Air Force Institute of Technology

AFIT Scholar

3-2006

Determining the Resistivity of Resistive Sheets Using Transmission Measurements

Milo W. Hyde IV

Follow this and additional works at: https://scholar.afit.edu/etd

Part of the Electromagnetics and Photonics Commons

Recommended Citation

**DETERMINING THE RESISTIVITY OF RESISTIVE SHEETS
USING TRANSMISSION MEASUREMENTS**

THESIS

Milo W. Hyde IV, Captain, USAF

AFIT/GE/ENG/06-24

**DEPARTMENT OF THE AIR FORCE
AIR UNIVERSITY**

AIR FORCE INSTITUTE OF TECHNOLOGY

Wright-Patterson Air Force Base, Ohio

AFIT/GE/ENG/06-24

**DETERMINING THE RESISTIVITY OF RESISTIVE SHEETS
USING TRANSMISSION MEASUREMENTS**

THESIS

Presented to the Faculty

Department of Electrical and Computer Engineering

Graduate School of Engineering and Management

Air Force Institute of Technology

Air University

Air Education and Training Command

In Partial Fulfillment of the Requirements for the

Degree of Master of Science in Electrical Engineering

Milo W. Hyde IV, BS

Captain, USAF

March 2006

AFIT/GE/ENG/06-24

**DETERMINING THE RESISTIVITY OF RESISTIVE SHEETS
USING TRANSMISSION MEASUREMENTS**

Milo W. Hyde IV, BS
Captain, USAF

Approved:

//signed//	
Dr. Michael J. Havrilla (Chairman)	Date

//signed//	
Dr. Andrew J. Terzuoli (Member)	Date

//signed//	
Dr. Paul E. Crittenden (Member)	Date

Acknowledgments

The person I have the most to thank is my advisor Dr. Michael Havrilla. Without his patience and his time, this thesis would have never been possible.

I would also like to thank Major Michael Hastriter for his help during my instructional quarters at AFIT.

I owe a great deal of gratitude to Rodney George at AFRL/SNS. Without his help, the free-space portion of this thesis would be significantly lacking.

Lastly, I would like to thank my parents for without them I certainly would not be here.

<div align="right">Milo W. Hyde IV</div>

Table of Contents

List of Figures

List of Tables

AFIT/GE/ENG/06-24

Abstract

In September 2005, radar cross section (RCS) measurements were made of resistive sheets, or R-cards, wrapped around a polystyrene foam cylinder to compare with a newly developed theoretical RCS prediction technique. The resistivities of the R-cards were initially measured with a direct current (DC) four-point probe. When the RCS measurements were compared to the theoretical predictions, it became clear that DC resistivity alone is not sufficient to accurately predict the scattering from an R-card. This thesis presents alternating current (AC) methods for determining the resistivity of an R-card. Both free-space and waveguide techniques are presented.

Experimental verification of the techniques is performed using two R-cards with DC resistivities 892 Ω/sq and 64 Ω/sq. The techniques are compared intra- and inter-measurement apparatus. An error analysis is also performed to demonstrate the sensitivity of the techniques to errors in the measurements of the thickness or the permittivity of the support backing.

DETERMINING THE RESISTIVITY OF RESISTIVE SHEETS

USING TRANSMISSION MEASUREMENTS

1. Introduction

A perfect electrical conductor (PEC) is a type of surface with which every student of electromagnetics is familiar. From the very first electromagnetics course, students are taught that at a PEC surface the total tangential electric field is forced to zero and that the total tangential magnetic field is related to the electric current density induced on that surface. Such a surface, being a PEC, offers no hindrance to the flow of electric current; therefore, it possesses infinite conductance and zero resistance. Although PECs do not exist naturally, iron, aluminum, copper, gold, and most other common metals can be safely approximated as PECs at microwave frequencies.

A dielectric is another material with which students of electromagnetics are familiar. An ideal dielectric is an electrical insulator; it does not permit electric current to flow through it or across its surface. This material, completely opposite of a PEC, has no conductance and infinite resistance. The tangential components of a field incident on a dielectric are continuous across the boundary. Common dielectrics are air, glass, and polystyrene foam.

A resistive sheet, or R-card, is a material which can be thought of as having properties of both a PEC and a dielectric. It is typically a non-magnetic, i.e. permeability equal to that of free-space, electrically thin, imperfect conductor of electric current;

therefore, it possesses a finite conductance and a greater than zero resistance. The total tangential electric field incident on an R-card is continuous across the boundary. Also since R-cards are typically electrically thin, the volume current induced by the field inside an R-card can be approximated as a surface current, therefore equivalently making the total tangential magnetic field discontinuous by the amount of electric current induced on the surface of the R-card. Since R-cards behave in a manner analogous to an electrical resistor, they are ideal for radiation absorbers. A radiation absorber device that makes use of R-cards is called a Jaumann absorber. A Jaumann absorber is designed by stacking resistive sheets in descending resistivity value order with the highest valued sheets closest to the source of the incident field and placing polystyrene foam or some other dielectric material between the sheets. Determining accurately the resistivity of an R-card is critical to the design of a Jaumann absorber. It is also imperative to theoretically predicting the scattering and ultimately the RCS of a resistive sheet. The resistivity of an R-card is typically measured with a four-point probe. This DC device measures the ohms per square of a resistive material simply by placing the probe's four points in contact with the material. Since electromagnetic fields induce alternating current on the surface of a conducting material, another method is to measure the material parameters of the resistive sheet in a free-space or waveguide system. This thesis will center on this latter method and present new techniques for determining the resistivity of a material from free-space and waveguide material measurements.

1.1 Problem Statement

In September 2005, RCS measurements were taken of two resistive sheets wrapped around a polystyrene foam cylinder (Figure 1-1) to compare with a physical optics approximation developed by Michael Havrilla of the Air Force Institute of Technology [1]. Measurements were also made of a PEC cylinder to validate the range data. Initial measurements of the two R-cards were quite discouraging, especially the 892 Ω/sq R-card shown in Figure 1-2. The RCS range was quickly exonerated as being a possible cause of the inaccuracies since the PEC cylinder measurements agreed well with theoretical predictions. Like the RCS range, the math behind the theoretical RCS

Figure 1-1. R-cards wrapped around a polystyrene foam cylinder. On the left is an R-card with a measured DC resistivity of 892 Ω/sq. On the right is another R-card with a measured DC resistivity of 64 Ω/sq.
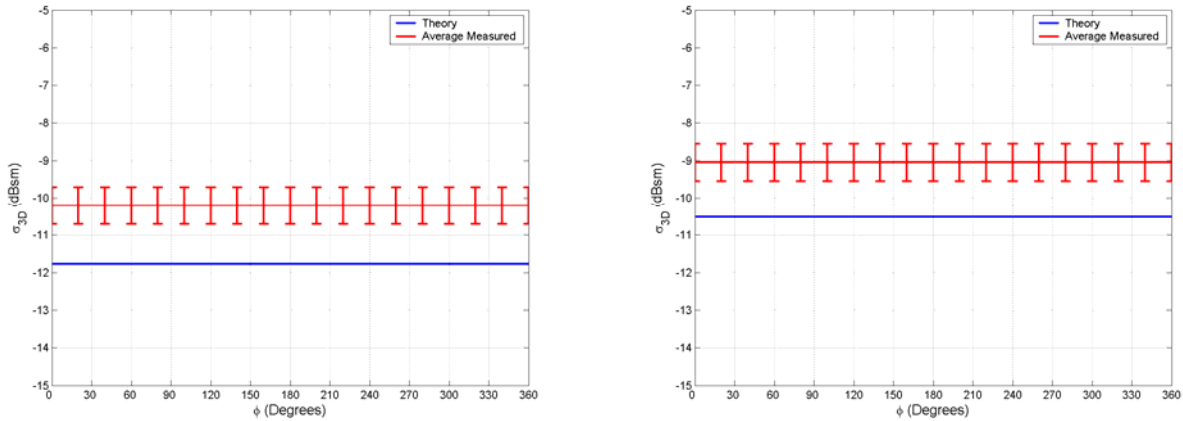
Figure 1-2. Vertical and horizontal polarization monostatic RCS plots of the 892 Ω/sq R-card. The RCS was predicted and measured at 7 GHz. In both polarizations, the theoretical RCS is approximately 1.5 dBsm lower than measured. Experience has shown a ±0.5 dBsm uncertainty in the RCS values obtained from the AFIT range.

prediction of the 892 Ω/sq R-card was double checked and determined to be accurate. The only other possible cause to the theory and measurement mismatches in Figure 1-2 is an error in the how the resistivity value of the R-card was determined.

The resistivity of the 892 Ω/sq R-card, shown in Figure 1-1, was initially measured with the four-point probe shown in Figure 1-3. In *Semiconductor Material and Device Characterization*, Schroder [2] derives the basic theory behind a four-point probe. The following background theory on four-point probes relies on his work. A four-point probe in contact with a semi-infinite material with current entering probe 1 and leaving probe 4 will experience a voltage drop across probes 2 and 3 according to the following expression

$$V = \frac{\rho I}{2\pi}\left(\frac{1}{r_1} - \frac{1}{r_4}\right),$$

(1.1)

1-4

Figure 1-3. Guardian model SRM-232 four-point probe.

where V is the voltage, ρ is the resistivity in ohms per meter, I is the current, and r_1 and r_4 are the radial distances from probes 1 and 4 respectively. Using the nomenclature for distances in Figure 1-4, the voltages measured at probe 2 and probe 3 are

$$V_2 = \frac{\rho I}{2\pi}\left(\frac{1}{s_1} - \frac{1}{s_2 + s_3}\right) \qquad (1.2)$$

and

$$V_3 = \frac{\rho I}{2\pi}\left(\frac{1}{s_1 + s_2} - \frac{1}{s_3}\right). \qquad (1.3)$$

Taking into account that the probe spacings of most four-point probes are equal and subtracting the voltage at probe 3 from the voltage at probe 2, one obtains

$$\rho = 2\pi s\left(\frac{V}{I}\right). \qquad (1.4)$$
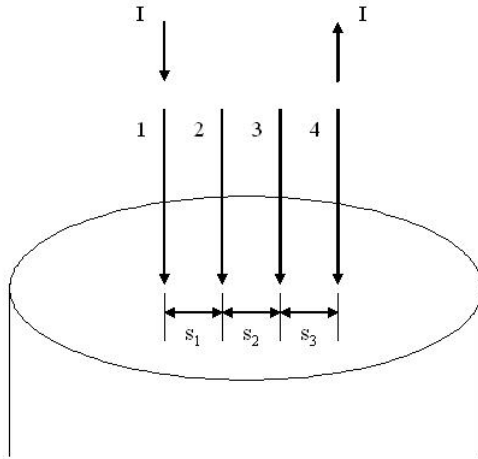
Figure 1-4. Four-point probe.

For thin materials, thicknesses less than or equal to half the probe spacing, (1.4) must be

corrected because the material cannot be considered to be semi-infinite in the vertical

direction. Considering the thickness of the material, τ, the resistivity ρ equals

$$\rho = \frac{\pi\tau}{\ln(2)}\left(\frac{V}{I}\right).$$

(1.5)

Dividing both sides of the above expression by τ results in

$$\rho_s = \frac{\rho}{\tau} = \frac{\pi}{\ln(2)}\left(\frac{V}{I}\right),$$

(1.6)

where ρ_s is the sheet resistance of the material and has the units ohms per square. For the

remainder of this thesis, resistivity will be used equivalently for sheet resistance.

Since the four-point probe pictured in Figure 1-3 is a DC device, it can only

measure the resistive properties and not any of the reactive properties that also have an

effect on the RCS of an R-card. Since DC methods have this shortfall, AC methods for

determining resistivity will be more accurate. This thesis will focus on two such AC

methods, free-space and waveguide material measurement systems. Both of these

systems take forward and reverse reflection, S_{11} and S_{22}, and forward and reverse

transmission, S_{21} and S_{12}, coefficient measurements. Both the reflection and transmission

measurements can be used to determine the resistivity of a material. In some cases it is

more advantageous to use the reflection measurements because a resistive sheet measured

at certain frequencies will be predominately reflective with very little energy transmitted.

While in other cases using the transmission measurements is more desirable because

unlike the reflection measurements, the transmission measurements do not depend on the

position of the material being measured relative to the calibration plane. Because of the

latter, this thesis will focus on methods for determining the resistivity of a material using

the transmission measurements.

1.2 Limitations

While the validity of the transmission measurements does not depend on the

position of the sample relative to the calibration plane, there are instances where it is not

possible to utilize them for determining resistivity. One such instance occurs when trying

to make resistivity measurements at low frequencies. Under these conditions resistive

sheets are highly reflective making the transmission measurements too near the noise

floor of the system for the resistivity of the sample to be accurately determined.

Knowledge of the conditions under which a resistive sheet will be used is imperative to

determining the validity of using transmission based resistivity measurements.

1.3 Scope

There are certainly other ways, including microstrip and coaxial systems, to determine the resistivity of a material. This thesis focuses only on free-space and waveguide system methods and validates those methods on the two R-cards shown in Figure 1-1. Further reducing its scope, this thesis focuses on using the forward transmission coefficient measurement, S_{21}, from those two systems to determine resistivity. Forward transmission measurement data gathered from the free-space system is from 2 to 18 GHz, while data gathered from the waveguide system is from the X-band (8.2 to 12.4 GHz). Although the data presented is from those particular frequencies, the methods developed relating resistivity to S_{21} are applicable at any frequency granted S_{21} can be accurately measured.

1.4 Thesis Organization

Chapter 2 provides the theoretical background starting with Maxwell's equations, working through vector potentials, and finally introducing transverse electromagnetic and transverse electric modes. Chapter 3 shows the development of free-space and waveguide methods for determining the resistivity of an R-card using the forward transmission coefficient measurement. The chapter begins with free-space techniques and introduces the root search, first, second, and Nth order approximations, and the thin sheet approximation methods. The chapter ends with waveguide techniques and introduces waveguide versions of the root search, first, second, and Nth order approximations, and the thin sheet approximation methods. It also introduces another waveguide method that relies on the principle of mode matching: the vertical mode

matching technique. Chapter 4 presents experimental results and compares the methods

introduced in chapter 3 to one another. Lastly, the thesis concludes in chapter 5 with

recommendations for future research.

2. Background

This chapter provides the theoretical background for the free-space and waveguide methods for determining resistivity shown in chapter 3. The theory presented in this chapter comes from the combined work of Collin [3], Harrington [4], and Balanis [5]. Any method for predicting the behavior of electromagnetic waves begins with Maxwell's equations,

$$\nabla \times \bar{E} = -\bar{M} - j\omega\bar{B} \tag{2.1}$$

$$\nabla \times \bar{H} = \bar{J} + j\omega\bar{D} \tag{2.2}$$

$$\nabla \cdot \bar{D} = q_{ev} \tag{2.3}$$

$$\nabla \cdot \bar{B} = q_{mv}, \tag{2.4}$$

shown here in time harmonic form. The curl equations, (2.1) and (2.2), are known as Faraday's Law and Ampere's Law respectively, where $\bar{E}$ is the electric field intensity, $\bar{H}$ is the magnetic field intensity, $\bar{M}$ is the magnetic current density, $\bar{J}$ is the electric current density, $\bar{B}$ is the magnetic flux density, $\bar{D}$ is the electric flux density, and ω is the radian frequency. Equations (2.3) and (2.4) are known as Gauss' Laws for electric and magnetic fields, where q_{ev} is the electric charge density and q_{mv} is the magnetic charge density. This thesis will deal with linear, homogeneous, isotropic materials for which

$$\begin{aligned} \bar{D} &= \varepsilon\bar{E} \\ \bar{B} &= \mu\bar{H} \end{aligned}, \tag{2.5}$$

where ε and μ are the permittivity and permeability of the material. This simplifies

Maxwell's equations to

$$\nabla \times \bar{E} = -\bar{M} - j\omega\mu\bar{H} \tag{2.6}$$

$$\nabla \times \bar{H} = \bar{J} + j\omega\varepsilon\bar{E} \tag{2.7}$$

$$\nabla \cdot \bar{E} = \frac{q_{ev}}{\varepsilon} \tag{2.8}$$

$$\nabla \cdot \bar{H} = \frac{q_{mv}}{\mu}. \tag{2.9}$$

2.1 Helmholtz Wave Equations and Vector Potentials

Using Maxwell's equations, (2.6) through (2.9), directly to determine the electric

and magnetic fields of a system is difficult because the equations are first-order, coupled,

partial differential equations. However, using those coupled equations, second-order,

uncoupled, partial differential equations can be formed which are more easily solved.

The Helmholtz electric field wave equation is formed by taking the curl of both sides of

Faraday's Law (2.6):

$$\nabla \times \nabla \times \bar{E} = -\nabla \times \bar{M} - j\omega\mu\nabla \times \bar{H} . \tag{2.10}$$

Making use of the vector identity

$$\nabla \times \nabla \times \bar{A} = \nabla\left(\nabla \cdot \bar{A}\right) - \nabla^2\bar{A}, \tag{2.11}$$

and Ampere's Law (2.7), equation (2.10) becomes

$$\nabla\left(\nabla \cdot \bar{E}\right) - \nabla^2\bar{E} = -\nabla \times \bar{M} - j\omega\mu\left(\bar{J} + j\omega\varepsilon\bar{E}\right). \tag{2.12}$$

Substituting in (2.8) and simplifying results in the Helmholtz electric field wave equation

with sources,

$$\nabla^2 \vec{E} + k^2 \vec{E} = \nabla \times \vec{M} + j\omega\mu\vec{J} + \frac{1}{\varepsilon}\nabla q_{ev}, \tag{2.13}$$

where

$$k^2 = \omega^2 \mu\varepsilon. \tag{2.14}$$

A very similar procedure can be done to Ampere's Law to arrive at the Helmholtz magnetic field wave equation with sources:

$$\nabla^2 \vec{H} + k^2 \vec{H} = -\nabla \times \vec{J} + j\omega\varepsilon\vec{M} + \frac{1}{\mu}\nabla q_{mv}. \tag{2.15}$$

If the sources are not contained in the region of interest, (2.13) and (2.15) simplify to the source-free Helmholtz wave equations:

$$\nabla^2 \vec{E} + k^2 \vec{E} = 0 \tag{2.16}$$

and

$$\nabla^2 \vec{H} + k^2 \vec{H} = 0. \tag{2.17}$$

Since (2.16) and (2.17) are of the same form, their solutions will also be of the same form. Expanding the electric field in (2.16) into its components results in

$$\nabla^2 \left(\hat{x} E_x + \hat{y} E_y + \hat{z} E_z\right) + k^2 \left(\hat{x} E_x + \hat{y} E_y + \hat{z} E_z\right) = 0. \tag{2.18}$$

Since the x, y, and z components of the electric field are orthogonal to each other, the solution of (2.18) in one direction is completely independent of the solution of (2.18) in another direction. Therefore, the vector equation, (2.18), can be expressed as three scalar equations of the form

$$\begin{aligned} \nabla^2 E_x + k^2 E_x &= 0 \\ \nabla^2 E_y + k^2 E_y &= 0. \\ \nabla^2 E_z + k^2 E_z &= 0 \end{aligned} \tag{2.19}$$

As before, since the three scalar equations have the same form, their solutions will have the same form. Expanding the Laplacian operator in the first scalar expression results in

$$\frac{\partial^2 E_x}{\partial x} + \frac{\partial^2 E_x}{\partial y} + \frac{\partial^2 E_x}{\partial z} + k^2 E_x = 0 . \qquad (2.20)$$

Using separation of variables, the solution is assumed to be of the form

$$E_x = f(x)g(y)h(z) \qquad (2.21)$$

for the purpose of transforming the partial derivatives into ordinary derivatives. This results in

$$gh\frac{d^2 f}{dx} + fh\frac{d^2 g}{dy} + fg\frac{d^2 h}{dz} + k^2 fgh = 0 . \qquad (2.22)$$

Dividing by fgh and subtracting k^2 from both sides of (2.22) yields

$$\frac{1}{f}\frac{d^2 f}{dx} + \frac{1}{g}\frac{d^2 g}{dy} + \frac{1}{h}\frac{d^2 h}{dz} = -k^2 . \qquad (2.23)$$

Since each of the three functions in (2.23) is of one variable independent of the other two and summed to equal a constant, one gets

$$\frac{1}{f}\frac{d^2 f}{dx} = -k_x^2 \qquad (2.24)$$

$$\frac{1}{g}\frac{d^2 g}{dy} = -k_y^2 ,$$

$$\frac{1}{h}\frac{d^2 h}{dz} = -k_z^2$$

where

$$k^2 = k_x^2 + k_y^2 + k_z^2 . \qquad (2.25)$$

2-4

The expressions in (2.24) are now second-order, linear, homogeneous differential equations and since they are of the same form, their solutions are also of the same form. The function f,

$$f(x) = A_1 e^{-jk_x x} + A_2 e^{jk_x x} \text{ or } f(x) = B_1 \cos(k_x x) + B_2 \sin(k_x x) \tag{2.26}$$

as well as g and h, can take either expression depending on the nature of the wave. If, for example, the wave travels in the x direction and stands in the other two, the solution to the Helmholtz electric field wave equation will be

$$E_x = \left(A_1 e^{-jk_x x} + A_2 e^{jk_x x}\right)\left(B_1 \cos k_y y + B_2 \sin k_y y\right)\left(C_1 \cos k_z z + C_2 \sin k_z z\right), \tag{2.27}$$

where A_1, A_2, B_1, B_2, C_1, and C_2 are constants whose values are obtained by enforcing the boundary conditions of the problem.

2.1.1 The Magnetic Vector Potential.

Since the Helmholtz wave equations are linear, superposition can be used to develop intermediate quantities. These intermediate quantities in electromagnetics are called vector potentials. There are two vector potentials in electromagnetics: the magnetic vector potential and the electric vector potential.

The magnetic vector potential, or $\vec{A}$, is associated with the magnetic flux density $\vec{B}$. In a source-free environment, $\nabla \cdot \vec{B} = 0$; therefore, one can set

$$\vec{B} = \nabla \times \vec{A}. \tag{2.28}$$

Using (2.28) and noting the relationship between the magnetic flux density and the magnetic field intensity (2.5) produces in an expression for the magnetic field due to the magnetic vector potential:

$$\bar{H}_A = \frac{1}{\mu} \nabla \times \bar{A}. \tag{2.29}$$

Substituting (2.29) into source-free Faraday's Law (2.6) and simplifying brings about the following expression

$$\nabla \times \left[\bar{E}_A + j\omega \bar{A} \right] = 0. \tag{2.30}$$

As a results of (2.30), there exists a scalar electric potential function, ϕ_e, such that

$$\bar{E}_A + j\omega \bar{A} = -\nabla \phi_e. \tag{2.31}$$

Solving (2.31) for the electric field due to the magnetic vector potential results in

$$\bar{E}_A = -\nabla \phi_e - j\omega \bar{A}. \tag{2.32}$$

Taking the curl of both sides of (2.29) and using vector identity (2.11) results in

$$\mu \nabla \times \bar{H}_A = \nabla \times \nabla \times \bar{A} = \nabla \left(\nabla \cdot \bar{A} \right) - \nabla^2 \bar{A}. \tag{2.33}$$

Substituting in Ampere's Law (2.7) where the electric current density is an electric current impressed by the field, brings about

$$\mu \bar{J} + j\omega\mu\varepsilon \bar{E}_A = \nabla \left(\nabla \cdot \bar{A} \right) - \nabla^2 \bar{A}. \tag{2.34}$$

Substituting (2.32) into (2.34) and simplifying produces

$$\nabla^2 \bar{A} + k^2 \bar{A} = -\mu \bar{J} + j\omega\mu\varepsilon \nabla \phi_e + \nabla \left(\nabla \cdot \bar{A} \right). \tag{2.35}$$

To fully characterize the magnetic vector potential both the curl and divergence of the vector must be specified. The curl of the magnetic vector potential was defined in (2.28); however, no value has been specified for the divergence of the magnetic vector potential. Letting

$$\nabla \cdot \bar{A} = -j\omega\mu\varepsilon\phi_e \tag{2.36}$$

and substituting it into (2.35) produces

$$\nabla^2 \vec{A} + k^2 \vec{A} = -\mu \vec{J} \, . \tag{2.37}$$

More importantly, simple expressions for the electric and magnetic fields in terms of the magnetic vector potential can be formed from (2.29) and from substituting (2.37) into (2.34):

$$\vec{E}_A = \frac{1}{j\omega\mu\varepsilon} \left(\nabla \left(\nabla \cdot \vec{A} \right) + k^2 \vec{A} \right) \tag{2.38}$$

$$\vec{H}_A = \frac{1}{\mu} \nabla \times \vec{A}$$

To get the total electric and magnetic fields however, the fields due to the magnetic vector potential must be added to the fields due to the electric vector potential. The electric vector potential will be introduced in the next subsection.

2.1.2 The Electric Vector Potential.

Following from the principle of superposition, the total fields are obtained when the contributions to the fields from both vector potentials are added together. In the previous subsection, the magnetic vector potential was introduced. In this subsection, the electric vector potential will be introduced. The electric vector potential, or $\vec{F}$, is linked to the electric flux density $\vec{D}$. In a source-free region, $\nabla \cdot \vec{D} = 0$; therefore, one can set

$$\vec{D} = -\nabla \times \vec{F} \, . \tag{2.39}$$

Using the relationship between the electric field intensity and the electric flux density (2.5), the electric field due to the electric vector potential becomes

$$\vec{E}_F = -\frac{1}{\varepsilon} \nabla \times \vec{F} \, . \tag{2.40}$$

Substituting (2.40) into source-free Ampere's Law (2.7) produces

$$\nabla \times \left[\bar{H}_F + j\omega \bar{F} \right] = 0 . \tag{2.41}$$

As a result of (2.41), there exists a scalar magnetic potential function, ϕ_m, such that

$$\bar{H}_F + j\omega \bar{F} = -\nabla \phi_m . \tag{2.42}$$

By solving (2.42) for $\bar{H}_F$, an expression for the magnetic field due to the electric vector potential can be obtained:

$$\bar{H}_F = -\nabla \phi_m - j\omega \bar{F} . \tag{2.43}$$

Taking the curl of both sides of (2.40), using Faraday's Law (2.6), substituting in (2.43), and simplifying brings about

$$\nabla^2 \bar{F} + k^2 \bar{F} = -\varepsilon \bar{M} + \nabla \left(\nabla \cdot \bar{F} \right) + j\omega\mu\varepsilon \nabla \phi_m . \tag{2.44}$$

Exactly like the magnetic vector potential, to fully characterize the electric vector potential, the divergence and curl of the vector must be defined. Expression (2.40) defines the curl of the electric vector potential. Letting

$$\nabla \cdot \bar{F} = -j\omega\mu\varepsilon \phi_m \tag{2.45}$$

results in the following wave equation for the electric vector potential

$$\nabla^2 \bar{F} + k^2 \bar{F} = -\varepsilon \bar{M} . \tag{2.46}$$

The expressions for the electric and magnetic fields due to the electric vector potential are

$$\bar{E}_F = -\frac{1}{\varepsilon} \nabla \times \bar{F} \tag{2.47}$$

$$\bar{H}_F = \frac{1}{j\omega\mu\varepsilon} \left(\nabla \left(\nabla \cdot \bar{F} \right) + k^2 \bar{F} \right)^{.}$$

Following from superposition, expressions for the total electric and magnetic fields can now be obtained by adding the field contributions from the magnetic and electric vector potentials together:

$$\bar{E} = \bar{E}_A + \bar{E}_F = \frac{1}{j\omega\mu\varepsilon}\left(\nabla\left(\nabla\cdot\bar{A}\right)+k^2\bar{A}\right)-\frac{1}{\varepsilon}\nabla\times\bar{F} \qquad (2.48)$$

$$\bar{H} = \bar{H}_A + \bar{H}_F = \frac{1}{\mu}\nabla\times\bar{A}+\frac{1}{j\omega\mu\varepsilon}\left(\nabla\left(\nabla\cdot\bar{F}\right)+k^2\bar{F}\right).$$

2.2 Transverse Electromagnetic Waves (TEM)

A transverse electromagnetic wave, or plane wave in Cartesian coordinates, is a wave in which the electric and magnetic fields are directed transverse to the direction the wave propagates. A *TEM* wave exists in free-space, coaxial cable, and microstrip environments. Expressions for the electric and magnetic fields of a *TEM* wave propagating in the z direction, TEM^Z, can be found using magnetic and electric vector potentials introduced in the previous subsections. Since a TEM^Z wave exists in environments where there are no sources or impressed sources, expressions for the electric and magnetic fields that compose it must come from

$$\nabla^2\bar{A}+k^2\bar{A}=0 \qquad (2.49)$$

$$\nabla^2\bar{F}+k^2\bar{F}=0.$$

The solutions of the equations in (2.49) are of the same form as the Helmholtz wave equation solutions shown in (2.26) and (2.27). Since the wave propagates in the z direction, only the magnetic and electric vector potentials in the z direction will be of consequence, therefore

$$A_z = \left(A_1 e^{-jk_x x} + A_2 e^{jk_x x}\right)\left(B_1 e^{-jk_y y} + B_2 e^{jk_y y}\right)\left(C_1 e^{-jk_z z} + C_2 e^{jk_z z}\right) \qquad (2.50)$$

$$F_z = \left(D_1 e^{-jk_x x} + D_2 e^{jk_x x}\right)\left(E_1 e^{-jk_y y} + E_2 e^{jk_y y}\right)\left(F_1 e^{-jk_z z} + F_2 e^{jk_z z}\right).$$

It follows from (2.25) that since the wave propagates completely in the z direction, the wave numbers in the x and y directions, k_x and k_y, must be zero. Rolling the

coefficients together, the expressions for the magnetic and electric vector potentials become

$$A_z = A_1 e^{-jkz} + A_2 e^{jkz}$$
$$F_z = F_1 e^{-jkz} + F_2 e^{jkz}$$

(2.51)

where the coefficients, A_1, A_2, F_1, and F_2, could be functions of x and y and k equals k_z.

Using the relationships in (2.48), the electric and magnetic fields in a TEM^Z wave are given by the following expressions

$$\bar{E} = \bar{E}_A + \bar{E}_F = \frac{1}{j\omega\mu\varepsilon}\left(\nabla\left(\nabla \cdot \hat{z}A_z\right) + k^2\hat{z}A_z\right) - \frac{1}{\varepsilon}\nabla \times \hat{z}F_z$$

(2.52)

$$\bar{H} = \bar{H}_A + \bar{H}_F = \frac{1}{\mu}\nabla \times \hat{z}A_z + \frac{1}{j\omega\mu\varepsilon}\left(\nabla\left(\nabla \cdot \hat{z}F_z\right) + k^2\hat{z}F_z\right)$$

Expanding and simplifying (2.52) produces

$$E_x = \left(\mp\frac{1}{\sqrt{\mu\varepsilon}}\frac{\partial A_1}{\partial x} - \frac{1}{\varepsilon}\frac{\partial F_1}{\partial y}\right)e^{\mp jkz} \equiv E_x^+ e^{-jkz} + E_x^- e^{jkz}$$

(2.53)

$$E_y = \left(\mp\frac{1}{\sqrt{\mu\varepsilon}}\frac{\partial A_1}{\partial y} + \frac{1}{\varepsilon}\frac{\partial F_1}{\partial x}\right)e^{\mp jkz} \equiv E_y^+ e^{-jkz} + E_y^- e^{jkz}$$

$$E_z = 0$$

$$H_x = \left(\mp\frac{1}{\sqrt{\mu\varepsilon}}\frac{\partial F_1}{\partial x} + \frac{1}{\mu}\frac{\partial A_1}{\partial y}\right)e^{\mp jkz} \equiv H_x^+ e^{-jkz} + H_x^- e^{jkz}$$

$$H_y = \left(\mp\frac{1}{\sqrt{\mu\varepsilon}}\frac{\partial F_1}{\partial y} - \frac{1}{\mu}\frac{\partial A_1}{\partial x}\right)e^{\mp jkz} \equiv H_y^+ e^{-jkz} + H_y^- e^{jkz}$$

$$H_z = 0$$

using the $e^{j\omega t}$ time convention. The constants in (2.53) are found by enforcing the boundary conditions of the problem. It is evident from (2.53) that the electric and magnetic fields of a TEM^Z wave are related by the following expression

$$\vec{H} = \frac{1}{\eta} \hat{k} \times \vec{E} ,$$
(2.54)

where η is the intrinsic impedance of the medium and equal to

$$\eta = \sqrt{\frac{\mu}{\varepsilon}}$$
(2.55)

and $\hat{k}$ is the unit vector pointing in the direction of propagation. In the case of a forward traveling TEM^Z wave, $\hat{k}$ is $\hat{z}$.

Transverse electromagnetic is the simplest form, or mode, a wave can take and therefore is commonly referred to as mode zero. Other more complicated modes, such as transverse electric (*TE*) and transverse magnetic (*TM*), exist. In the next section, transverse electric modes will be introduced.

2.3 Transverse Electric Waves (TE)

In the last section, the transverse electromagnetic mode was introduced. This section will introduce transverse electric modes. A *TE* mode is formed when the energy is constrained inside a waveguide. Like a *TEM* mode, the electric field in a *TE* mode is directed transverse to the direction of propagation; unlike a *TEM* mode, the directions of the magnetic field in a *TE* mode are under no such requirement. Expressions for the electric and magnetic fields for a transverse electric mode traveling in a *z* directed, TE^Z, waveguide can be found by using magnetic and electric vector potentials. In this case, the electric vector potential in the *z* direction is the only quantity necessary and it must satisfy the following scalar wave equation

$$\nabla^2 F_z + k^2 F_z = 0 \ [5].$$
(2.56)

2-11
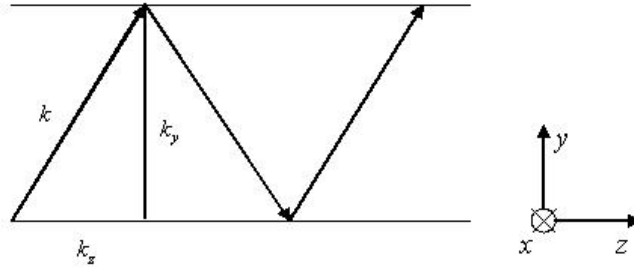
Figure 2-1. Wave propagating in a z directed waveguide.

The solutions to (2.56) are of the same form as (2.26) and (2.27). Since the energy is confined in the x and y directions and free to propagate in the z direction, the solutions to (2.56) are of the form

$$F_z = \left(A_1 \cos k_x x + A_2 \sin k_x x\right)\left(B_1 \cos k_y y + B_2 \sin k_y y\right)\left(C_1 e^{-jk_z z} + C_2 e^{jk_z z}\right). \qquad (2.57)$$

Figure 2-1 shows how the wave propagates down the guide in the z direction. Since it does not completely travel in the z direction, the wave numbers in the x and y directions could have values and cannot be set equal to zero. Using (2.48), the electric and magnetic fields of a TE^Z mode are given by the following expressions

$$\bar{E} = \bar{E}_F = -\frac{1}{\varepsilon} \nabla \times \hat{z} F_z \qquad (2.58)$$

$$\bar{H} = \bar{H}_F = \frac{1}{j\omega\mu\varepsilon}\left(\nabla\left(\nabla \cdot \hat{z} F_z\right) + k^2 \hat{z} F_z\right)$$

Expanding and simplifying (2.58) results in

$$E_x = \frac{k_y}{\varepsilon}\left(A_1 \cos k_x x + A_2 \sin k_x x\right)\left(B_1 \sin k_y y - B_2 \cos k_y y\right)\left(C_1 e^{-jk_z z} + C_2 e^{jk_z z}\right) \qquad (2.59)$$

$$E_y = -\frac{k_x}{\varepsilon}\left(A_1 \sin k_x x - A_2 \cos k_x x\right)\left(B_1 \cos k_y y + B_2 \sin k_y y\right)\left(C_1 e^{-jk_z z} + C_2 e^{jk_z z}\right)$$

$$E_z = 0$$

$$H_x = \frac{k_x k_z}{\omega\mu\varepsilon}\left(A_1 \sin k_x x - A_2 \cos k_x x\right)\left(B_1 \cos k_y y + B_2 \sin k_y y\right)\left(C_1 e^{-jk_z z} - C_2 e^{jk_z z}\right)$$

$$H_y = \frac{k_y k_z}{\omega\mu\varepsilon}\left(A_1 \cos k_x x + A_2 \sin k_x x\right)\left(B_1 \sin k_y y - B_2 \cos k_y y\right)\left(C_1 e^{-jk_z z} - C_2 e^{jk_z z}\right) \quad,$$

$$H_z = \frac{k^2 - k_z^2}{j\omega\mu\varepsilon}\left(A_1 \cos k_x x + A_2 \sin k_x x\right)\left(B_1 \cos k_y y + B_2 \sin k_y y\right)\left(C_1 e^{-jk_z z} + C_2 e^{jk_z z}\right)$$

where the constants A_1, A_2, B_1, B_2, C_1, and C_2 are found by imposing the boundary conditions of the problem. The tangential electric and tangential magnetic fields in a TE^Z mode are related by the following expression

$$\vec{H}_t = \frac{1}{Z}\hat{k} \times \vec{E}_t , \tag{2.60}$$

where Z is the wave impedance of the medium filling the waveguide and equal to

$$Z = \frac{j\omega\mu}{\gamma} \tag{2.61}$$

$$\gamma = jk_z$$

and $\hat{k}$ is the unit vector pointing in the direction of traveling wave propagation. In the case of a forward traveling TE^Z wave, $\hat{k}$ is $\hat{z}$. Setting the wave number in the z direction equal to zero in (2.25) results in

$$k_c = \sqrt{k_x^2 + k_y^2} , \tag{2.62}$$

where k_c is the cut-off wave number. Since k is related to frequency by (2.14), equation (2.62) actually gives the cut-off frequency. Physically, the cut-off frequency is the frequency at which wave propagation in the z direction commences. Waves with frequencies above the cut-off frequency will propagate in the waveguide; whereas, waves with frequencies below the cut-off frequency will be heavily damped, or evanescent. Cut-off frequency will be re-examined in chapter 3.

2.4 Summary

In this chapter, the background behind transverse electromagnetic and transverse electric modes was introduced. These two concepts will form the basis of the theoretical work shown in chapter 3. Transverse magnetic modes were not introduced in this chapter because they will not be used in this thesis. Their development can be found in Collin [3], Harrington [4], and Balanis [5].

3. Methodology

Building on the theoretical background presented in chapter 2, this chapter will show the development of several techniques for extracting the resistivity of an R-card in free-space and waveguide systems using the forward transmission measurement. The theory presented in this chapter will follow the same basic format: derive the fields in each region of the problem, enforce boundary conditions, and solve for the electromagnetic parameters of the material. Free-space methods will be presented first followed by waveguide techniques.

3.1 Free-Space Methods

A free-space material measurement system, or focused arch system, is a technique for material parameter extraction in which a *TEM* wave is transmitted from a horn antenna and focused through lenses. The wave then passes through or is reflected from an unknown material and is received by another horn antenna (Figure 3-1). Since the material sample size is large in its lateral dimensions compared to the wavelength of the incident *TEM* wave and to the size of the focused illuminated area produced by the lenses, the sample can be approximated as infinite in extent and scattering effects such as diffraction from the material's edges can be ignored. Figure 3-2 shows the geometry of the free-space problem. The electric and magnetic fields in region I, II, and III have the same form as (2.53) and are
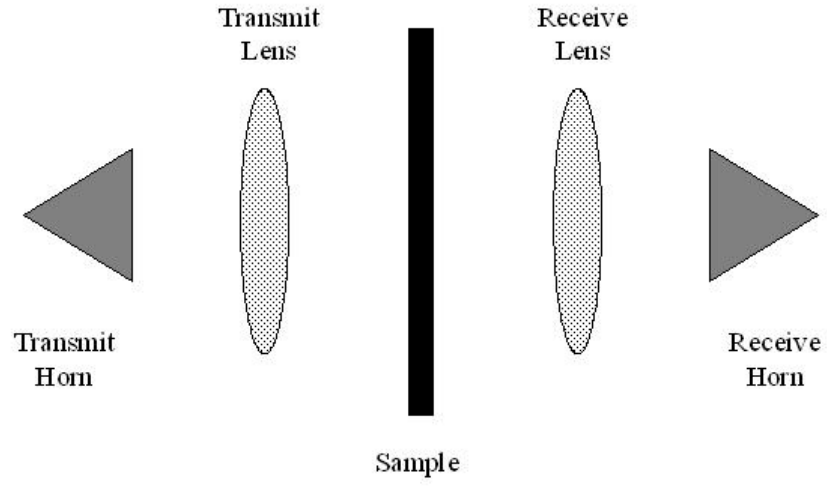
Figure 3-1. Free-space, or focused arch material measurement system.
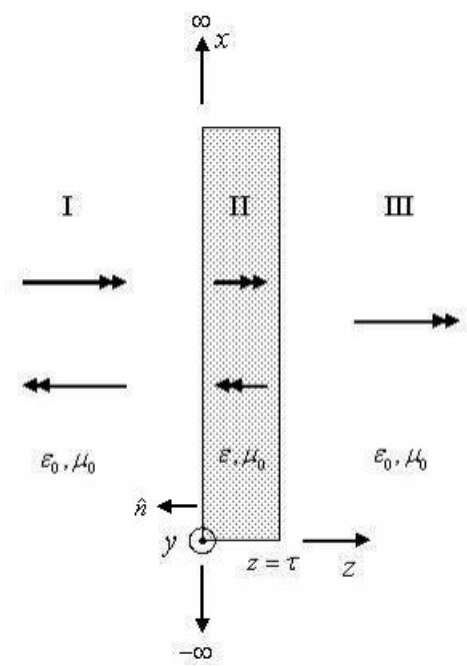
Figure 3-2. Geometry of the free-space problem.

$$\bar{E}_I = \begin{bmatrix} \hat{x} \\ \hat{y} \end{bmatrix} \left(E_I^+ e^{-jk_0 z} + E_I^- e^{jk_0 z} \right) \tag{3.1}$$

$$\bar{H}_I = \frac{\hat{k} \times \bar{E}_I}{\eta_0} = \frac{1}{\eta_0} \left(\begin{bmatrix} \hat{y} \\ -\hat{x} \end{bmatrix} E_I^+ e^{-jk_0 z} + \begin{bmatrix} -\hat{y} \\ \hat{x} \end{bmatrix} E_I^- e^{jk_0 z} \right)$$

$$\bar{E}_{II} = \begin{bmatrix} \hat{x} \\ \hat{y} \end{bmatrix} \left(E_{II}^+ e^{-jkz} + E_{II}^- e^{jkz} \right)$$

$$\bar{H}_{II} = \frac{\hat{k} \times \bar{E}_{II}}{\eta} = \frac{1}{\eta} \left(\begin{bmatrix} \hat{y} \\ -\hat{x} \end{bmatrix} E_{II}^+ e^{-jkz} + \begin{bmatrix} -\hat{y} \\ \hat{x} \end{bmatrix} E_{II}^- e^{jkz} \right) \quad ,$$

$$\bar{E}_{III} = \begin{bmatrix} \hat{x} \\ \hat{y} \end{bmatrix} E_{III}^+ e^{-jk_0 (z-\tau)}$$

$$\bar{H}_{III} = \frac{\hat{k} \times \bar{E}_{III}}{\eta_0} = \frac{1}{\eta_0} \begin{bmatrix} \hat{y} \\ -\hat{x} \end{bmatrix} E_{III}^+ e^{-jk_0 (z-\tau)}$$

where k_0, η_0, k, and η are the wave numbers (2.14) and intrinsic impedances (2.55) of free-space and the unknown material respectively.

3.1.1 Root Search Method.

Applying tangential continuity boundary conditions to the fields of each region at $z = 0$ and $z = \tau$ results in the following expressions

$$E_I^+ + E_I^- = E_{II}^+ + E_{II}^- \tag{3.2}$$

$$\frac{E_I^+}{\eta_0} - \frac{E_I^-}{\eta_0} = \frac{E_{II}^+}{\eta} - \frac{E_{II}^-}{\eta}$$

$$E_{II}^+ e^{-jk\tau} + E_{II}^- e^{jk\tau} = E_{III}^+ \quad .$$

$$\frac{E_{II}^+}{\eta} e^{-jk\tau} - \frac{E_{II}^-}{\eta} e^{jk\tau} = \frac{E_{III}^+}{\eta_0}$$

Since an expression for the forward transmission coefficient, S_{21}, is desired and it is equal to the field received at antenna 2 divided by the field transmitted from antenna 1 (Figure 3-1), the expressions in (3.2) must be divided by E_I^+ resulting in

3-3

$$1 + \frac{E_I^-}{E_I^+} = \frac{E_{II}^+}{E_I^+} + \frac{E_{II}^-}{E_I^+}$$

$$\frac{1}{\eta_0} - \frac{1}{\eta_0}\frac{E_I^-}{E_I^+} = \frac{1}{\eta}\frac{E_{II}^+}{E_I^+} - \frac{1}{\eta}\frac{E_{II}^-}{E_I^+}$$

$$\frac{E_{II}^+}{E_I^+}e^{-jk\tau} + \frac{E_{II}^-}{E_I^+}e^{jk\tau} = \frac{E_{III}^+}{E_I^+}$$

$$\frac{1}{\eta}\frac{E_{II}^+}{E_I^+}e^{-jk\tau} - \frac{1}{\eta}\frac{E_{II}^-}{E_I^+}e^{jk\tau} = \frac{1}{\eta_0}\frac{E_{III}^+}{E_I^+}$$

(3.3)

Rearranging (3.3) into matrix form produces

$$
\begin{bmatrix}
1 & -1 & -1 & 0 \\
\dfrac{-1}{\eta_0} & \dfrac{-1}{\eta} & \dfrac{1}{\eta} & 0 \\
0 & e^{-jk\tau} & e^{jk\tau} & -1 \\
0 & \dfrac{1}{\eta}e^{-jk\tau} & \dfrac{-1}{\eta}e^{jk\tau} & \dfrac{-1}{\eta_0}
\end{bmatrix}
\begin{bmatrix}
\Gamma \\ t \\ r \\ T
\end{bmatrix}
=
\begin{bmatrix}
-1 \\ \dfrac{-1}{\eta_0} \\ 0 \\ 0
\end{bmatrix},
$$

(3.4)

where

$$\Gamma = \frac{E_I^-}{E_I^+}, \ t = \frac{E_{II}^+}{E_I^+}, \ r = \frac{E_{II}^-}{E_I^+}, \ \text{and T} = \frac{E_{III}^+}{E_I^+}.$$

(3.5)

An expression for T, which is related to the forward transmission coefficient by the following expression

$$S_{21} = Te^{jk_0\tau},$$

(3.6)

can now be obtained by solving the system of linear equations. After Gaussian elimination to reduce the matrix in (3.4) to the identity matrix and using (3.6), S_{21} equals

$$S_{21} = \frac{4\eta\eta_0}{\left(\eta_0^2 + \eta^2\right)\left(e^{jk\tau} - e^{-jk\tau}\right) + 2\eta\eta_0\left(e^{jk\tau} + e^{-jk\tau}\right)}e^{jk_0\tau}.$$

(3.7)

Using the following forms of the Euler formula

$$e^{j\theta} + e^{-j\theta} = 2\cos\theta \qquad (3.8)$$
$$e^{j\theta} - e^{-j\theta} = 2j\sin\theta \, '$$

(2.55), (2.14), and the fact that R-cards are non-magnetic, (3.7) becomes

$$S_{21} = \frac{2\sqrt{\varepsilon_r}}{j\varepsilon_r \sin\left(\dfrac{\omega\tau}{c}\sqrt{\varepsilon_r}\right) + 2\sqrt{\varepsilon_r}\cos\left(\dfrac{\omega\tau}{c}\sqrt{\varepsilon_r}\right) + j\sin\left(\dfrac{\omega\tau}{c}\sqrt{\varepsilon_r}\right)} e^{j\frac{\omega\tau}{c}} , \qquad (3.9)$$

where $\varepsilon_r = \dfrac{\varepsilon}{\varepsilon_0}$ is the relative permittivity of the R-card and c,

$$c = \frac{1}{\sqrt{\varepsilon_0\mu_0}} = 299792458 \, \frac{\text{m}}{\text{s}} , \qquad (3.10)$$

is the speed of light in a vacuum. It is not possible to analytically solve (3.9) for ε_r in

terms of S_{21}; therefore, a solution to (3.9) must be found using numerical techniques

which compare the theoretical expression on the right hand side of (3.9) to measured S_{21}

data. The simplest numerical technique to implement is the complex one-dimensional

Newton's method. It attempts to solve the expression

$$S_{21}^{thy}(\varepsilon_r,\omega) - S_{21}^{meas}(\omega) = 0 \qquad (3.11)$$

within a certain precision and is a derivative based technique. The initial guess is

supplied by the user while subsequent guesses are supplied by the following expression

$$\varepsilon_{r\,n+1} = \varepsilon_{r\,n} - \frac{S_{21}^{thy}(\varepsilon_{r\,n},\omega) - S_{21}^{meas}(\omega)}{\dfrac{d}{d\varepsilon_r}\left(S_{21}^{thy}(\varepsilon_r,\omega) - S_{21}^{meas}(\omega)\right)\bigg|_{\varepsilon_r=\varepsilon_{r\,n}}} . \qquad (3.12)$$

In expressions (3.11) and (3.12), S_{21}^{thy} and S_{21}^{meas} are

$$S_{21}^{thy} = S_{21}e^{-j\frac{\omega\tau}{c}}$$

$$S_{21}^{meas} = S_{21}^{raw}e^{-j\frac{\omega\tau}{c}},$$

(3.13)

where S_{21}^{raw} is measured forward transmission data directly from the network analyzer. With this technique, highly accurate values for ε_r can be obtained which are related to the resistivity of the R-card by

$$R_e = \frac{-j\eta_0}{k_0\tau(\varepsilon_r - 1)} \ [6].$$

(3.14)

Since Newton's method is highly sensitive to the initial guess, it would be much more convenient if a function of relative permittivity, resistivity by (3.14), in terms of S_{21} could be derived. Although it is impossible to create such an expression using (3.9) directly, it becomes possible when approximations are made using Maclaurin series.

3.1.2 First, Second, and Nth Order Approximations.

As stated in the previous subsection, (3.9) cannot be solved explicitly for ε_r in terms of S_{21}. However, approximate solutions can be obtained by making use of the Maclaurin series for sine and cosine. A paper written by Sarabandi and Ulaby [7] use this concept to determine the relative permittivity of foliage using the forward reflection measurement. This is the first time such an idea has been applied to material parameter extraction using the forward transmission measurement. If the value of the wave number times the thickness of the R-card is much less than one, then the first order terms from the Maclaurin series for sine and cosine,

$$\sin x \approx x$$

$$\cos x \approx 1,$$

(3.15)

can be substituted into (3.9) to form

$$S_{21}e^{-j\frac{\omega\tau}{c}} \approx \frac{2\sqrt{\varepsilon_r}}{j\varepsilon_r \frac{\omega\tau}{c}\sqrt{\varepsilon_r} + 2\sqrt{\varepsilon_r} + j\frac{\omega\tau}{c}\sqrt{\varepsilon_r}} \quad \text{(3.16)}$$

Substituting S_{21}^{raw} for S_{21} in (3.16) and simplifying produces a function of ε_r in terms of S_{21}^{meas} (3.13):

$$\varepsilon_r \approx \frac{2c - 2cS_{21}^{meas} - j\omega\tau S_{21}^{meas}}{j\omega\tau S_{21}^{meas}} \quad \text{(3.17)}$$

An expression for the resistivity of the R-card can now be obtained by substituting in (3.14) and simplifying:

$$R_e \approx \frac{\eta_0 cS_{21}^{meas}}{2c - 2cS_{21}^{meas} - j2\omega\tau S_{21}^{meas}} \quad \text{(3.18)}$$

Since the above expression is formed from only the first order terms of the Maclaurin series, (3.18) is called the first order approximation.

If in addition to the first order terms the second order terms of the Maclaurin series for sine and cosine are retained, another approximate function of resistivity in terms of S_{21}^{meas} can be obtained. The Maclaurin series for sine and cosine, retaining first and second order terms only, are

$$\sin x \approx x \quad \text{(3.19)}$$
$$\cos x \approx 1 - \frac{x^2}{2}.$$

Substituting (3.19) into (3.9) produces the following expression

$$S_{21}^{meas} \approx \frac{2\sqrt{\varepsilon_r}}{j\varepsilon_r \frac{\omega\tau}{c}\sqrt{\varepsilon_r} + 2\sqrt{\varepsilon_r} - \sqrt{\varepsilon_r}\frac{\omega^2\tau^2}{c^2}\varepsilon_r + j\frac{\omega\tau}{c}\sqrt{\varepsilon_r}} \quad \text{(3.20)}$$

After some algebraic manipulation, a function of ε_r in terms of S_{21}^{meas} can be written:

$$\varepsilon_r \approx \frac{2c^2 - 2c^2 S_{21}^{meas} - j\omega\tau c S_{21}^{meas}}{S_{21}^{meas}\left(j\omega\tau c - \omega^2\tau^2\right)}. \tag{3.21}$$

Substituting in (3.14) and simplifying results in

$$R_e \approx \frac{\eta_0 c^2 S_{21}^{meas} + j\eta_0 \omega\tau c S_{21}^{meas}}{2c^2 - 2c^2 S_{21}^{meas} - j2\omega\tau c S_{21}^{meas} + \omega^2\tau^2 S_{21}^{meas}}. \tag{3.22}$$

Like the first order approximation, (3.22) is known as the second order approximation since it makes use of the second order terms in the Maclaurin series for sine and cosine.

In general, any order approximate function can be obtained by retaining the desired order terms from the Maclaurin series for sine and cosine. Starting at third order, however, the expressions relating ε_r and S_{21}^{meas} become polynomials and are not able to be manipulated into simple functions like (3.17) and (3.21). This is not to say that higher than second order approximations are worthless. In many cases it is easier to find the roots of a polynomial, especially quadratic, cubic, or other low order polynomials, than it is to solve a transcendental equation like (3.9). For a general N order expression, the following Maclaurin series are substituted into (3.9)

$$\begin{array}{c} \sin x = \displaystyle\sum_{n=0}^{\infty} \frac{(-1)^n}{(2n+1)!} x^{2n+1} \\ \cos x = \displaystyle\sum_{n=0}^{\infty} \frac{(-1)^n}{(2n)!} x^{2n} \end{array}, \tag{3.23}$$

producing this expression after some simplification

$$\frac{2\sqrt{\varepsilon_r}}{S_{21}^{meas}} = j\varepsilon_r \sum_{n=0}^{\infty} \frac{(-1)^n}{(2n+1)!}\left(\frac{\omega\tau}{c}\right)^{2n+1}\left(\sqrt{\varepsilon_r}\right)^{2n+1}$$

$$+2\sqrt{\varepsilon_r}\sum_{n=0}^{\infty}\frac{(-1)^n}{(2n)!}\left(\frac{\omega\tau}{c}\right)^{2n}\left(\sqrt{\varepsilon_r}\right)^{2n}$$

$$+j\sum_{n=0}^{\infty}\frac{(-1)^n}{(2n+1)!}\left(\frac{\omega\tau}{c}\right)^{2n+1}\left(\sqrt{\varepsilon_r}\right)^{2n+1}$$

(3.24)

Further simplification and expansion of (3.24) results in

$$0 = 2 + \frac{j\omega\tau}{c} - \frac{2}{S_{21}^{meas}}$$

$$+\varepsilon_r\left[\frac{j\omega\tau}{c} - \frac{2}{2!}\left(\frac{\omega\tau}{c}\right)^2 - \frac{j}{3!}\left(\frac{\omega\tau}{c}\right)^3\right]$$

$$+\varepsilon_r^2\left[-\frac{j}{3!}\left(\frac{\omega\tau}{c}\right)^3 + \frac{2}{4!}\left(\frac{\omega\tau}{c}\right)^4 + \frac{j}{5!}\left(\frac{\omega\tau}{c}\right)^5\right]$$

$$+...+$$

$$\varepsilon_r^N\left[\frac{j(-1)^{N-1}}{(2N-1)!}\left(\frac{\omega\tau}{c}\right)^{2N-1} + \frac{2(-1)^N}{(2N)!}\left(\frac{\omega\tau}{c}\right)^{2N} + \frac{j(-1)^N}{(2N+1)!}\left(\frac{\omega\tau}{c}\right)^{2N+1}\right]$$

$$+...$$

(3.25)

or in summation form

$$\frac{2}{\omega\tau S_{21}^{meas}} - \frac{2}{\omega\tau} - \frac{j}{c} = \sum_{n=1}^{\infty}\frac{\varepsilon_r^n}{c^{2n+1}(2n+1)!}\left[\begin{array}{l} jc^2(2n)(2n+1)(-1)^{n-1}(\omega\tau)^{2n-2} \\ +2c(2n+1)(-1)^n(\omega\tau)^{2n-1} \\ +j(-1)^n(\omega\tau)^{2n} \end{array}\right].$$

(3.26)

The first order approximation, (3.17), comes from a combination of the terms on the right hand side of (3.25) up until the first term in the first bracketed quantity. The second order approximation, (3.21), comes from a combination of the terms on the right hand side of (3.25) up until the first two terms in the first bracketed quantity. The third order

approximation would be formed from a combination of the terms on the right hand side

of (3.25) up until the first term from the second bracketed quantity:

$$\frac{2}{S_{21}^{meas}} - 2 - \frac{j\omega\tau}{c} \approx \varepsilon_r \left[\frac{j\omega\tau}{c} - \frac{2}{2!}\left(\frac{\omega\tau}{c}\right)^2 - \frac{j}{3!}\left(\frac{\omega\tau}{c}\right)^3 \right] + \varepsilon_r^2 \left[-\frac{j}{3!}\left(\frac{\omega\tau}{c}\right)^3 \right]. \tag{3.27}$$

This pattern of order approximations continues indefinitely. Once ε_r is found, its values

can be inserted into (3.14) to determine the resistivity of the R-card.

3.1.3 Thin Sheet Approximation.

The last free-space technique presented is the thin sheet approximation. The thin

sheet approximation derives its name from the resistive boundary conditions that are used

to derive it. In *Approximate Boundary Conditions in Electromagnetics*, by Senior and

Volakis [6], the resistive boundary conditions,

$$\left[\hat{n} \times \vec{E} \right]_{-}^{+} = 0 \tag{3.28}$$

and

$$\hat{n} \times \vec{E} = R_e \hat{n} \times \left[\hat{n} \times \vec{H} \right]_{-}^{+}, \tag{3.29}$$

where $\hat{n}$ is the unit normal pointing in direction away from the R-card's surface, are

derived electromagnetically. Physically (3.28) implies that the electric field is continuous

across the R-card boundary; whereas, (3.29) states that the magnetic field is

discontinuous across the R-card boundary by the amount of electric current induced in

the resistive sheet. It is easy to visualize physically what is taking place by an equivalent

circuit theory model. Figure 3-3 shows a lumped resistor, which models the electrically-

thin R-card, in a classic parallel configuration. The voltage, which relates to the electric

field, on the either side of a parallel connection is equal; however, the current, which
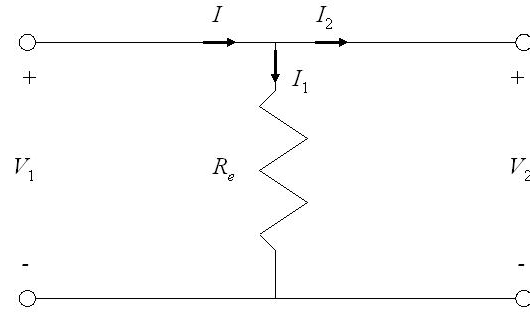
Figure 3-3. Resistive boundary conditions circuit analogy.

relates to the magnetic field, is discontinuous by the amount of current that flows through the resistor in parallel. It is in this way that (3.29) very closely resembles Ohm's Law.

To apply the resistive boundary conditions some changes need to be made to the fields expressions in (3.1):

$$\vec{E}_I = \begin{bmatrix} \hat{x} \\ \hat{y} \end{bmatrix} \left(E_I^+ e^{-jk_0 z} + E_I^- e^{jk_0 z} \right) \tag{3.30}$$

$$\vec{H}_I = \frac{\hat{k} \times \vec{E}_I}{\eta_0} = \frac{1}{\eta_0} \left(\begin{bmatrix} \hat{y} \\ -\hat{x} \end{bmatrix} E_I^+ e^{-jk_0 z} + \begin{bmatrix} -\hat{y} \\ \hat{x} \end{bmatrix} E_I^- e^{jk_0 z} \right)$$

$$\vec{E}_{III} = \begin{bmatrix} \hat{x} \\ \hat{y} \end{bmatrix} E_{III}^+ e^{-jk_0 z}$$

$$\vec{H}_{III} = \frac{\hat{k} \times \vec{E}_{III}}{\eta_0} = \frac{1}{\eta_0} \begin{bmatrix} \hat{y} \\ -\hat{x} \end{bmatrix} E_{III}^+ e^{-jk_0 z}$$

Applying (3.28) and (3.29), where $\hat{n}$ in accordance with Figure 3-2 is $-\hat{z}$, results in the following two expressions

$$E_I^+ + E_I^- = E_{III}^+ \tag{3.31}$$

$$E_I^+ + E_I^- = R_e \frac{1}{\eta_0} \left[E_I^+ - E_I^- - E_{III}^+ \right]$$

Dividing both expressions by E_I^+ and rearranging (3.31) into matrix form produces

$$\begin{bmatrix} 1 & -1 \\ 1 + \dfrac{R_e}{\eta_0} & \dfrac{R_e}{\eta_0} \end{bmatrix} \begin{bmatrix} \Gamma \\ T \end{bmatrix} = \begin{bmatrix} -1 \\ \dfrac{R_e}{\eta_0} - 1 \end{bmatrix}, \tag{3.32}$$

where

$$\Gamma = \frac{E_I^-}{E_I^+}, \quad T = \frac{E_{III}^+}{E_I^+}, \tag{3.33}$$

and in this case

$$S_{21} = T = S_{21}^{meas} = S_{21}^{raw}, \tag{3.34}$$

no phase shift required. As in the root search technique, an expression for S_{21}^{meas} can be found by inverting the 2x2 matrix,

$$A = \begin{bmatrix} a_{11} & a_{12} \\ a_{21} & a_{22} \end{bmatrix} \tag{3.35}$$

$$A^{-1} = \frac{1}{a_{11}a_{22} - a_{12}a_{21}} \begin{bmatrix} a_{22} & -a_{12} \\ -a_{21} & a_{11} \end{bmatrix},$$

in (3.32) and multiplying it by the known vector on the right hand side of the expression. After matrix multiplication and some algebra, S_{21}^{meas} equals

$$S_{21}^{meas} = \frac{2R_e}{\eta_0 + 2R_e}. \tag{3.36}$$

Solving (3.36) for R_e in terms of S_{21}^{meas} results in the following function

$$R_e = \frac{\eta_0 S_{21}^{meas}}{2 - 2S_{21}^{meas}}. \tag{3.37}$$

Expression (3.37) is known as the thin sheet approximation for the resistivity of an R-card as shown in *Radar Cross Section*, by Knott, Shaeffer, and Tuley [8]. The authors, however, do not present a derivation of the expression.
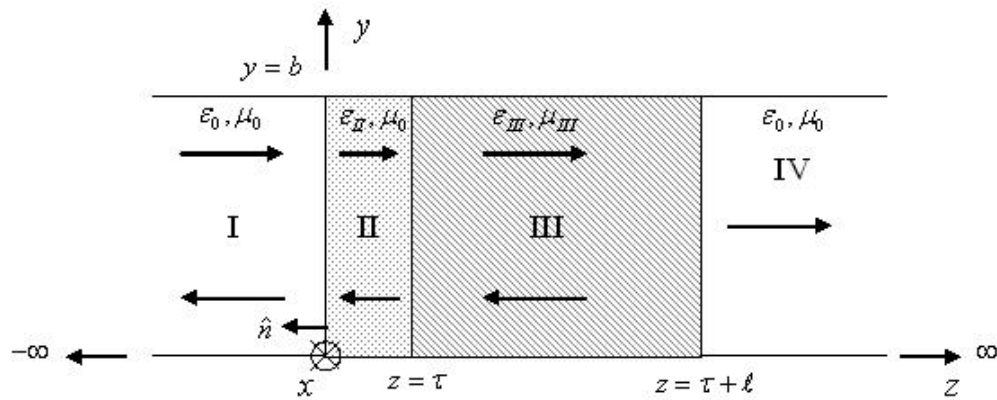
Figure 3-4. Geometry of the waveguide problem.

The value of the thin sheet approximation is its simplicity when compared to the root search and Nth order approximations. Generally it turns out to be an order 2.1 approximation in terms of accuracy, being slightly more accurate than the second order approximation. In the next section, waveguide methods will be introduced, including waveguide versions of the methods presented in this section.

3.2 Waveguide Methods

In the previous section, the root search method, the first, second, and Nth order, and the thin sheet approximations for a free-space system were introduced. In this section, waveguide versions of those methods and also a mode matching measurement technique will be derived. Figure 3-4 shows the geometry of the TE_{10}^{Z} excitation, fully-filled waveguide problem. Regions I and IV in Figure 3-4 are air filled regions and region II is the R-card region. Since R-cards are thin and cannot support themselves in a waveguide sample holder, they are typically supported by a known backing material, such as acrylic or polystyrene foam. This known support backing is represented by

region III. The fields in regions I, II, III, and IV take the form of (2.59). Enforcing the

boundary condition at the walls of the waveguide—that is, the tangential electric field

must be zero at the surface of a PEC—for all regions results in

$$\bar{E}_{I,II} = -\hat{y}\frac{\pi}{a\varepsilon_{I,II}}\sin\left(\frac{\pi}{a}x\right)\left(E_{I,II}^+ e^{-\gamma_{I,II}z} + E_{I,II}^- e^{\gamma_{I,II}z}\right) \tag{3.38}$$

$$\bar{H}_{I,II} = \hat{x}\frac{\pi}{a\varepsilon_{I,II}Z_{I,II}}\sin\left(\frac{\pi}{a}x\right)\left(E_{I,II}^+ e^{-\gamma_{I,II}z} - E_{I,II}^- e^{\gamma_{I,II}z}\right)$$

$$+\hat{z}\frac{\pi^2}{j\omega\mu_{I,II}\varepsilon_{I,II}a^2}\cos\left(\frac{\pi}{a}x\right)\left(E_{I,II}^+ e^{-\gamma_{I,II}z} + E_{I,II}^- e^{\gamma_{I,II}z}\right)$$

$$\bar{E}_{III} = -\hat{y}\frac{\pi}{a\varepsilon_{III}}\sin\left(\frac{\pi}{a}x\right)\left(E_{III}^+ e^{-\gamma_{III}(z-\tau)} + E_{III}^- e^{\gamma_{III}(z-\tau)}\right)$$

$$\bar{H}_{III} = \hat{x}\frac{\pi}{a\varepsilon_{III}Z_{III}}\sin\left(\frac{\pi}{a}x\right)\left(E_{III}^+ e^{-\gamma_{III}(z-\tau)} - E_{III}^- e^{\gamma_{III}(z-\tau)}\right)$$

$$+\hat{z}\frac{\pi^2}{j\omega\mu_{III}\varepsilon_{III}a^2}\cos\left(\frac{\pi}{a}x\right)\left(E_{III}^+ e^{-\gamma_{III}(z-\tau)} + E_{III}^- e^{\gamma_{III}(z-\tau)}\right)$$

$$\bar{E}_{IV} = -\hat{y}\frac{\pi}{a\varepsilon_{IV}}\sin\left(\frac{\pi}{a}x\right)E_{IV}^+ e^{-\gamma_{IV}(z-\tau-\ell)}$$

$$\bar{H}_{IV} = \left[\hat{x}\frac{\pi}{a\varepsilon_{IV}Z_{IV}}\sin\left(\frac{\pi}{a}x\right) + \hat{z}\frac{\pi^2}{j\omega\mu_{IV}\varepsilon_{IV}a^2}\cos\left(\frac{\pi}{a}x\right)\right]E_{IV}^+ e^{-\gamma_{IV}(z-\tau-\ell)},$$

where

$$k_x = \frac{\pi}{a} \tag{3.39}$$

$$k_y = 0$$

$$\varepsilon_I = \varepsilon_{IV} = \varepsilon_0$$

$$\mu_I = \mu_{II} = \mu_{IV} = \mu_0$$

$$Z_{I,II,III,IV} = \frac{j\omega\mu_{I,II,III,IV}}{\gamma_{I,II,III,IV}}$$

$$\gamma_{I,II,III,IV} = jk_{zI,II,III,IV} = \sqrt{\left(\frac{\pi}{a}\right)^2 - \omega^2\varepsilon_{I,II,III,IV}\mu_{I,II,III,IV}}$$

and a is the dimension of the waveguide in the x direction [5]. The forward transmission

coefficient, S_{21}, is found by dividing the electric field expression in region IV by the

forward traveling electric field expression in region I:

$$S_{21} = \frac{\bar{E}_{IV}}{\bar{E}_I^+} = \frac{E_{IV}^+}{E_I^+} e^{\gamma_0(\tau+\ell)} . \tag{3.40}$$

Finding an expression for the ratio in (3.40) will be the purpose of the next several

subsections.

3.2.1 Root Search Method.

Enforcing the continuity of tangential fields at $z = 0$, $z = \tau$, and $z = \tau + \ell$, results

in the following expressions

$$
\begin{aligned}
&\frac{1}{\varepsilon_I}\left(E_I^+ + E_I^-\right) = \frac{1}{\varepsilon_{II}}\left(E_{II}^+ + E_{II}^-\right) \\
&\frac{1}{\varepsilon_I Z_I}\left(E_I^+ - E_I^-\right) = \frac{1}{\varepsilon_{II} Z_{II}}\left(E_{II}^+ - E_{II}^-\right) \\
&\frac{1}{\varepsilon_{II}}\left(E_{II}^+ e^{-\gamma_{II}\tau} + E_{II}^- e^{\gamma_{II}\tau}\right) = \frac{1}{\varepsilon_{III}}\left(E_{III}^+ + E_{III}^-\right) \\
&\frac{1}{\varepsilon_{II} Z_{II}}\left(E_{II}^+ e^{-\gamma_{II}\tau} - E_{II}^- e^{\gamma_{II}\tau}\right) = \frac{1}{\varepsilon_{III} Z_{III}}\left(E_{III}^+ - E_{III}^-\right) \\
&\frac{1}{\varepsilon_{III}}\left(E_{III}^+ e^{-\gamma_{III}\ell} + E_{III}^- e^{\gamma_{III}\ell}\right) = \frac{1}{\varepsilon_{IV}} E_{IV}^+ \\
&\frac{1}{\varepsilon_{III} Z_{III}}\left(E_{III}^+ e^{-\gamma_{III}\ell} - E_{III}^- e^{\gamma_{III}\ell}\right) = \frac{1}{\varepsilon_{IV} Z_{IV}} E_{IV}^+
\end{aligned}
\tag{3.41}
$$

Dividing each expression by E_I^+ and rearranging (3.41) into matrix form produces

$$
\begin{bmatrix}
\dfrac{1}{\varepsilon_I} & \dfrac{-1}{\varepsilon_{II}} & \dfrac{-1}{\varepsilon_{II}} & 0 & 0 & 0 \\[2mm]
\dfrac{-1}{\varepsilon_I Z_I} & \dfrac{-1}{\varepsilon_{II} Z_{II}} & \dfrac{1}{\varepsilon_{II} Z_{II}} & 0 & 0 & 0 \\[2mm]
0 & \dfrac{e^{-\gamma_{II}\tau}}{\varepsilon_{II}} & \dfrac{e^{\gamma_{II}\tau}}{\varepsilon_{II}} & \dfrac{-1}{\varepsilon_{III}} & \dfrac{-1}{\varepsilon_{III}} & 0 \\[2mm]
0 & \dfrac{e^{-\gamma_{II}\tau}}{\varepsilon_{II} Z_{II}} & \dfrac{-e^{\gamma_{II}\tau}}{\varepsilon_{II} Z_{II}} & \dfrac{-1}{\varepsilon_{III} Z_{III}} & \dfrac{1}{\varepsilon_{III} Z_{III}} & 0 \\[2mm]
0 & 0 & 0 & \dfrac{e^{-\gamma_{III}\ell}}{\varepsilon_{III}} & \dfrac{e^{\gamma_{III}\ell}}{\varepsilon_{III}} & \dfrac{-1}{\varepsilon_{IV}} \\[2mm]
0 & 0 & 0 & \dfrac{e^{-\gamma_{III}\ell}}{\varepsilon_{III} Z_{III}} & \dfrac{-e^{\gamma_{III}\ell}}{\varepsilon_{III} Z_{III}} & \dfrac{-1}{\varepsilon_{IV} Z_{IV}}
\end{bmatrix}
\begin{bmatrix}
\Gamma \\ t_1 \\ r_1 \\ t_2 \\ r_2 \\ T
\end{bmatrix}
=
\begin{bmatrix}
\dfrac{-1}{\varepsilon_I} \\[2mm] \dfrac{-1}{\varepsilon_I Z_I} \\[2mm] 0 \\ 0 \\ 0 \\ 0
\end{bmatrix}.
\tag{3.42}
$$

After performing Gaussian elimination to transform the 6x6 matrix to the identity matrix in (3.42) and taking into account the expressions in (3.39), S_{21} equals

$$
S_{21} = \frac{8 Z_0 Z_{II} Z_{III}}{e^{\gamma_{III}\ell}\left(Z_{III}+Z_0\right)Y^+ + e^{-\gamma_{III}\ell}\left(Z_0 - Z_{III}\right)Y^-}\, e^{\gamma_0(\tau+\ell)},
\tag{3.43}
$$

where

$$
Y^{\pm} = 2 Z_{II} Z_{III}\cos k_{zII}\tau \pm 2 j Z_{II}^2 \sin k_{zII}\tau + 2 j Z_0 Z_{III}\sin k_{zII}\tau \pm 2 Z_0 Z_{II}\cos k_{zII}\tau.
\tag{3.44}
$$

It is not possible to analytically solve (3.43) for the relative permittivity of the R-card in terms of the forward transmission coefficient; therefore, (3.43) must be solved numerically by a root search routine. Very similar to the free-space system, S_{21}^{thy} and S_{21}^{meas} become

$$
S_{21}^{thy} = S_{21}e^{-\gamma_0(\tau+\ell)}
\tag{3.45}
$$
$$
S_{21}^{meas} = S_{21}^{raw}e^{-\gamma_0(\tau+\ell)}
$$

and values of ε_r are iterated until (3.11) is satisfied to within a specified tolerance. Once the R-card's ε_r values have been solved for, (3.14) can be used to obtain the resistivity.

It would be much easier if expressions could be derived from (3.43) that take forward transmission data as an input and output the relative permittivity without having to worry about an initial guess or precision. In the next subsection, expressions that do exactly that will be derived.

3.2.2 First, Second, and Nth Order Approximations.

In the previous subsection, the exact solution, (3.43), for the forward transmission coefficient was derived. As in the free-space techniques, if the first order or second order terms from the Maclaurin series are substituted in for the sine and cosine expressions in (3.43), an approximate function of relative permittivity in terms of measured S_{21} can be obtained. The first order approximations for sine and cosine are shown in (3.15). Substituting (3.15) into (3.43) and (3.44) results in

$$S_{21}^{meas} \approx \frac{8 Z_0 Z_{III} \omega \eta_0}{e^{\gamma_{III}\ell}\left(Z_{III} + Z_0\right) Y^+ + e^{-\gamma_{III}\ell}\left(Z_0 - Z_{III}\right) Y^-} \tag{3.46}$$

$$Y^\pm \approx 2 Z_{III} \omega \eta_0 \pm 2j \frac{\omega^2 \eta_0^2 \tau}{c} + 2 j Z_0 Z_{III} c k_{z\,II}^2 \tau \pm 2 Z_0 \omega \eta_0$$

Rearranging (3.46) and substituting in the equivalent expression for $k_{z\,II}$ (3.39) produces

$$\frac{4 Z_0 Z_{III} \omega \eta_0}{S_{21}^{meas}} \approx Z_{III} \omega \eta_0 e^{\gamma_{III}\ell}\left(Z_{III} + Z_0\right) + j \frac{\omega^2 \eta_0^2 \tau}{c} e^{\gamma_{III}\ell}\left(Z_{III} + Z_0\right) \tag{3.47}$$

$$+ j Z_0 Z_{III} c \tau \frac{\pi^2}{a^2 c^2}\left(4a^2 f^2 \varepsilon_r - c^2\right) e^{\gamma_{III}\ell}\left(Z_{III} + Z_0\right)$$

$$+ Z_0 \omega \eta_0 e^{\gamma_{III}\ell}\left(Z_{III} + Z_0\right)$$

$$+ Z_{III} \omega \eta_0 e^{-\gamma_{III}\ell}\left(Z_0 - Z_{III}\right) - j \frac{\omega^2 \eta_0^2 \tau}{c} e^{-\gamma_{III}\ell}\left(Z_0 - Z_{III}\right)$$

$$+ j Z_0 Z_{III} c \tau \frac{\pi^2}{a^2 c^2}\left(4a^2 f^2 \varepsilon_r - c^2\right) e^{-\gamma_{III}\ell}\left(Z_0 - Z_{III}\right)$$

$$- Z_0 \omega \eta_0 e^{-\gamma_{III}\ell}\left(Z_0 - Z_{III}\right)$$

Solving (3.47) for ε_r produces the following approximate function

$$\varepsilon_r \approx A\left(\frac{\Omega_6}{S_{21}^{meas}}\right) + A\left[\Psi_1\left(-\Omega_4 - \Omega_5 + \Omega_3 - \Omega_2\right)\right] + A\left[\Psi_2\left(-\Omega_4 + \Omega_5 + \Omega_3 + \Omega_2\right)\right], \tag{3.48}$$

where

$$A = \frac{1}{\Omega_1\Psi_1 + \Omega_1\Psi_2} \tag{3.49}$$

$$\Psi_1 = e^{\gamma_{III}\ell}(Z_0 + Z_{III}), \ \Psi_2 = e^{-\gamma_{III}\ell}(Z_0 - Z_{III})$$

$$\Omega_1 = jZ_0 Z_{III}\frac{\omega^2\tau}{c}, \ \Omega_2 = Z_0\omega\eta_0, \ \Omega_3 = jZ_0 Z_{III}\frac{\pi^2\tau c}{a^2}$$

$$\Omega_4 = Z_{III}\omega\eta_0, \ \Omega_5 = j\frac{\omega^2\eta_0^2\tau}{c}, \ \Omega_6 = 4Z_0 Z_{III}\omega\eta_0$$

The resistivity of the R-card can now be found by using (3.14). This expression is known as the first order approximation because it uses only the first order terms of the Maclaurin series for sine and cosine.

Exactly like the free-space case, if in addition to the first order terms the second order terms are retained, a more accurate approximate function can be derived. Expanding the denominator in (3.43) to second order terms produces

$$S_{21}^{meas} \approx \frac{8Z_0 Z_{III}\omega\eta_0}{e^{\gamma_{III}\ell}(Z_{III} + Z_0)Y^+ + e^{-\gamma_{III}\ell}(Z_0 - Z_{III})Y^-} \tag{3.50}$$

$$Y^\pm \approx 2Z_{III}\omega\eta_0\left(1 - \frac{1}{2}k_{zII}^2\tau^2\right) \pm 2j\frac{\omega^2\eta_0^2\tau}{c} + 2jZ_0 Z_{III}ck_{zII}^2\tau \pm 2Z_0\omega\eta_0\left(1 - \frac{1}{2}k_{zII}^2\tau^2\right)$$

Rearranging (3.50) and substituting in the equivalent expression for k_{zII} (3.39) results in

$$\frac{8Z_0 Z_{III}\omega\eta_0}{S_{21}^{meas}} \approx 2Z_{III}\omega\eta_0 e^{\gamma_{III}\ell}\left(Z_{III}+Z_0\right) + 2j\frac{\omega^2\eta_0^2\tau}{c}e^{\gamma_{III}\ell}\left(Z_{III}+Z_0\right) \tag{3.51}$$

$$+2Z_{III}\omega\eta_0 e^{-\gamma_{III}\ell}\left(Z_0-Z_{III}\right) - 2j\frac{\omega^2\eta_0^2\tau}{c}e^{-\gamma_{III}\ell}\left(Z_0-Z_{III}\right)$$

$$-Z_{III}\omega\eta_0\frac{\pi^2\tau^2}{a^2c^2}\left(4a^2f^2\varepsilon_r-c^2\right)e^{\gamma_{III}\ell}\left(Z_{III}+Z_0\right)$$

$$-Z_{III}\omega\eta_0\frac{\pi^2}{a^2c^2}\left(4a^2f^2\varepsilon_r-c^2\right)e^{-\gamma_{III}\ell}\left(Z_0-Z_{III}\right)$$

$$+2jZ_0Z_{III}c\tau\frac{\pi^2}{a^2c^2}\left(4a^2f^2\varepsilon_r-c^2\right)e^{\gamma_{III}\ell}\left(Z_{III}+Z_0\right)$$

$$+2jZ_0Z_{III}c\tau\frac{\pi^2}{a^2c^2}\left(4a^2f^2\varepsilon_r-c^2\right)e^{-\gamma_{III}\ell}\left(Z_0-Z_{III}\right)$$

$$-Z_0\omega\eta_0\frac{\pi^2}{a^2c^2}\left(4a^2f^2\varepsilon_r-c^2\right)e^{\gamma_{III}\ell}\left(Z_{III}+Z_0\right)$$

$$+Z_0\omega\eta_0\frac{\pi^2}{a^2c^2}\left(4a^2f^2\varepsilon_r-c^2\right)e^{-\gamma_{III}\ell}\left(Z_0-Z_{III}\right)$$

$$+2Z_0\omega\eta_0 e^{\gamma_{III}\ell}\left(Z_{III}+Z_0\right) - 2Z_0\omega\eta_0 e^{-\gamma_{III}\ell}\left(Z_0-Z_{III}\right) \quad .$$

Solving for ε_r brings about the following approximate function

$$\varepsilon_r \approx A\left(\frac{\Omega_4}{S_{21}^{meas}}\right) + A\left[\Psi_1\left(-\Omega_5-\Omega_6-\Omega_7-\Omega_8+\Omega_9-\Omega_{10}\right)\right] \tag{3.52}$$
$$+A\left[\Psi_2\left(-\Omega_5+\Omega_6+\Omega_7-\Omega_8+\Omega_9+\Omega_{10}\right)\right]$$,

where

$$A=\frac{1}{\Psi_1\left(-\Omega_1+\Omega_2-\Omega_3\right)+\Psi_2\left(-\Omega_1+\Omega_2+\Omega_3\right)} \tag{3.53}$$

$$\Psi_1 = e^{\gamma_{III}\ell}\left(Z_0+Z_{III}\right),\ \Psi_2 = e^{-\gamma_{III}\ell}\left(Z_0-Z_{III}\right)$$

$$\Omega_1 = Z_{III}\eta_0\frac{\omega^3\tau^2}{c^2},\ \Omega_2 = 2jZ_0Z_{III}\frac{\omega^3\tau}{c},\ \Omega_3 = Z_0\eta_0\frac{\omega^3\tau^2}{c^2},\ \Omega_4 = 8Z_0Z_{III}\omega\eta_0\ .$$

$$\Omega_5 = 2Z_{III}\omega\eta_0,\ \Omega_6 = 2j\frac{\omega^2\eta_0^2\tau}{c},\ \Omega_7 = 2Z_0\omega\eta_0,\ \Omega_8 = Z_{III}\omega\eta_0\frac{\pi^2\tau^2}{a^2}$$

$$\Omega_9 = 2jZ_0Z_{III}\frac{\pi^2\tau c}{a^2},\ \Omega_{10} = Z_0\omega\eta_0\frac{\pi^2\tau^2}{a^2}$$

Once ε_r has been obtained using (3.52), the resistivity of the R-card can be found by using (3.14). Expression (3.52) is known as the second order approximation because it uses the second order terms from the Maclaurin series for sine and cosine.

By retaining higher order terms from the Maclaurin series for sine and cosine, a general Nth order waveguide approximation can be derived. Once again, polynomial expressions involving ε_r are the result. Substituting the Maclaurin series for sine and cosine, (3.23), into (3.43) and (3.44) and simplifying produces

$$0 = \Omega_1\left(\Psi_1 + \Psi_2\right) + \tau\Omega_2\left(\Psi_1 - \Psi_2\right) + \Omega_4\left(\Psi_1 - \Psi_2\right) - \frac{4Z_0 Z_{III}\omega\eta_0}{S_{21}^{meas}} \tag{3.54}$$

$$+ k_{zII}^2\left[\tau\Omega_3\left(\Psi_1 + \Psi_2\right) - \frac{\tau^2}{2!}\Omega_1\left(\Psi_1 + \Psi_2\right) - \frac{\tau^2}{2!}\Omega_4\left(\Psi_1 - \Psi_2\right) - \frac{\tau^3}{3!}\Omega_2\left(\Psi_1 - \Psi_2\right)\right]$$

$$+ k_{zII}^4\left[\frac{-\tau}{3!}\Omega_3\left(\Psi_1 + \Psi_2\right) + \frac{\tau^4}{4!}\Omega_1\left(\Psi_1 + \Psi_2\right) + \frac{\tau^4}{4!}\Omega_4\left(\Psi_1 - \Psi_2\right) + \frac{\tau^5}{5!}\Omega_2\left(\Psi_1 - \Psi_2\right)\right],$$

$$+ ... + k_{zII}^{2n}\left[\begin{array}{l}\dfrac{(-1)^{n-1}\,\tau^{2n-1}}{(2n-1)!}\Omega_3\left(\Psi_1 + \Psi_2\right) + \dfrac{(-1)^n\,\tau^{2n}}{(2n)!}\Omega_1\left(\Psi_1 + \Psi_2\right) \\[2mm] + \dfrac{(-1)^n\,\tau^{2n}}{(2n)!}\Omega_4\left(\Psi_1 - \Psi_2\right) + \dfrac{(-1)^n\,\tau^{2n+1}}{(2n+1)!}\Omega_2\left(\Psi_1 - \Psi_2\right)\end{array}\right] + ...$$

where

$$\Psi_1 = e^{\gamma_{III}\ell}\left(Z_0 + Z_{III}\right), \quad \Psi_2 = e^{-\gamma_{III}\ell}\left(Z_0 - Z_{III}\right) \tag{3.55}$$

$$\Omega_1 = \omega\eta_0 Z_{III}, \quad \Omega_2 = j\frac{\omega^2\eta_0^2}{c}, \quad \Omega_3 = jcZ_0 Z_{III}, \quad \Omega_4 = \omega\eta_0 Z_0$$

and k_{zII} is

$$k_{zII} = \frac{\pi}{ac}\sqrt{4a^2 f^2 \varepsilon_r - c^2}\ . \tag{3.56}$$

The first order approximation, (3.48), is formed from a combination of the terms on the right hand side of (3.54) up until the first term in the first bracketed expression. The

second order approximation, (3.52), is formed from a combination of the terms on the

right hand side of (3.54) up until the first three terms in the first bracketed expression.

The third order approximation is a combination of the terms on the right hand side of

(3.54) up until the first term from the second bracketed expression:

$$
\begin{aligned}
0 \approx{} & \Omega_1\left(\Psi_1 + \Psi_2\right) + \tau\Omega_2\left(\Psi_1 - \Psi_2\right) + \Omega_4\left(\Psi_1 - \Psi_2\right) - \frac{4Z_0 Z_{III}\omega\eta_0}{S_{21}^{meas}} \\
& + k_{z\,II}^2 \left[
\begin{aligned}
& \tau\Omega_3\left(\Psi_1 + \Psi_2\right) - \frac{\tau^2}{2!}\Omega_1\left(\Psi_1 + \Psi_2\right) \\
& - \frac{\tau^2}{2!}\Omega_4\left(\Psi_1 - \Psi_2\right) - \frac{\tau^3}{3!}\Omega_2\left(\Psi_1 - \Psi_2\right)
\end{aligned}
\right] \\
& + k_{z\,II}^4 \left[\frac{-\tau^3}{3!}\Omega_3\left(\Psi_1 + \Psi_2\right)\right]
\end{aligned}
\tag{3.57}
$$

This pattern continues indefinitely. Once $k_{z\,II}$ has been found, (3.56) can be used to get

ε_r , which is related to resistivity by (3.14).

3.2.3 Thin Sheet Approximation.

There are many similarities between the waveguide thin sheet approximation and

the free-space thin sheet approximation. Like the free-space thin sheet approximation,

the fields in region II, (3.38), can be neglected since the R-card is assumed to be very

thin. Taking this into account, the expressions for the fields become

$$
\begin{aligned}
\bar{E}_{I,III} ={} & -\hat{y}\,\frac{\pi}{a\varepsilon_{I,III}}\sin\left(\frac{\pi}{a}x\right)\left(E_{I,III}^+ e^{-\gamma_{I,III}z} + E_{I,III}^- e^{\gamma_{I,III}z}\right) \\
\bar{H}_{I,III} ={} & \hat{x}\,\frac{\pi}{a\varepsilon_{I,III}Z_{I,III}}\sin\left(\frac{\pi}{a}x\right)\left(E_{I,III}^+ e^{-\gamma_{I,III}z} - E_{I,III}^- e^{\gamma_{I,III}z}\right) \\
& + \hat{z}\,\frac{\pi^2}{j\omega\mu_{I,III}\varepsilon_{I,III}a^2}\cos\left(\frac{\pi}{a}x\right)\left(E_{I,III}^+ e^{-\gamma_{I,III}z} + E_{I,III}^- e^{\gamma_{I,III}z}\right)
\end{aligned}
\tag{3.58}
$$

$$\bar{E}_{IV} = -\hat{y}\,\frac{\pi}{a\varepsilon_{IV}}\sin\left(\frac{\pi}{a}x\right)E_{IV}^{+}e^{-\gamma_{IV}(z-\ell)}$$

$$\bar{H}_{IV} = \left[\hat{x}\,\frac{\pi}{a\varepsilon_{IV}Z_{IV}}\sin\left(\frac{\pi}{a}x\right) + \hat{z}\,\frac{\pi^{2}}{j\omega\mu_{IV}\varepsilon_{IV}a^{2}}\cos\left(\frac{\pi}{a}x\right)\right]E_{IV}^{+}e^{-\gamma_{IV}(z-\ell)}$$

Enforcing (3.28) and (3.29) at $z = 0$ and the continuity of tangential fields at $z = \ell$

results in the following equations

$$\frac{1}{\varepsilon_{I}}\left(E_{I}^{+} + E_{I}^{-}\right) = \frac{1}{\varepsilon_{III}}\left(E_{III}^{+} + E_{III}^{-}\right) \tag{3.59}$$

$$\frac{1}{\varepsilon_{I}}\left(E_{I}^{+} + E_{I}^{-}\right) = R_{e}\left(\frac{1}{\varepsilon_{I}Z_{I}}E_{I}^{+} - \frac{1}{\varepsilon_{I}Z_{I}}E_{I}^{-} - \frac{1}{\varepsilon_{III}Z_{III}}E_{III}^{+} + \frac{1}{\varepsilon_{III}Z_{III}}E_{III}^{-}\right)$$

$$\frac{1}{\varepsilon_{III}}\left(E_{III}^{+}e^{-\gamma_{III}\ell} + E_{III}^{-}e^{\gamma_{III}\ell}\right) = \frac{1}{\varepsilon_{IV}}E_{IV}^{+}$$

$$\frac{1}{\varepsilon_{III}Z_{III}}\left(E_{III}^{+}e^{-\gamma_{III}\ell} - E_{III}^{-}e^{\gamma_{III}\ell}\right) = \frac{1}{\varepsilon_{IV}Z_{IV}}E_{IV}^{+}$$

Dividing each equation by E_{I}^{+} and rearranging (3.59) into matrix form produces

$$\begin{bmatrix} \dfrac{1}{\varepsilon_{I}} & \dfrac{-1}{\varepsilon_{III}} & \dfrac{-1}{\varepsilon_{III}} & 0 \\[2mm] \dfrac{1}{\varepsilon_{I}} + \dfrac{R_{e}}{\varepsilon_{I}Z_{I}} & \dfrac{R_{e}}{\varepsilon_{III}Z_{III}} & \dfrac{-R_{e}}{\varepsilon_{III}Z_{III}} & 0 \\[2mm] 0 & \dfrac{e^{-\gamma_{III}\ell}}{\varepsilon_{III}} & \dfrac{e^{\gamma_{III}\ell}}{\varepsilon_{III}} & \dfrac{-1}{\varepsilon_{IV}} \\[2mm] 0 & \dfrac{e^{-\gamma_{III}\ell}}{\varepsilon_{III}Z_{III}} & \dfrac{-e^{\gamma_{III}\ell}}{\varepsilon_{III}Z_{III}} & \dfrac{-1}{\varepsilon_{IV}Z_{IV}} \end{bmatrix} \begin{bmatrix} \Gamma \\ t \\ r \\ T \end{bmatrix} = \begin{bmatrix} \dfrac{-1}{\varepsilon_{I}} \\[2mm] \dfrac{R_{e}}{\varepsilon_{I}Z_{I}} - \dfrac{1}{\varepsilon_{I}} \\[2mm] 0 \\[2mm] 0 \end{bmatrix}, \tag{3.60}$$

where S_{21}, the electric field in region IV divided by the forward traveling electric field in

region I, equals

$$S_{21} = \frac{\bar{E}_{IV}}{\bar{E}_{I}^{+}} = \frac{E_{IV}^{+}}{E_{I}^{+}}e^{\gamma_{0}\ell} = Te^{\gamma_{0}\ell} \tag{3.61}$$

$$S_{21}^{meas} = S_{21}^{raw}e^{-\gamma_{0}\ell}$$

Inverting the matrix in (3.60), multiplying it by the known vector on the right hand side

of the expression, and simplifying results in the following relation for S_{21}^{meas}

$$S_{21}^{meas} = \frac{2R_e Z_0 Z_{III}}{R_e \Psi_1 + \Psi_2},$$

(3.62)

where

$$\Psi_1 = jZ_{III}^2 \sin k_{zIII}\ell + 2Z_0 Z_{III} \cos k_{zIII}\ell + jZ_0^2 \sin k_{zIII}\ell$$
$$\Psi_2 = jZ_0 Z_{III}^2 \sin k_{zIII}\ell + Z_0^2 Z_{III} \cos k_{zIII}\ell$$

(3.63)

Solving (3.62) for the resistivity of the R-card results in the following expression

$$R_e = \frac{S_{21}^{meas}\Psi_2}{2Z_0 Z_{III} - S_{21}^{meas}\Psi_1}.$$

(3.64)

Expression (3.64) is the waveguide thin sheet approximation. Just like the free-space thin

sheet approximation, the waveguide version is slightly more accurate than the second

order waveguide approximation.

The waveguide methods that were introduced take advantage of the sample fully

filling the waveguide. This certainly makes the math easier, but has the drawback that

the R-card is being measured along its most diminutive dimension. Since the R-card is so

thin, its resistivity values are extremely sensitive and depend highly on accurate relative

permittivity values for its support backing. With no free-space measurements available

to verify waveguide data, ensuring accurate resistivity values with just waveguide

methods alone could be a problem. If, however, the R-card sample is rotated 90 degrees

in the holder and measured along its largest dimension, more stable resistivity values

should result. In the next section, an expression for the resistivity of an R-card will be

derived with this waveguide geometry.

3.2.4 Vertical Mode Matching Technique.

The method derived in this subsection will be the vertical mode matching technique. In this technique a root search, similar to the ones introduced previously, will be used to solve for the relative permittivity of the R-card. Similar work was done by Bogle [9] in his thesis, "Electromagnetic Material Characterization Using a Partially Filled Rectangular Waveguide." In his work, he derives a method for extracting the material parameters of a substance when it does not uniformly fill the waveguide holder. His derivation, however, assumes that the sample is placed exactly in the center of the waveguide holder. In the derivation to follow, no such assumption will be made. Figures 3-5 and 3-6 show the geometry of the problem. Since the sample being measured does not uniformly fill the waveguide, higher order *TE* modes, in addition to the TE_{10} mode, will be generated. These higher order modes will take the form of TE_{m0} because the geometry shown Figures 3-5 and 3-6 has no variation in the *y* direction. Equation (2.62) gives the general expression for the cut-off frequency. Substituting in (2.14), making use of the expressions in (3.39), and noting that the fields generated in the waveguide will be TE_{m0} modes, (2.62) becomes

$$\omega_{c,m} = \frac{m\pi}{a\sqrt{\mu\varepsilon}} \; .$$

(3.65)

In this thesis, an X-band waveguide, $a = 2.286 \text{ cm}$, was used; therefore, the first two cut-off frequencies corresponding to the first two modes generated in an air filled waveguide are
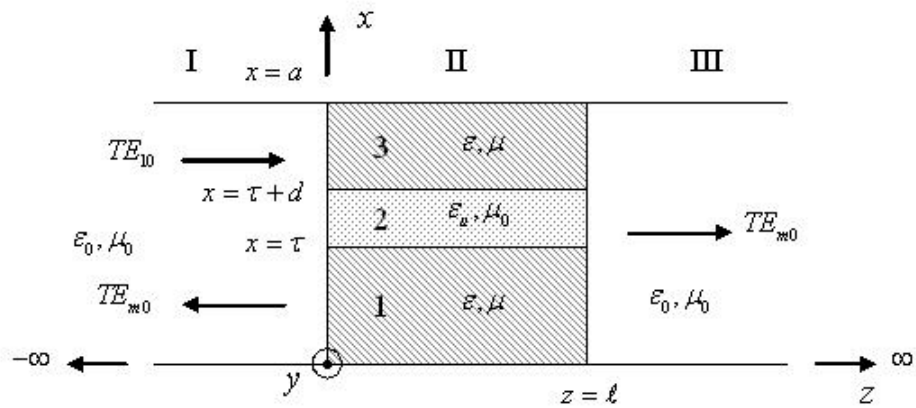
Figure 3-5. Cross sectional view of the vertical mode matching technique.
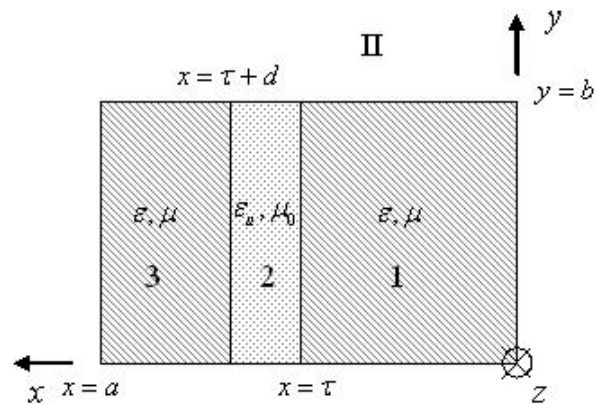
Figure 3-6. View of the vertical mode matching technique looking down the waveguide.

$$
\left.\begin{aligned}
\omega_{c,1} &\approx 41.2 \text{ rad} \cdot \text{GHz} \\
f_{c,1} &\approx 6.557 \text{ GHz}
\end{aligned}\right\} \Rightarrow TE_{10}
\tag{3.66}
$$

$$
\left.\begin{aligned}
\omega_{c,2} &\approx 82.4 \text{ rad} \cdot \text{GHz} \\
f_{c,2} &\approx 13.114 \text{ GHz}
\end{aligned}\right\} \Rightarrow TE_{20}
$$

The frequency range at which the R-cards were measured in the waveguide system was

8.2 GHz to 12.4 GHz. This means that only the TE_{10} mode will propagate. All other

modes generated by the non-uniformly filled sample will be highly evanescent and will not make it to the detector to be measured. These modes however must be accounted for since they are generated from the power of the incident TE_{10} mode and no power is added to the system. To an observer not taking into account the existence of these modes, the forward transmission coefficient would appear to be lower in magnitude than it should be.

The fields in region I and III of Figure 3-5 are of the same form as the uniformly filled fields shown in (3.38) with the exception that higher order modes are generated. Taking this into account, the fields in region I and III are of the form

$$\vec{E}_I = -\hat{y}\frac{\pi}{a\varepsilon_0}\sin\left(\frac{\pi}{a}x\right)A_1^+ e^{-\gamma_{0,1}z} - \hat{y}\sum_{m=1}^{\infty}\frac{m\pi}{a\varepsilon_0}\sin\left(\frac{m\pi}{a}x\right)A_m^- e^{\gamma_{0,m}z} \tag{3.67}$$

$$\vec{H}_I = \hat{x}\left[\frac{\pi}{a\varepsilon_0 Z_{0,1}}\sin\left(\frac{\pi}{a}x\right)A_1^+ e^{-\gamma_{0,1}z} - \sum_{m=1}^{\infty}\frac{m\pi}{a\varepsilon_0 Z_{0,m}}\sin\left(\frac{m\pi}{a}x\right)A_m^- e^{\gamma_{0,m}z}\right]$$

$$+\hat{z}\left[\frac{\pi^2}{j\omega\mu_0\varepsilon_0 a^2}\cos\left(\frac{\pi}{a}x\right)A_1^+ e^{-\gamma_{0,1}z} + \sum_{m=1}^{\infty}\frac{m^2\pi^2}{j\omega\mu_0\varepsilon_0 a^2}\cos\left(\frac{m\pi}{a}x\right)A_m^- e^{\gamma_{0,m}z}\right].$$

$$\vec{E}_{III} = -\hat{y}\sum_{m=1}^{\infty}\frac{m\pi}{a\varepsilon_0}\sin\left(\frac{m\pi}{a}x\right)C_m^+ e^{-\gamma_{0,m}(z-\ell)}$$

$$\vec{H}_{III} = \hat{x}\sum_{m=1}^{\infty}\frac{m\pi}{a\varepsilon_0 Z_{0,m}}\sin\left(\frac{m\pi}{a}x\right)C_m^+ e^{-\gamma_{0,m}(z-\ell)}$$

$$+\hat{z}\sum_{m=1}^{\infty}\frac{m^2\pi^2}{j\omega\mu_0\varepsilon_0 a^2}\cos\left(\frac{m\pi}{a}x\right)C_m^+ e^{-\gamma_{0,m}(z-\ell)}$$

In region II of Figure 3-5, there are three subregions. Subregions 1 and 3 are the same material, but may not necessarily have the same physical dimension in the x direction. Subregion 2 is the unknown, non-magnetic R-card. To get expressions for the fields in region II of Figure 3-5, the electric vector potential must be used. Note that since each subregion of region II is different in some way, it will have its own electric vector

potential expression. The expressions for the electric vector potentials of subregions 1, 2, and 3 are

$$\overset{1}{F}_{z,m} = \frac{\varepsilon}{k_{x,m}} \left[\overset{1}{E}_m \cos k_{x,m} x + \overset{1}{F}_m \sin k_{x,m} x \right] \left(B_m^+ e^{-\gamma_m z} + B_m^- e^{\gamma_m z} \right) \tag{3.68}$$

$$\overset{2}{F}_{z,m} = \frac{\varepsilon_u}{k_{xu,m}} \left[\overset{2}{E}_m \cos k_{xu,m} (x-\tau) + \overset{2}{F}_m \sin k_{xu,m} (x-\tau) \right] \left(B_m^+ e^{-\gamma_m z} + B_m^- e^{\gamma_m z} \right).$$

$$\overset{3}{F}_{z,m} = \frac{\varepsilon}{k_{x,m}} \left[\overset{3}{E}_m \cos k_{x,m} (a-x) + \overset{3}{F}_m \sin k_{x,m} (a-x) \right] \left(B_m^+ e^{-\gamma_m z} + B_m^- e^{\gamma_m z} \right)$$

Constants were placed in front of the expressions in (3.68), which differ from the electric vector potential expression shown in (2.57), to simplify the expressions of the fields. The wave numbers in the x direction in region II are unknown and are not equal to the k_x shown in (3.39) or (3.67). Since expressions for the electric vector potentials for subregions 1, 2, and 3 have been found, (2.48) can be used to find expressions for the fields in each subregion:

$$\overset{1}{\bar{E}} = -\hat{y} \left[\overset{1}{E}_m \sin k_{x,m} x - \overset{1}{F}_m \cos k_{x,m} x \right] \left(B_m^+ e^{-\gamma_m z} + B_m^- e^{\gamma_m z} \right) \tag{3.69}$$

$$\overset{1}{\bar{H}} = \hat{x} \frac{1}{Z_m} \left[\overset{1}{E}_m \sin k_{x,m} x - \overset{1}{F}_m \cos k_{x,m} x \right] \left(B_m^+ e^{-\gamma_m z} - B_m^- e^{\gamma_m z} \right)$$

$$+ \hat{z} \frac{k_{x,m}}{j\omega\mu} \left[\overset{1}{E}_m \cos k_{x,m} x + \overset{1}{F}_m \sin k_{x,m} x \right] \left(B_m^+ e^{-\gamma_m z} + B_m^- e^{\gamma_m z} \right)$$

$$\overset{2}{\bar{E}} = -\hat{y} \left[\overset{2}{E}_m \sin k_{xu,m} (x-\tau) - \overset{2}{F}_m \cos k_{xu,m} (x-\tau) \right] \left(B_m^+ e^{-\gamma_m z} + B_m^- e^{\gamma_m z} \right)$$

$$\overset{2}{\bar{H}} = \hat{x} \frac{1}{Z_{u,m}} \left[\overset{2}{E}_m \sin k_{xu,m} (x-\tau) - \overset{2}{F}_m \cos k_{xu,m} (x-\tau) \right] \left(B_m^+ e^{-\gamma_m z} - B_m^- e^{\gamma_m z} \right)$$

$$+ \hat{z} \frac{k_{xu,m}}{j\omega\mu_0} \left[\overset{2}{E}_m \cos k_{xu,m} (x-\tau) + \overset{2}{F}_m \sin k_{xu,m} (x-\tau) \right] \left(B_m^+ e^{-\gamma_m z} + B_m^- e^{\gamma_m z} \right)$$

$$\overset{3}{\bar{E}} = \hat{y} \left[\overset{3}{E}_m \sin k_{x,m} (a-x) - \overset{3}{F}_m \cos k_{x,m} (a-x) \right] \left(B_m^+ e^{-\gamma_m z} + B_m^- e^{\gamma_m z} \right)$$

$$\vec{H} = -\hat{x}\frac{1}{Z_m}\left[\overset{3}{E_m}\sin k_{x,m}\left(a-x\right)-\overset{3}{F_m}\cos k_{x,m}\left(a-x\right)\right]\left(B_m^+e^{-\gamma_m z}-B_m^-e^{\gamma_m z}\right)$$

$$+\hat{z}\frac{k_{x,m}}{j\omega\mu}\left[\overset{3}{E_m}\cos k_{x,m}\left(a-x\right)+\overset{3}{F_m}\sin k_{x,m}\left(a-x\right)\right]\left(B_m^+e^{-\gamma_m z}+B_m^-e^{\gamma_m z}\right)$$

Applying the tangential electric field boundary conditions at the walls, $x=0$ and $x=a$, of the waveguide—that is, the tangential electric field at the surface of a PEC must be zero—results in

$$\overset{1}{F_m}=0$$
$$\overset{3}{F_m}=0$$

(3.70)

Enforcing the continuity of tangential fields at $x=\tau$ and $x=\tau+d$, produces the following expressions

$$\overset{2}{F_m}=-\overset{1}{E_m}\sin k_{x,m}\tau$$

$$\overset{2}{E_m}=\frac{k_{x,m}\mu_0}{\mu k_{xu,m}}\overset{1}{E_m}\cos k_{x,m}\tau$$

$$-\overset{2}{E_m}\sin k_{xu,m}d+\overset{2}{F_m}\cos k_{xu,m}d=\overset{3}{E_m}\sin k_{x,m}\left(a-\tau-d\right)$$

$$\overset{2}{E_m}\cos k_{xu,m}d+\overset{2}{F_m}\sin k_{xu,m}d=\frac{k_{x,m}\mu_0}{\mu k_{xu,m}}\overset{3}{E_m}\cos k_{x,m}\left(a-\tau-d\right)$$

(3.71)

Substituting the first two expression of (3.71) into the last two and then dividing the two resulting equations by each other, brings about

$$\frac{\dfrac{-k_{x,m}\mu_0}{\mu k_{xu,m}}\cos k_{x,m}\tau\sin k_{xu,m}d-\sin k_{x,m}\tau\cos k_{xu,m}d}{\dfrac{k_{x,m}\mu_0}{\mu k_{xu,m}}\cos k_{x,m}\tau\cos k_{xu,m}d-\sin k_{x,m}\tau\sin k_{xu,m}d}=\frac{\mu k_{xu,m}\sin k_{x,m}\left(a-\tau-d\right)}{k_{x,m}\mu_0\cos k_{x,m}\left(a-\tau-d\right)}$$

(3.72)

Simplifying (3.72) results in

$$0 = \cos k_{xu,m} d \sin k_{x,m} (a-d) + \sin k_{xu,m} d \frac{k_{x,m} \mu_0}{\mu k_{xu,m}} \cos k_{x,m} (a-\tau-d) \cos k_{x,m} \tau \qquad (3.73)$$

$$- \sin k_{xu,m} d \frac{\mu k_{xu,m}}{k_{x,m} \mu_0} \sin k_{x,m} (a-\tau-d) \sin k_{x,m} \tau$$

Equation (3.73) is known as an eigenvalue equation. Without further information, solving the eigenvalue equation is impossible since it contains two unknowns. Realizing that both unknown x directed wave numbers must satisfy (2.25) and substituting in γ for the z directed wave number, (3.73) becomes

$$0 = \cos\left[d\sqrt{\omega^2 \varepsilon_u \mu_0 + \gamma_m^2} \right] \sin\left[(a-d)\sqrt{\omega^2 \varepsilon \mu + \gamma_m^2} \right] + \sin\left[d\sqrt{\omega^2 \varepsilon_u \mu_0 + \gamma_m^2} \right] \qquad (3.74)$$

$$\left[\begin{array}{l} \dfrac{\mu_0 \sqrt{\omega^2 \varepsilon \mu + \gamma_m^2}}{\mu\sqrt{\omega^2 \varepsilon_u \mu_0 + \gamma_m^2}} \cos\left[(a-\tau-d)\sqrt{\omega^2 \varepsilon \mu + \gamma_m^2} \right] \cos\left[\tau\sqrt{\omega^2 \varepsilon \mu + \gamma_m^2} \right] \\[2ex] - \dfrac{\mu\sqrt{\omega^2 \varepsilon_u \mu_0 + \gamma_m^2}}{\mu_0\sqrt{\omega^2 \varepsilon \mu + \gamma_m^2}} \sin\left[(a-\tau-d)\sqrt{\omega^2 \varepsilon \mu + \gamma_m^2} \right] \sin\left[\tau\sqrt{\omega^2 \varepsilon \mu + \gamma_m^2} \right] \end{array} \right].$$

Since the value of ε_u is supplied as the initial guess to the root search routine, (3.74) is now an equation of one unknown, γ_m. Unfortunately, (3.74) cannot be solved directly for γ_m and another root search must be performed on (3.74) to obtain γ_m. Supplying initial guesses for γ_m, which has a different value for each mode, can be tricky. However, the values of γ_m are known when the waveguide is either completely filled or completely empty. Using those values as the initial guesses and solving (3.74) repeatedly, each solution becoming the next iterations initial guesses and incrementing the R-card's thickness, d from merely a fraction of d to its actual value, produces the correct results for γ_m. Before the continuity of tangential fields can be enforced in the z

direction, the constants in (3.71) must be found. Dividing each expression in (3.71) by

$\overset{1}{E}_m$ and simplifying results in

$$\frac{\overset{2}{E}_m}{\overset{1}{E}_m} = \Psi_{1,m} = \frac{k_{x,m}\mu_0}{\mu k_{xu,m}}\cos k_{x,m}\tau \qquad\qquad (3.75)$$

$$\frac{\overset{2}{F}_m}{\overset{1}{E}_m} = \Psi_{2,m} = -\sin k_{x,m}\tau \qquad\qquad .$$

$$\frac{\overset{3}{E}_m}{\overset{1}{E}_m} = Y_m = \frac{-\Psi_{1,m}\sin k_{xu,m}d + \Psi_{2,m}\cos k_{xu,m}d}{\sin k_{x,m}(a-\tau-d)}$$

Plugging these expressions back into (3.69) produces the following expressions for the

fields in region II

$$\overset{1}{\bar{E}} = -\hat{y}\sin k_{x,m}x\left(B_m^+ e^{-\gamma_m z} + B_m^- e^{\gamma_m z}\right) \qquad\qquad (3.76)$$

$$\overset{1}{\bar{H}} = \hat{x}\frac{1}{Z_m}\sin k_{x,m}x\left(B_m^+ e^{-\gamma_m z} - B_m^- e^{\gamma_m z}\right) + \hat{z}\frac{k_{x.m}}{j\omega\mu}\cos k_{x,m}x\left(B_m^+ e^{-\gamma_m z} + B_m^- e^{\gamma_m z}\right)$$

$$\overset{2}{\bar{E}} = -\hat{y}\left[\Psi_{1,m}\sin k_{xu,m}(x-\tau) - \Psi_{2,m}\cos k_{xu,m}(x-\tau)\right]\left(B_m^+ e^{-\gamma_m z} + B_m^- e^{\gamma_m z}\right)$$

$$\overset{2}{\bar{H}} = \hat{x}\frac{1}{Z_{u,m}}\left[\Psi_{1,m}\sin k_{xu,m}(x-\tau) - \Psi_{2,m}\cos k_{xu,m}(x-\tau)\right]\left(B_m^+ e^{-\gamma_m z} - B_m^- e^{\gamma_m z}\right)$$

$$+\hat{z}\frac{k_{xu.m}}{j\omega\mu_0}\left[\Psi_{1,m}\cos k_{xu,m}(x-\tau) + \Psi_{2,m}\sin k_{xu,m}(x-\tau)\right]\left(B_m^+ e^{-\gamma_m z} + B_m^- e^{\gamma_m z}\right)$$

$$\overset{3}{\bar{E}} = \hat{y}Y_m\sin k_{x,m}(a-x)\left(B_m^+ e^{-\gamma_m z} + B_m^- e^{\gamma_m z}\right)$$

$$\overset{3}{\bar{H}} = -\hat{x}\frac{1}{Z_m}Y_m\sin k_{x,m}(a-x)\left(B_m^+ e^{-\gamma_m z} - B_m^- e^{\gamma_m z}\right)$$

$$+\hat{z}\frac{k_{x.m}}{j\omega\mu}Y_m\cos k_{x,m}(a-x)\left(B_m^+ e^{-\gamma_m z} + B_m^- e^{\gamma_m z}\right) \qquad .$$

Now that complete expressions for the fields in region II have been found, the

constants A_m^-, B_m^+, B_m^-, and C_m^+ can be found by enforcing the continuity of tangential

fields at the z directed boundaries, $z = 0$ and $z = \ell$. Doing so, rolling the like constants

into the z propagation coefficients in the fields expressions in regions I and III, and

dividing each expression by A_1^+ brings about equations of the following basic form

$$-\overset{1}{\bar{e}_1} - \sum_{m=1}^{\infty} \Gamma_m \overset{1}{\bar{e}_m} = -\sum_{m=1}^{\infty} t_m \overset{2}{\bar{e}_m} - \sum_{m=1}^{\infty} r_m \overset{2}{\bar{e}_m} \tag{3.77}$$

$$\overset{1}{\bar{h}_1} - \sum_{m=1}^{\infty} \Gamma_m \overset{1}{\bar{h}_m} = \sum_{m=1}^{\infty} t_m \overset{2}{\bar{h}_m} - \sum_{m=1}^{\infty} r_m \overset{2}{\bar{h}_m}$$

$$-\sum_{m=1}^{\infty} t_m \overset{2}{\bar{e}_m} e^{-\gamma_m \ell} - \sum_{m=1}^{\infty} r_m \overset{2}{\bar{e}_m} e^{\gamma_m \ell} = -\sum_{m=1}^{\infty} \mathrm{T}_m \overset{3}{\bar{e}_m} ^{,}$$

$$\sum_{m=1}^{\infty} t_m \overset{2}{\bar{h}_m} e^{-\gamma_m \ell} - \sum_{m=1}^{\infty} r_m \overset{2}{\bar{h}_m} e^{\gamma_m \ell} = \sum_{m=1}^{\infty} \mathrm{T}_m \overset{3}{\bar{h}_m}$$

where

$$\overset{1}{\bar{e}_m} = \overset{3}{\bar{e}_m}, \quad \overset{1}{\bar{h}_m} = \overset{3}{\bar{h}_m} \tag{3.78}$$

$$\Gamma_m = \frac{A_m^-}{A_1^+}, \quad t_m = \frac{B_m^+}{A_1^+}, \quad r_m = \frac{B_m^-}{A_1^+}, \quad \mathrm{T}_m = \frac{C_m^+}{A_1^+} \cdot$$

The forward transmission coefficient, S_{21}, is found by dividing the TE_{10} mode electric

field expression in region III, since all other modes will evanesce before reaching the

detector, by the forward traveling electric field expression in region I:

$$S_{21} = \frac{\bar{E}_{III,10}}{\bar{E}_I^+} = \frac{C_1^+}{A_1^+} e^{\gamma_{0,1} \ell} = \mathrm{T}_1 e^{\gamma_{0,1} \ell}. \tag{3.79}$$

In (3.77), there are four equations and an infinite number of unknowns. Even if the

infinite summations were truncated to become finite summations, there would still be

more unknowns than equations. This however can be overcome by using testing

operators. A testing operator is basically an inner product,

$$\langle \psi_1(x,y), \psi_2(x,y) \rangle = \int_y \int_x \psi_1(x,y) \psi_2(x,y) \, dxdy, \tag{3.80}$$

where ψ_1 can be any function and ψ_2 in this problem would be equal to the sine and cosine expressions in (3.77). Typically ψ_1 is chosen to be a function that is at least in part orthogonal to ψ_2 to ease the mathematics. Letting

$$\psi_1 = \sin\left(\frac{n\pi}{a} x\right) \tag{3.81}$$

and performing the inner product with each term in (3.77) results in

$$-M_{n1} - \sum_{m=1}^{\infty} \Gamma_m M_{nm} = \sum_{m=1}^{\infty} t_m U_{1,nm} + \sum_{m=1}^{\infty} r_m U_{1,nm} \tag{3.82}$$

$$N_{n1} - \sum_{m=1}^{\infty} \Gamma_m N_{nm} = \sum_{m=1}^{\infty} t_m U_{2,nm} + \sum_{m=1}^{\infty} r_m U_{3,nm}$$

$$-\sum_{m=1}^{\infty} T_m M_{nm} = \sum_{m=1}^{\infty} t_m V_{1,nm}^- + \sum_{m=1}^{\infty} r_m V_{1,nm}^+ \qquad,$$

$$\sum_{m=1}^{\infty} T_m N_{nm} = \sum_{m=1}^{\infty} t_m V_{2,nm} + \sum_{m=1}^{\infty} r_m V_{3,nm}$$

where

$$N_{nm} = \frac{M_{nm}}{Z_{0,m}} \tag{3.83}$$

$$U_{1,nm} = -O_{nm} - \Psi_{1,m} P_{nm} + \Psi_{2,m} Q_{nm} + Y_m R_{nm}$$

$$U_{2,nm} = \frac{O_{nm}}{Z_m} + \frac{\Psi_{1,m}}{Z_{u,m}} P_{nm} - \frac{\Psi_{2,m}}{Z_{u,m}} Q_{nm} - \frac{Y_m}{Z_m} R_{nm}$$

$$U_{3,nm} = \frac{-O_{nm}}{Z_m} - \frac{\Psi_{1,m}}{Z_{u,m}} P_{nm} + \frac{\Psi_{2,m}}{Z_{u,m}} Q_{nm} + \frac{Y_m}{Z_m} R_{nm}$$

$$V_{1,nm}^{\pm} = U_{1,nm} e^{\pm \gamma_m \ell}$$

$$V_{2,nm} = U_{2,nm} e^{-\gamma_m \ell}$$

$$V_{3,nm} = U_{3,nm} e^{\gamma_m \ell}$$

and M_{nm}, N_{nm}, O_{nm}, P_{nm}, Q_{nm}, and R_{nm} are

$$M_{nm} = \int_0^b \int_0^a \sin\left(\frac{n\pi}{a}x\right)\sin\left(\frac{m\pi}{a}x\right)dxdy = \begin{cases} 0 & \ldots n \neq m \\ \dfrac{ab}{2} & \ldots n = m \end{cases} \qquad (3.84)$$

$$N_{nm} = \frac{M_{nm}}{Z_{0,m}} = \begin{cases} 0 & \ldots n \neq m \\ \dfrac{ab}{2Z_{0,m}} & \ldots n = m \end{cases}$$

$$O_{nm} = \int_0^b \int_0^\tau \sin\left(\frac{n\pi}{a}x\right)\sin\left(k_{x,m}x\right)dxdy$$

$$= \frac{b}{2}\left(\frac{a}{n\pi - ak_{x,m}}\right)\sin\tau\left(\frac{n\pi}{a}-k_{x,m}\right) - \frac{b}{2}\left(\frac{a}{n\pi + ak_{x,m}}\right)\sin\tau\left(\frac{n\pi}{a}+k_{x,m}\right)$$

$$P_{nm} = \int_0^b \int_\tau^{\tau+d} \sin\left(\frac{n\pi}{a}x\right)\sin\left(k_{xu,m}(x-\tau)\right)dxdy$$

$$= \frac{b}{2}\left(\frac{a}{n\pi - ak_{xu,m}}\right)\left[\sin\left(\frac{n\pi}{a}(\tau+d)-k_{xu,m}d\right)-\sin\frac{n\pi}{a}\tau\right]$$

$$\quad - \frac{b}{2}\left(\frac{a}{n\pi + ak_{xu,m}}\right)\left[\sin\left(\frac{n\pi}{a}(\tau+d)+k_{xu,m}d\right)-\sin\frac{n\pi}{a}\tau\right]$$

$$Q_{nm} = \int_0^b \int_\tau^{\tau+d} \sin\left(\frac{n\pi}{a}x\right)\cos\left(k_{xu,m}(x-\tau)\right)dxdy$$

$$= \frac{b}{2}\left(\frac{a}{n\pi + ak_{xu,m}}\right)\left[\cos\frac{n\pi}{a}\tau - \cos\left(\frac{n\pi}{a}(\tau+d)+k_{xu,m}d\right)\right]$$

$$\quad + \frac{b}{2}\left(\frac{a}{n\pi - ak_{xu,m}}\right)\left[\cos\frac{n\pi}{a}\tau - \cos\left(\frac{n\pi}{a}(\tau+d)-k_{xu,m}d\right)\right]$$

$$R_{nm} = \int_0^b \int_{\tau+d}^a \sin\left(\frac{n\pi}{a}x\right)\sin\left(k_{x,m}(a-x)\right)dxdy$$

$$= \frac{b}{2}\left(\frac{a}{n\pi - ak_{x,m}}\right)\sin\left(\frac{n\pi}{a}(\tau+d)+k_{x,m}(a-\tau-d)\right)$$

$$\quad - \frac{b}{2}\left(\frac{a}{n\pi + ak_{x,m}}\right)\sin\left(\frac{n\pi}{a}(\tau+d)+k_{x,m}(\tau+d-a)\right)$$

(details in Appendix A). Assuming *M* modes are modeled and rearranging (3.82) into

matrix form produces

$$
\begin{bmatrix}
-M & -U_1 & -U_1 & 0 \\
-N & -U_2 & -U_3 & 0 \\
0 & V_1^- & V_1^+ & M \\
0 & V_2 & V_3 & -N
\end{bmatrix}
\begin{bmatrix}
\Gamma \\
t \\
r \\
T
\end{bmatrix}
=
\begin{bmatrix}
x_1 \\
-x_2 \\
0 \\
0
\end{bmatrix},
\qquad (3.85)
$$

where M, N, U_1, U_2, U_3, $V_1^{\pm}$, V_2, and V_3 are MxM submatrices and x_1 and x_2 are

column vectors,

$$
x_1 =
\begin{bmatrix}
M_{11} \\
\vdots \\
M_{1M}
\end{bmatrix}, \quad
x_2 =
\begin{bmatrix}
\dfrac{M_{11}}{Z_{0,1}} \\
\vdots \\
\dfrac{M_{1M}}{Z_{0,M}}
\end{bmatrix}.
\qquad (3.86)
$$

To get the values for T, which is related to S_{21} by (3.79), the inverse of the $4M$x$4M$

matrix must be taken and then multiplied by the known column vector on the right hand

side of (3.85). Once a theoretical value of S_{21} has been obtained, it is compared to

measured S_{21} data. If the theoretical solution is within a certain precision of the measured

data, then the relative permittivity of the R-card is returned. If not, then a new value is

iterated for the relative permittivity of the R-card and the whole process begins again

with the γ_m root search, filling the matrix in (3.85), and solving for the theoretical value

of S_{21}.

3.3 Summary

In this chapter, free-space and waveguide techniques for obtaining the resistivity

of an R-card were developed. They ranged from the computationally complex vertical

mode matching technique to simple functions, like the thin sheet approximations. Each

technique has its own advantages and disadvantages. In the next chapter, the techniques

will be compared to each other with measured, R-card forward transmission data.

4. Results

In the previous chapter, methods for determining the resistivity of an R-card were derived. Those methods will be verified in this chapter. Measurements of the 892 Ω/sq and 64 Ω/sq R-cards, Figure 1-1, were made with free-space and waveguide material measurement systems. The R-cards were measured from 2 to 18 GHz using the free-space, or focused arch, system and from 8.2 to 12.4 GHz, or X-band, using the waveguide system. While there is nothing invalid mathematically with using the S_{21} methods developed in the previous chapter at any frequency, the forward transmission data with which they depend may be too near the noise floor of the measurement system to be accurately obtained. R-cards, as will be shown, are highly dependent upon frequency. At some frequencies they are highly reflective, while at others they are more transparent. The frequency ranges chosen to measure the 892 Ω/sq and 64 Ω/sq R-cards were selected so that S_{21} data was easily measured and for convenient proof of concept demonstrations.

4.1 Experimental Setups

Free-space measurements were made using AFRL/SNS's focused arch system (Figure 4-1). Since the size of the beam focused by the lenses increases with wavelength, the R-card samples, shown in Figure 4-2, were cut to 1 foot by 1 foot squares. This ensured that at the lowest frequency measured (2 GHz), only the sample and none of the apparatus holding the sample was illuminated. Two measurements were then made. The first was a thru measurement—empty sample holder—to establish the system's
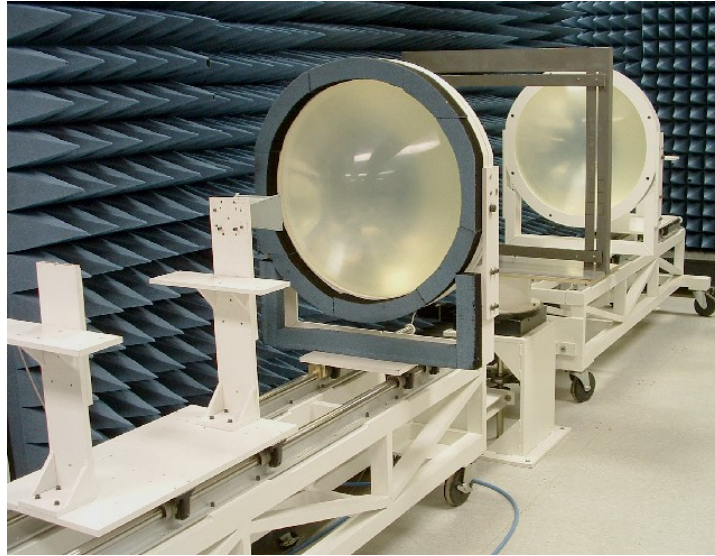
Figure 4-1. Focused arch material measurement system owned and operated by AFRL/SNS.
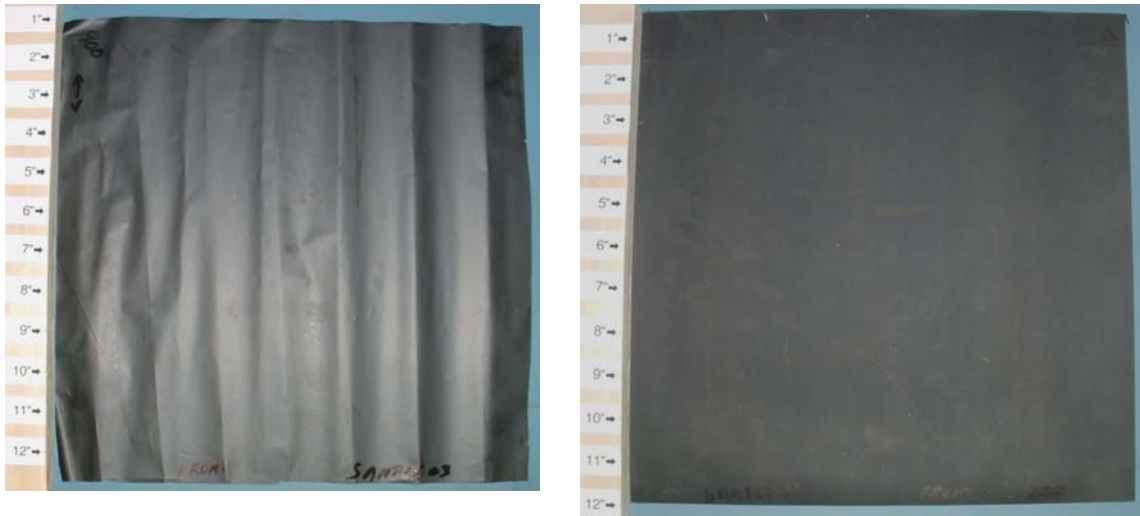
Figure 4-2. 1 foot by 1 foot R-card samples. On the left, is the 892 Ω/sq DC resistivity R-card. On the right, is the 64 Ω/sq DC resistivity R-card.

transmission response. The second was a reflect measurement using a metal plate to establish the system's isolation response. The samples (Figure 4-2) were then measured

and the raw data was calibrated using the results from the thru and reflect measurements and the following expression

$$S_{21}^{cal} = \frac{S_{21}^{raw} - S_{21}^{reflect}}{S_{21}^{thru} - S_{21}^{reflect}} \ [10].$$

(4.1)

After the R-card samples in Figure 4-2 were measured and the focused arch system was calibrated, the S_{21} data was software time gated. Software time gating is a post process technique which removes unwanted returns from the system. It is typically done in systems where it is not possible to perform full two port calibrations, like microstrip and free-space systems. Time gating requires transforming frequency domain data into time domain data via an inverse Fourier transform. Data in the time domain shows scattering from objects as they occur spatially; therefore, in a time domain image, it is quite easy to tell which scattering is due to the sample and which is due to unwanted phenomena, like cable connections in the system. Once the return from the sample has been identified, it is kept and all other data is made zero. The data is then transformed back into the frequency domain via a Fourier transform. Software time gating significantly improves the quality of measured data; however, it has the unintended effect of making data at the lower and upper limits of the measured frequency range inaccurate. This undesirable effect occurs because of the abrupt change from measured data to zero introduced by the gate. For more information on this phenomena see Cassell's [11] thesis, "Investigation of Time-Domain and Frequency-Domain Free-Space Material Measurements." Since the frequency range of interest is from 7 to 14 GHz, this time gating effect has no impact on the results presented in this thesis. R-card resistivity data

will be presented at 2 GHz and 18 GHz; however, it is only used for proof of concept demonstrations.

Waveguide measurements were made with the system shown in Figure 4-3. The waveguide used was a WR90 waveguide, where WR stands for waveguide rectangular and 90 is the waveguide aperture width—0.90 inches. The ends of the waveguide were connected to a HP8510C Vector Network Analyzer by coaxial cables. The X-band sample holder and the R-card samples are shown in Figure 4-4.

Before gathering S_{21} data, the system was calibrated, including the sample holder, using a full two port, thru, reflect, line (TRL) calibration technique. The TRL calibration makes three basic measurements. The first is called the thru measurement and involves

Figure 4-3. X-band waveguide WR90 attached to HP8510C Vector Network Analyzer with coaxial cables.
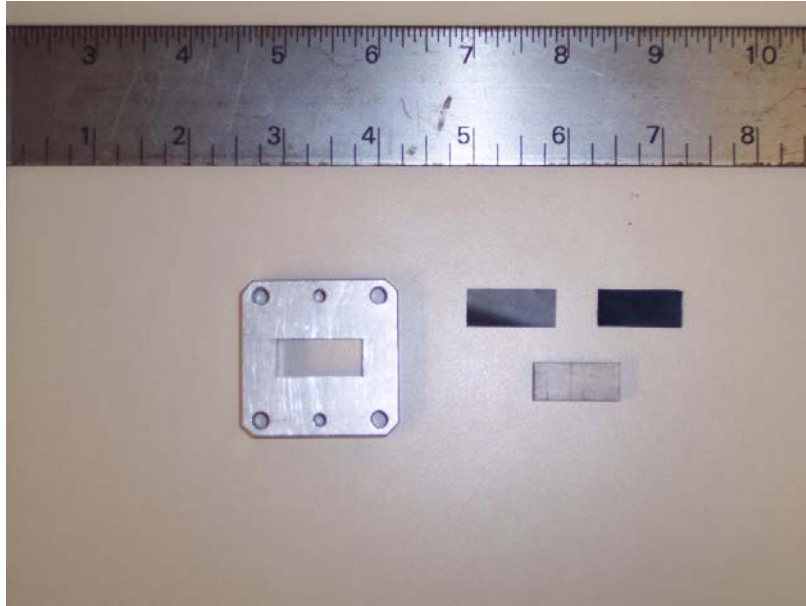
Figure 4-4. X-band waveguide sample holder and R-card samples. The leftmost sample is the 892 Ω/sq DC resistivity R-card. The rightmost sample is the 64 Ω/sq DC resistivity R-card. The other material shown in the figure is acrylic, used as a support backing to the R-card samples.

measuring the response of the system with the empty sample holder included. The second is the reflect measurement and consists of measuring the response of the system when a short, or metal plate, is placed at one end of the waveguide. The third and final measurement is called the line measurement and consists of measuring the response of the system without the sample holder. These measurements are used to nullify returns from coax to waveguide couplers and waveguide segment to waveguide segment linkages. After performing the TRL calibration, the forward reflection coefficient, S_{11}, was measured with the short in place to ensure that $S_{11} \approx -1 \approx 1\angle \pm 180°$. This was done to verify that the calibration was successful.

4.2 892 Ω/sq R-card

The 892 Ω/sq R-card measured in this thesis was a dark, opaque material. It was extremely thin, approximately 0.001 inches, and had the consistency of tissue paper. Extreme care had to be taken when handling it because it was very easy to tear the material. Figure 4-5 shows the VV relative permittivity of the material using the root search method derived from the focused arch system data. Figure 4-6 shows the resistivity of the R-card using the relative permittivity shown in Figure 4-5 and applying (3.14). These root search values, which are solutions to (3.11) with a 10^{-7} tolerance, will be used as a baseline to compare the accuracy of the other free-space methods. Figures 4-7 and 4-8 compare the root search relative permittivity and resistivity values with the first order and thin sheet approximations' values. The first order approximation's success can be explained by looking at Figure 4-9, which shows the magnitude of the R-card's wave number times its thickness. Since $|k\tau|$ is about 10 times less than 1, the first order approximation is extremely accurate. The thin sheet approximation performs very similarly to the first order approximation. Its accuracy depends upon the sheet thickness being much less than the wavelength of the incident field. The wavelength of electromagnetic energy at 18 GHz is 0.6557 inches, which is 655 times larger than the thickness of the sheet. The results are very similar for the HH case. Table 4-1 summarizes the results and shows average errors for the first, second, third, fifth, and tenth order approximations, as well as the average error for the thin sheet approximation. Figure 4-10 communicates the results shown in Table 4-1 pictorially.
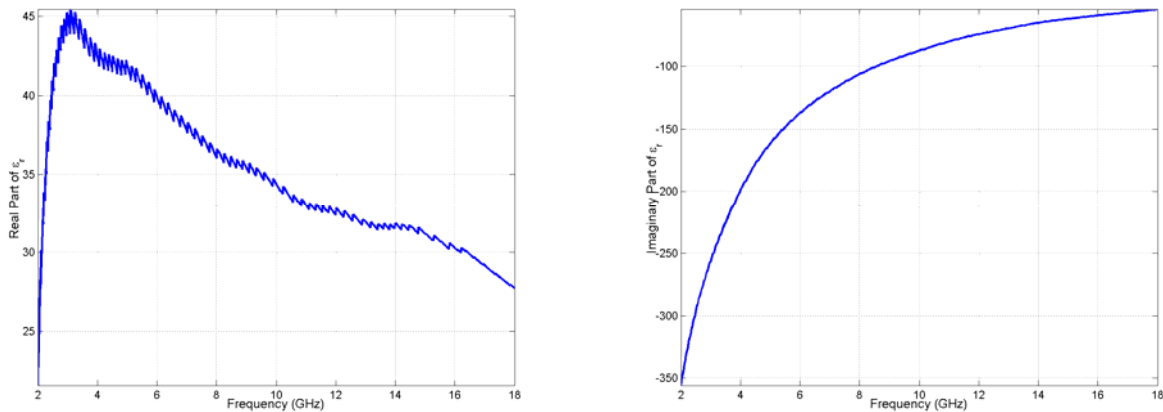
Figure 4-5. 892 Ω/sq R-card, free-space, VV, relative permittivity using the root search method. On the left is the real part of the relative permittivity. On the right is the imaginary part of the relative permittivity. Values are solutions to (3.11) with a 10^{-7} tolerance.
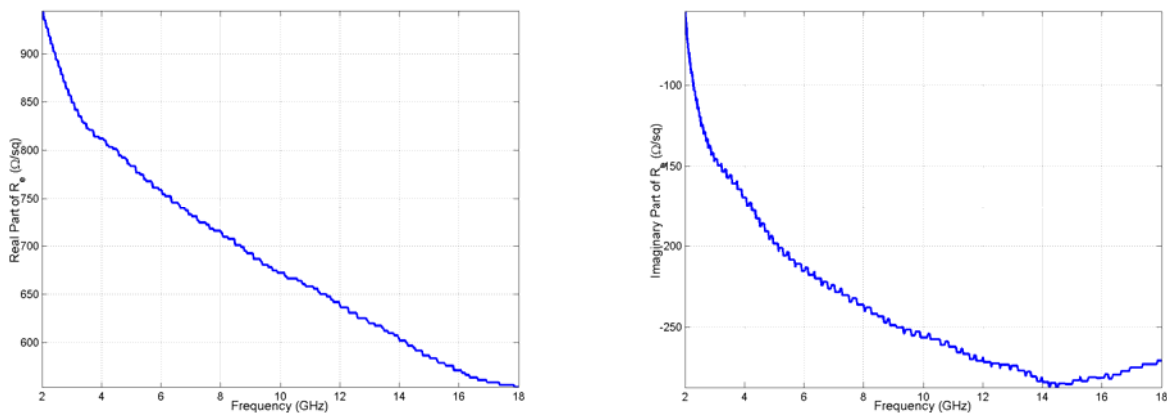
Figure 4-6. 892 Ω/sq R-card, free-space, VV, resistivity using the root search method. On the left is the real part of the resistivity. On the right is the imaginary part of the resistivity. Values are solutions to (3.11) with a 10^{-7} tolerance.
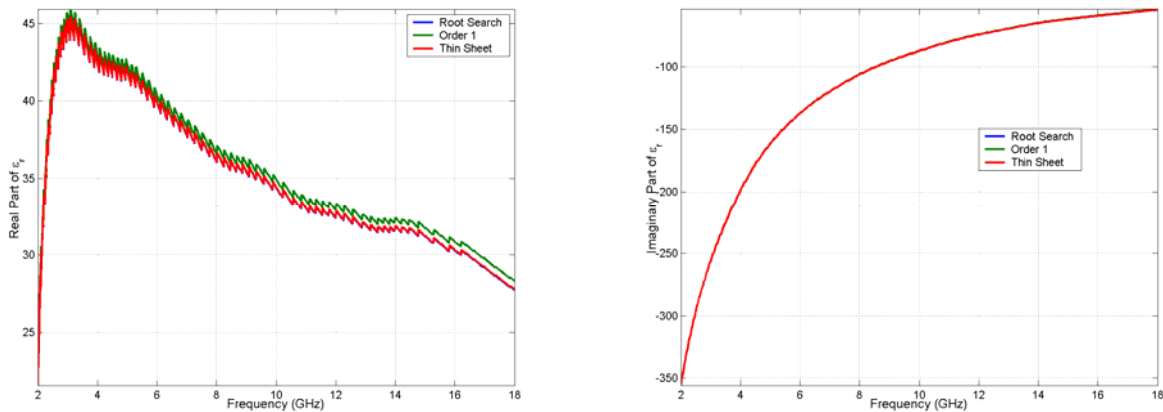
Figure 4-7. 892 Ω/sq R-card, free-space, VV, relative permittivity comparing the first order approximation and the thin sheet approximation to the root search method. On the left is the real part of the relative permittivity. On the right is the imaginary part of the relative permittivity.
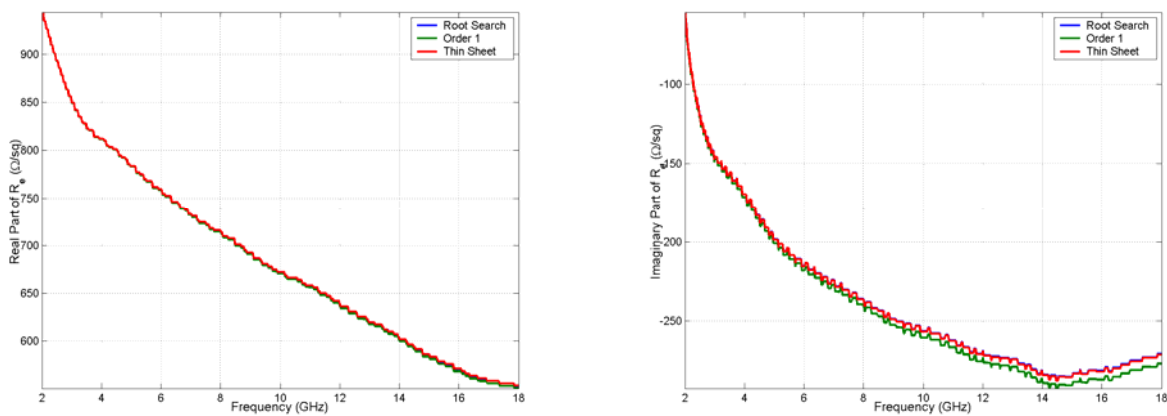
Figure 4-8. 892 Ω/sq R-card, free-space, VV, resistivity comparing the first order approximation and the thin sheet approximation to the root search method. On the left is the real part of the resistivity. On the right is the imaginary part of the resistivity.
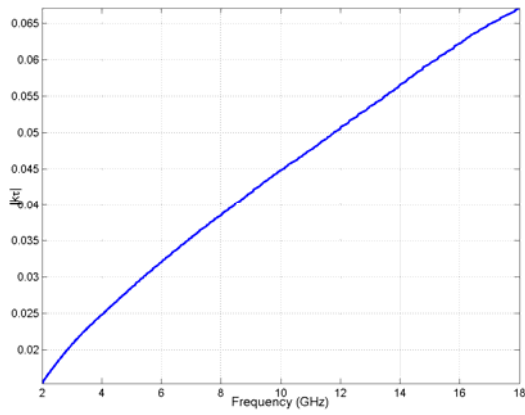
Figure 4-9. 892 Ω/sq R-card, free-space, VV, $|k\tau|$ values versus frequency.

Figure 4-10. 892 Ω/sq R-card, free-space methods' error magnitude versus frequency.
On the left are the results for VV. On the right are the results for HH.

Table 4-1. 892 Ω/sq R-card, free-space methods comparison summary.

	VV Average Error Magnitude (Ω/sq)	VV Max Error Frequency (GHz)	HH Average Error Magnitude (Ω/sq)	HH Max Error Frequency (GHz)
Order 1	4.2315	18.0	4.1093	18.0
Order 2	0.3563	18.0	0.3563	18.0
Order 3	0.0013	18.0	0.0013	18.0
Order 5	2.4683×10^{-7}	18.0	2.8687×10^{-7}	18.0
Order 10	7.9883×10^{-8}	17.98	1.1335×10^{-7}	18.0
Thin Sheet	0.3510	18.0	0.3510	18.0

Comparing the values returned from the waveguide root search to that of the waveguide first order and thin sheet approximations produces conclusions similar to that of the free-space methods comparison. The real point of interest is when the results from the fully filled waveguide techniques are compared to the 8.2 GHz to 12.4 GHz frequency range of the free-space techniques. Since all the approximations eventually converge to the root search method, it will be the only technique whose results are compared across material measurement apparatuses. Figure 4-11 shows the 892 Ω/sq R-card's relative permittivity, real and imaginary, obtained by using the free-space root search method compared to the relative permittivity returned by the waveguide root search method. Note that there is a significant disagreement between the two measurement systems, especially when it comes to the real part of the dielectric constant. Two possible causes are that the R-card is inhomogeneous and its permittivity depends on the polarization of the incident field or the dielectric constant of the R-card's acrylic support backing used in the waveguide experiments is not accurate. Since VV and HH free-space experiments produce similar relative permittivity values for the 892 Ω/sq R-card, the former cause does not seem likely in this case. This leaves the latter. Figure 4-

12 shows the relative permittivity of the acrylic support backing measured in the X-band waveguide. Its permittivity values differ by 1.02 % around the mean ($\varepsilon_r = 2.7479 - j0.0160$), which was the value used for acrylic in the waveguide root search method shown in Figure 4-11. Figure 4-13 shows the impact that changing the acrylic's permittivity to any value within the range shown in Figure 4-12 has on the values returned for the 892 Ω/sq R-card's relative permittivity by the waveguide root search method. Note the profound effect that changing the acrylic's permittivity value by only approximately 0.5 % has on the R-card's permittivity values. To accurately reproduce the free-space root search values with the waveguide root search requires an acrylic relative permittivity value of $\varepsilon_r = 2.81 - j0.0$, which is only about 2 % away from the mean acrylic value. This 2 % can easily be accounted for by any number of possible measurement errors, for instance the acrylic sample not fully filling the waveguide or imperfections in the surface of the material such as scratches or nicks.
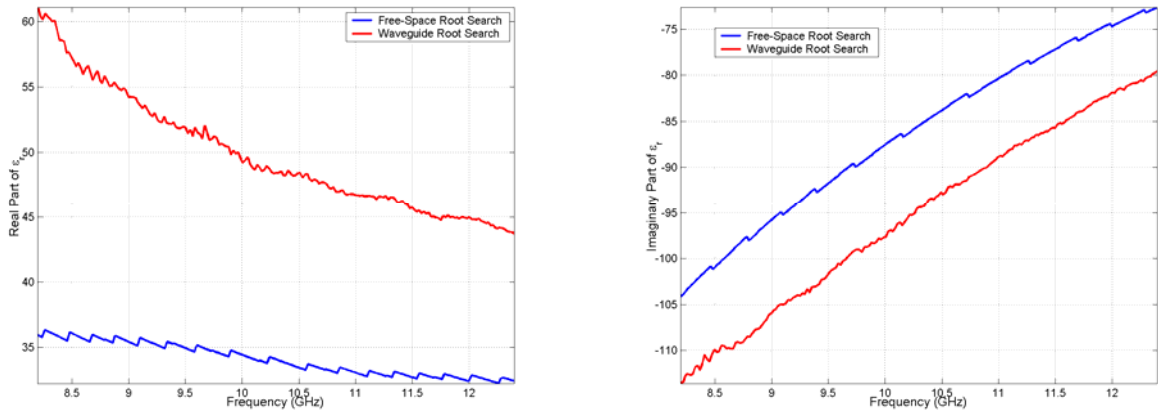
Figure 4-11. 892 Ω/sq R-card relative permittivity, free-space root search compared to the waveguide root search. On the left is the real part of the relative permittivity. On the right is the imaginary part of the relative permittivity.
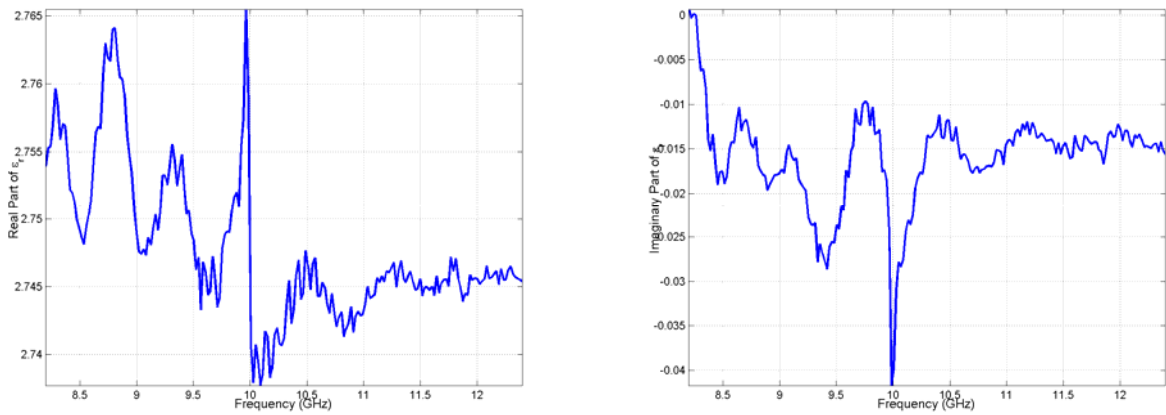
Figure 4-12. X-band relative permittivity of acrylic obtained by the waveguide root search method. On the left is the real part of the relative permittivity. On the right is the imaginary part of the relative permittivity.
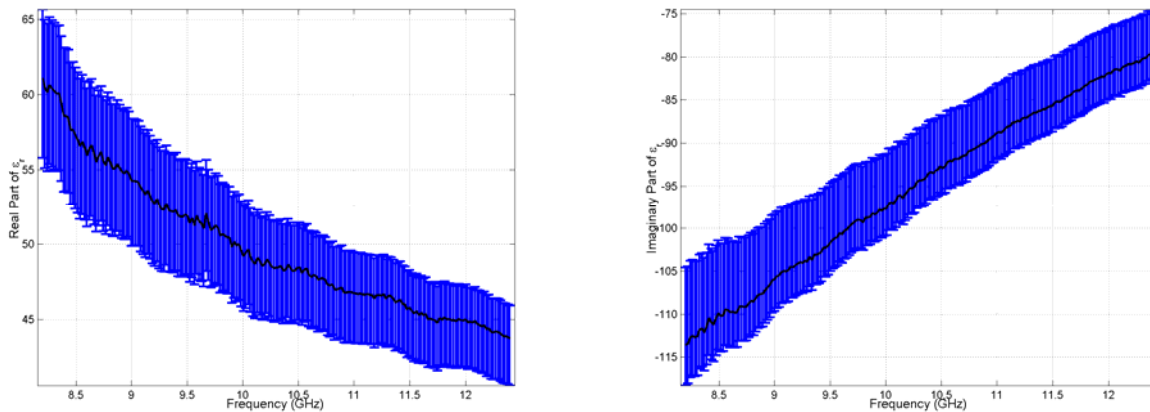
Figure 4-13. 892 Ω/sq R-card relative permittivity values obtained by the waveguide root search method when the acrylic support backing is any value within the range of Figure 4-12. On the left is the real part of the relative permittivity. On the right is the imaginary part of the relative permittivity.

To verify the vertical mode matching technique, the 892 Ω/sq R-card was sandwiched between two pieces of polystyrene foam as shown in Figures 3-5 and 3-6. The permittivity of foam was measured independently and is shown in Figure 4-14. The results of the vertical mode matching technique for the 892 Ω/sq R-card are shown in Figure 4-15 (1, 5, and 10 modes). The results are disappointing in terms of accuracy, especially for the real part of the dielectric constant; however, they are encouraging in terms of consistency. Figure 4-16 shows the variation in the values of the 892 Ω/sq R-card if any value in the range of Figure 4-14 is used as foam's permittivity in the vertical mode matching algorithm. It was hoped that measuring the R-card along its length, rather than its thickness, would produce more consistent results and it appears it has. Even with more variance in the value of its support backing—foam 1.23 % versus acrylic 1.02 %—the method produces more consistent results than the fully filled waveguide root search routine shown in Figure 4-13.

A major drawback of this method, especially for measuring the permittivity of a thin material which cannot support itself, is in the difficulty of machining the sample. In the fully filled waveguide methods, one sample at a time can be fabricated. While in the vertical mode matching technique a sample "sandwich" has to be made. Using the nomenclature in Figure 3-5, the values for permittivity are pretty resistant to inaccuracies in the measurement of τ as shown in Figure 4-17. However, inaccuracies in the measurement of ℓ are costly (Figure 4-18). Measuring ℓ accurately is not a problem for rigid substances like acrylic or even the R-cards; on the other hand, an accurate ℓ measurement is nearly impossible for a substance like polystyrene foam. Using a substance like acrylic for the sample sandwich, which was not available for this experiment, would certainly reduce the variability of the results.
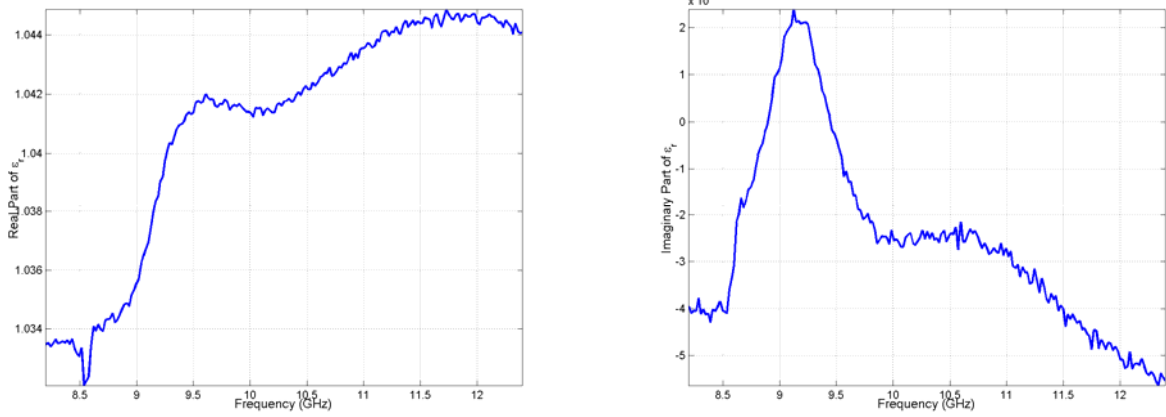
Figure 4-14. X-band relative permittivity of polystyrene foam obtained by the waveguide root search method. On the left is the real part of the relative permittivity. On the right is the imaginary part of the relative permittivity.
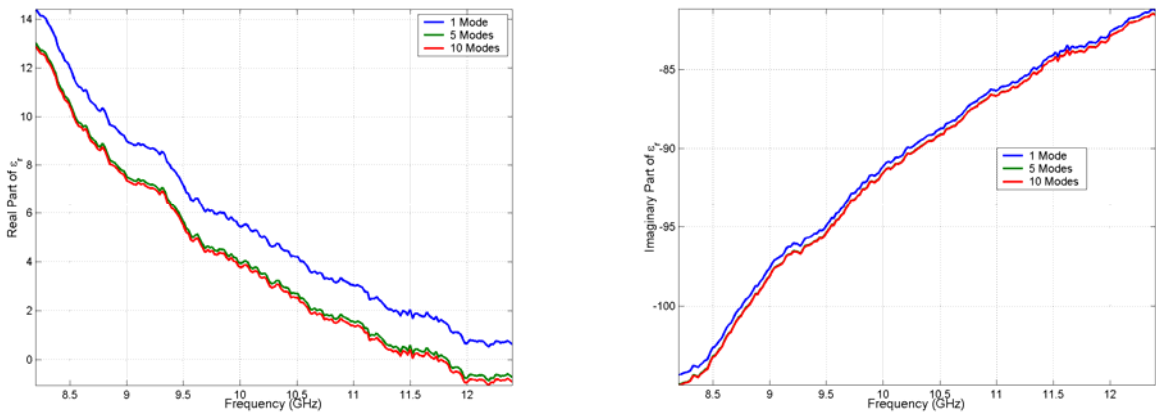
Figure 4-15. 892 Ω/sq R-card relative permittivity using 1, 5, and 10 modes of the vertical mode matching technique. On the left is the real part of the relative permittivity. On the right is the imaginary part of the relative permittivity. Values are solutions to (3.11) with a 10^{-7} tolerance.
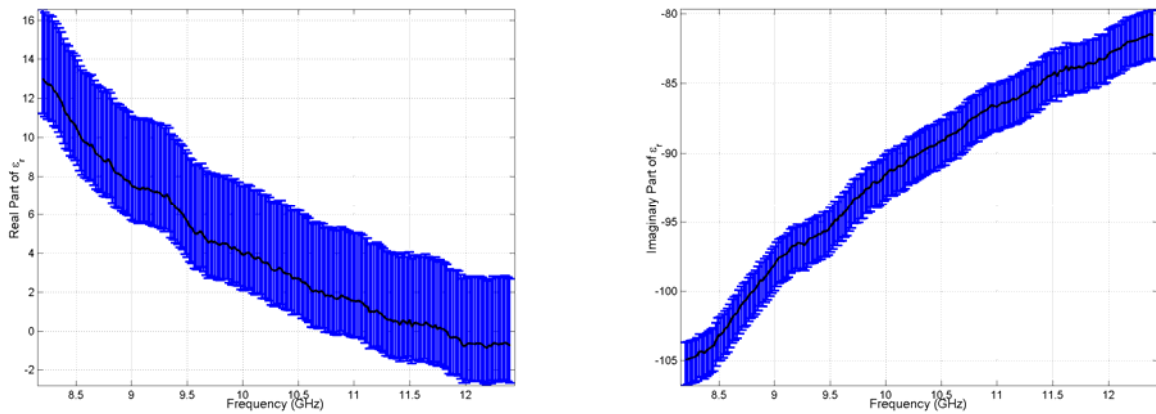
Figure 4-16. 892 Ω/sq R-card relative permittivity values obtained by the vertical mode matching technique, 5 modes, when the foam sandwich is any value within the range of Figure 4-14. On the left is the real part of the relative permittivity. On the right is the imaginary part of the relative permittivity.
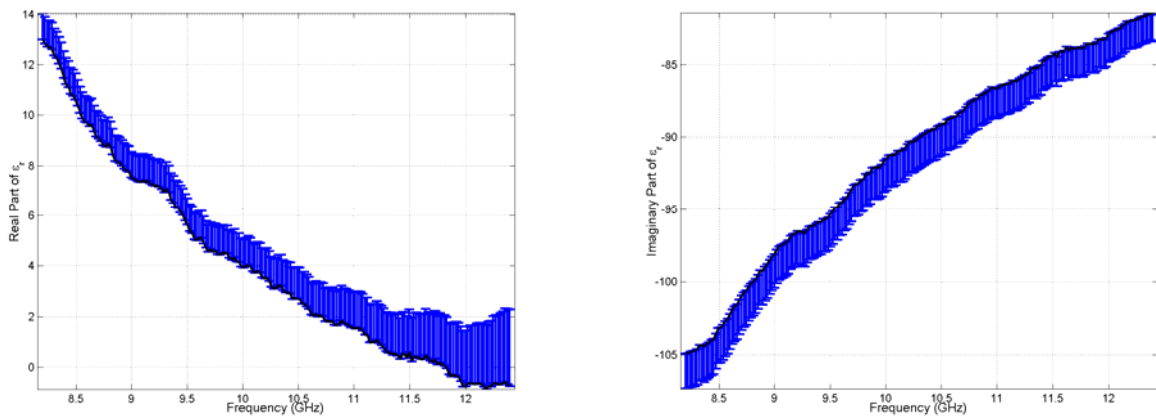
Figure 4-17. 892 Ω/sq R-card relative permittivity values obtained by the vertical mode matching technique, 5 modes, when the value of τ is changed by $\pm\,10\,\%$. On the left is the real part of the relative permittivity. On the right is the imaginary part of the relative permittivity.
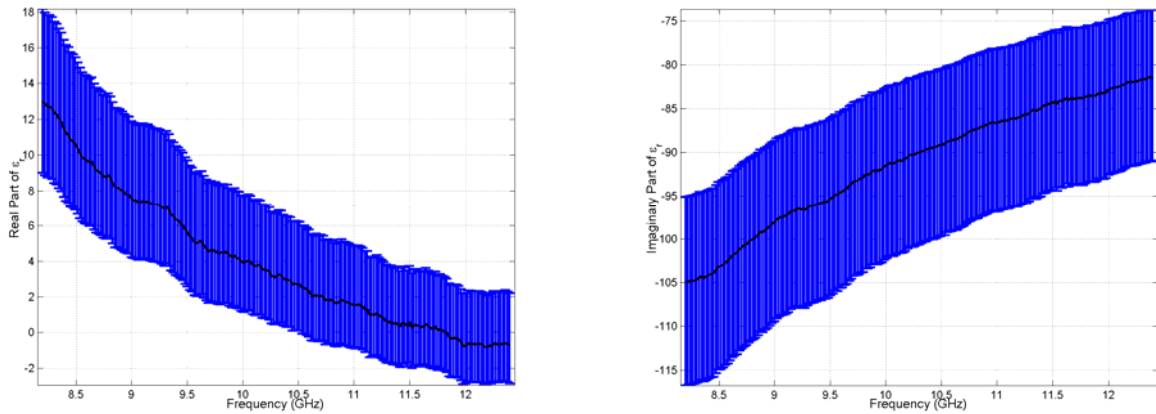
Figure 4-18. 892 Ω/sq R-card relative permittivity values obtained by the vertical mode matching technique, 5 modes, when the value of ℓ is changed by $\pm 10\%$. On the left is the real part of the relative permittivity. On the right is the imaginary part of the relative permittivity.

4.3 64 Ω/sq R-card

Like the 892 Ω/sq R-card, the 64 Ω/sq R-card was a dark, opaque material. It

however was 30 times thicker than the 892 Ω/sq R-card, approximately 0.030 inches, and

had a rubber-like consistency. Figures 4-19 and 4-20 show the R-card's relative

permittivity and resistivity respectively using the root search method. The results shown

in Figures 4-19 and 4-20, solutions to (3.11) with a 10^{-7} tolerance, will be used as a

baseline to compare all the other free-space methods. Figures 4-21 and 4-22 show the

first, second, third, and fifth order approximations, as well as the thin sheet

approximation, compared to the root search method. Note that it takes fifth order terms

of the Maclaurin series for sine and cosine to converge on the true values. Figure 4-23

shows the magnitude of the R-card's wave number times its thickness versus frequency.

The plot shows that $|k\tau|$ at a minimum is equal to approximately 0.5, which is only 2

times less than 1. This explains why the first order and second order approximations are

not accurate. The thin sheet approximation also returns erroneous values. Its accuracy

depends upon the thickness of the sheet being much less than the wavelength of the

incident field so that the fields induced inside the R-card are negligible. The longest and

shortest measured wavelengths are at 2 GHz and 18 GHz—5.9015 inches and 0.6557

inches. This explains why the thin sheet approximation's accuracy decreases as

frequency increases, or wavelength shortens. At the lowest frequency, the wavelength is

197 times larger than the thickness of the R-card. At 18 GHz, the wavelength is only 22

times larger than the thickness of the R-card, as opposed to 655 times larger in the 892

Ω/sq R-card case. Table 4-2 summarizes the results and shows average errors for the

first, second, third, fifth, and tenth order approximations, as well as the average error for

the thin sheet approximation. Figure 4-24 communicates the results shown in Table 4-2

pictorially.

Figure 4-19. 64 Ω/sq R-card, free-space, VV, relative permittivity using the root search method. On the left is the real part of the relative permittivity. On the right is the imaginary part of the relative permittivity. Values are solutions to (3.11) with a 10^{-7} tolerance.
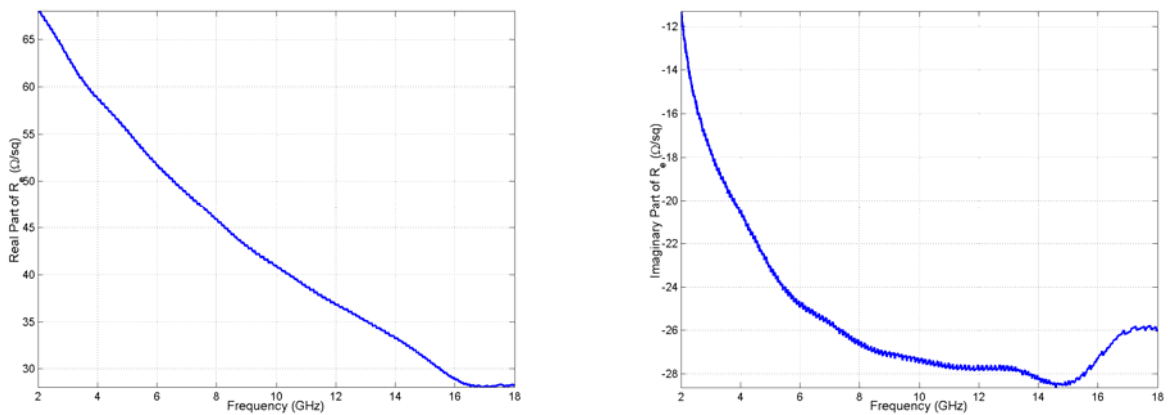
Figure 4-20. 64 Ω/sq R-card, free-space, VV, resistivity using the root search method. On the left is the real part of the resistivity. On the right is the imaginary part of the resistivity. Values are solutions to (3.11) with a 10^{-7} tolerance.

Figure 4-21. 64 Ω/sq R-card, free-space, VV, relative permittivity comparing the first, second, third, and fifth order approximations, as well as the thin sheet approximation, to the root search method. On the left is the real part of the relative permittivity. On the right is the imaginary part of the relative permittivity.
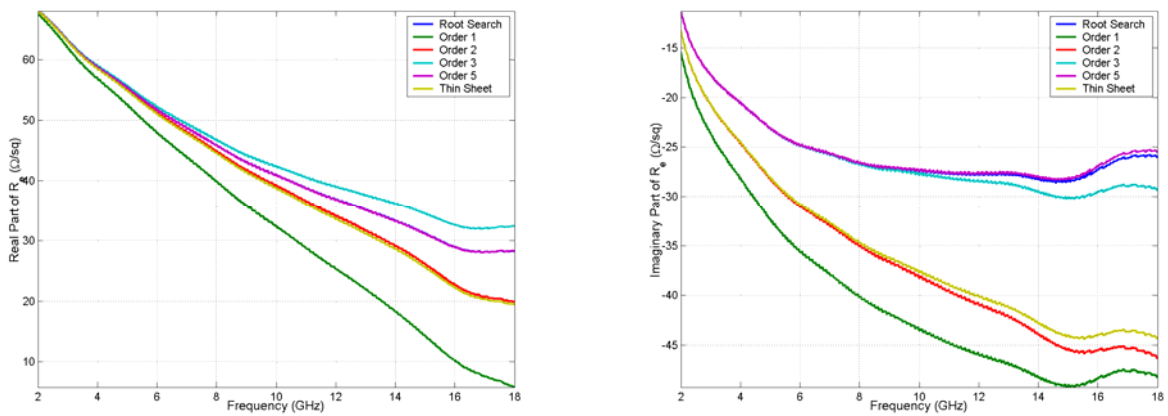
Figure 4-22. 64 Ω/sq R-card, free-space, VV, resistivity comparing the first, second, third, and fifth order approximations, as well as the thin sheet approximation, to the root search method. On the left is the real part of the resistivity. On the right is the imaginary part of the resisitivity.
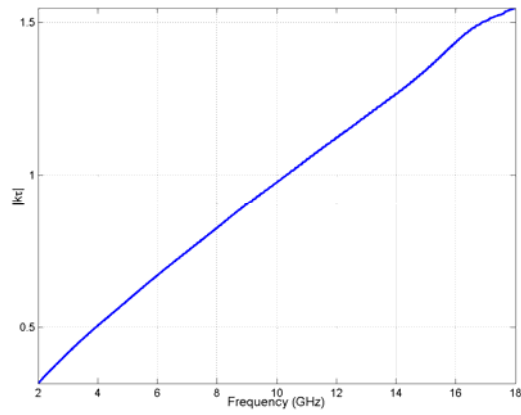
Figure 4-23. 64 Ω/sq R-card, free-space, VV, $|k\tau|$ values versus frequency.

Figure 4-24. 64 Ω/sq R-card, free-space methods' error magnitude versus frequency. On the left are the results for VV. On the right are the results for HH.

Table 4-2. 64 Ω/sq R-card, free-space methods comparison summary.

	VV Average Error Magnitude (Ω/sq)	VV Max Error Frequency (GHz)	HH Average Error Magnitude (Ω/sq)	HH Max Error Frequency (GHz)
Order 1	18.0952	18.0	16.1680	18.0
Order 2	11.2984	18.0	10.8126	18.0
Order 3	1.9221	18.0	1.9091	18.0
Order 5	0.1270	18.0	0.1498	18.0
Order 10	3.6422×10^{-5}	18.0	6.5499×10^{-5}	18.0
Thin Sheet	10.7447	18.0	10.4571	18.0

When comparing methods intra-measurement systems, the fully filled waveguide techniques produce very similar results to the free-space methods. Like the 892 Ω/sq R-card, the real point of interest is when the methods are compared inter-measurement systems. Once again, since all other methods converge to values obtained by root searches, only comparisons of the free-space root search and waveguide root search methods will be shown. Figure 4-25 shows the 64 Ω/sq R-card's relative permittivity values obtained by free-space S_{21} measurement compared to those obtained by waveguide S_{21} measurement. The discrepancy between the two is far less pronounced than in the 892 Ω/sq R-card case; however, it is still significant. The likely causes are the same as the 892 Ω/sq R-card case: the R-card is inhomogeneous or the permittivity value for the acrylic support backing is inaccurate. In this case, the former cause cannot be so easily dismissed. Figure 4-26 shows the VV and HH relative permittivity values of the 64 Ω/sq R-card as measured by the focused arch system. From Figure 4-26, it is clear that there is a significant dependence of the 64 Ω/sq R-card's relative permittivity on polarization, especially the imaginary part of relative permittivity. Therefore, it is entirely plausible to receive different results for relative permittivity when comparing values obtained from

measuring the 64 Ω/sq R-card with a *TEM* mode to those obtained when measuring the

64 Ω/sq R-card with a *TE*$_{10}$ mode. In addition to the former cause, the latter—inaccurate

value for permittivity of acrylic—can also be a source of the difference in Figure 4-25. A

small change in acrylic's permittivity, however, does not have nearly as drastic an effect

on the relative permittivity value of the 64 Ω/sq R-card as it did on the 892 Ω/sq R-card.

Figure 4-27 shows the relative permittivity of the 64 Ω/sq R-card when any value in

Figure 4-12 is used for the permittivity of acrylic in the waveguide root search algorithm.

Note that there is only a slight change in the relative permittivity of the 64 Ω/sq R-card.

Since it is 30 times thicker than the 892 Ω/sq R-card, its relative permittivity is much less

vulnerable to the value entered as the permittivity of acrylic in the root search algorithm.

An electrically thicker sample makes phase shifts caused by that sample easier to

measure. Since the shift a material puts on the phase of the scattered field is linked to the

material's reactive properties, which in turn are linked to the real part of the material's

permittivity, the discrepancy shown in Figure 4-25 is much less of a discrepancy than the

one shown in Figure 4-11.
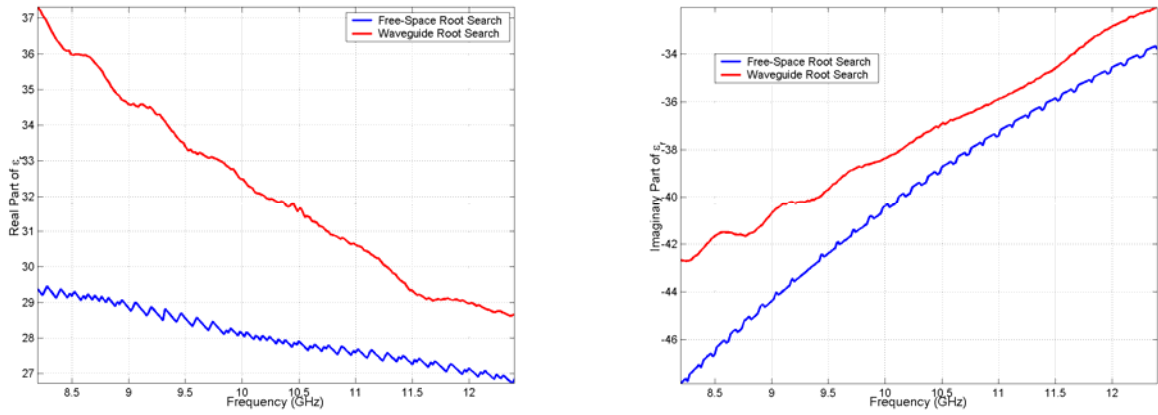
Figure 4-25. 64 Ω/sq R-card relative permittivity, free-space root search compared to the waveguide root search. On the left is the real part of the relative permittivity. On the right is the imaginary part of the relative permittivity.
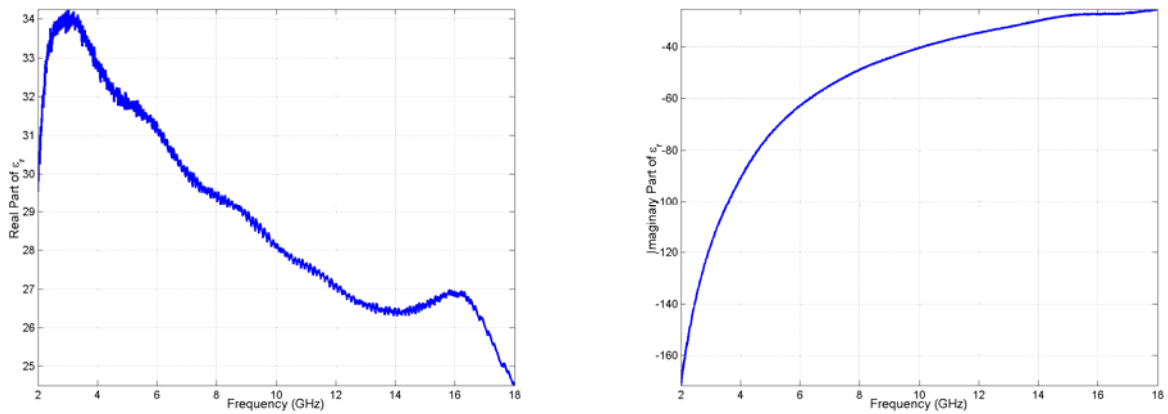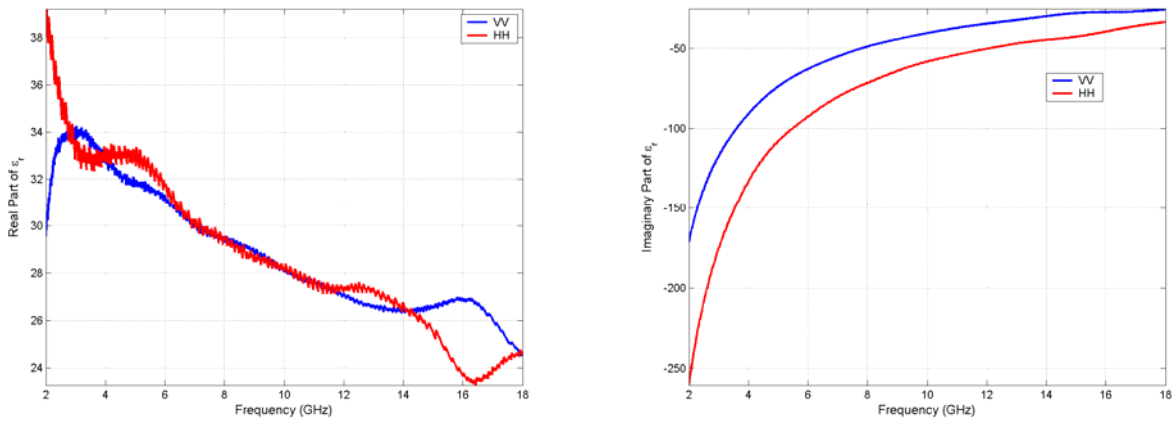

Figure 4-26. 64 Ω/sq R-card, free-space, VV and HH, relative permittivity using the free-space root search method. On the left is the real part of the relative permittivity. On the right is the imaginary part of the relative permittivity. Values are solutions to (3.11) with a 10^{-7} tolerance.
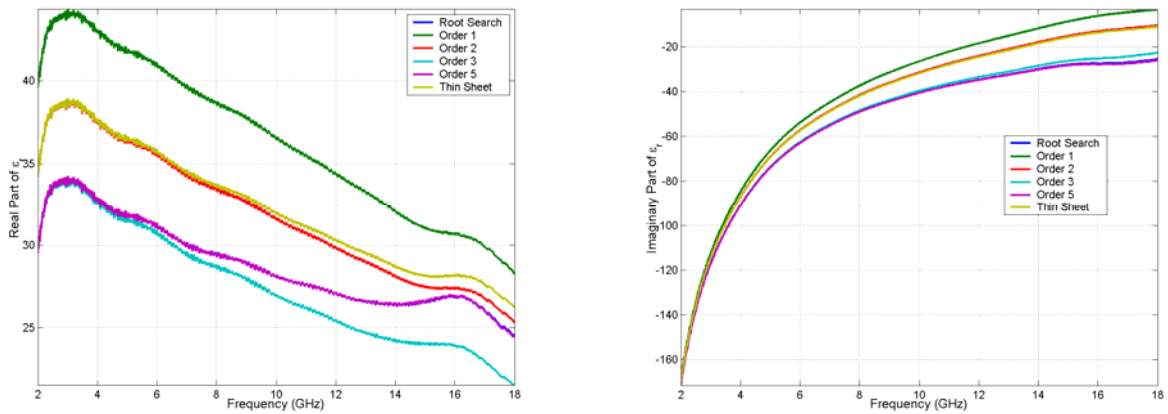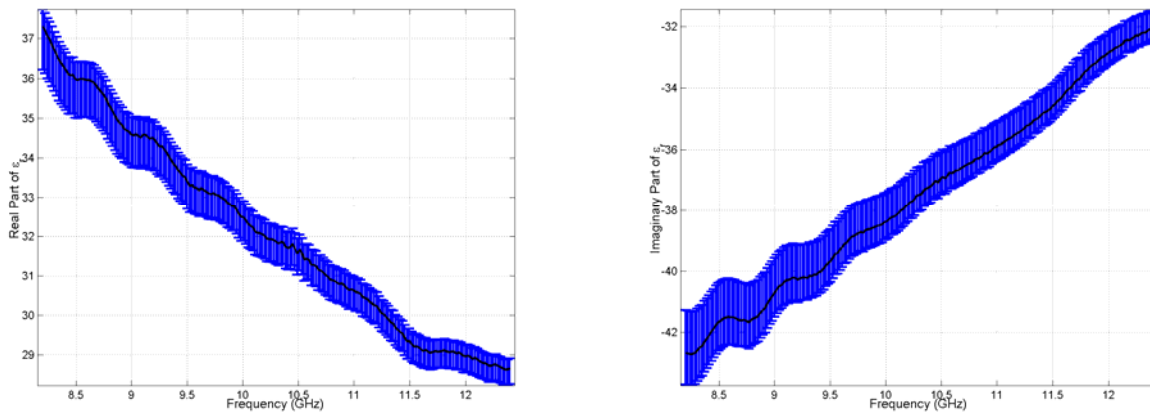
Figure 4-27. 64 Ω/sq R-card relative permittivity values obtained by the waveguide root search method when the acrylic support backing is any value within the range of Figure 4-12. On the left is the real part of the relative permittivity. On the right is the imaginary part of the relative permittivity.

The results for the 64 Ω/sq R-card using the vertical mode matching technique are very similar to those of the 892 Ω/sq R-card. Like the 892 Ω/sq R-card, layers 1 and 3 of Figures 3-5 and 3-6 were polystyrene foam (Figure 4-14). Figure 4-28 shows the results for the 64 Ω/sq R-card using 5, 10, and 15 modes of the vertical mode matching technique. This time the method produces much more accurate results for both the real and imaginary parts of the dielectric constant. The method also continues to demonstrate its stability to changes in the permittivity of foam entered in the algorithm (Figure 4-29).

Although the results are better for this R-card, the difficulty with the vertical mode matching technique lies in machining the sample. Using a material that can be compacted like foam helps with the sandwich; however, it makes it much harder to get accurate values for τ and ℓ (Figure 3-5). The good news is that like the 892 Ω/sq R-card, the results for the 64 Ω/sq R-card are pretty resistant to inaccuracies in the measurement of τ as shown in Figure 4-30. However, the same is not true for ℓ, shown

4-25

in Figure 4-31. Using a substance like acrylic for the sandwich would make it much easier to accurately measure τ and ℓ, which as a result would make the returned permittivity values more accurate. However, the sandwich would have to be machined very precisely to fully fill the waveguide (Figure 3-6).
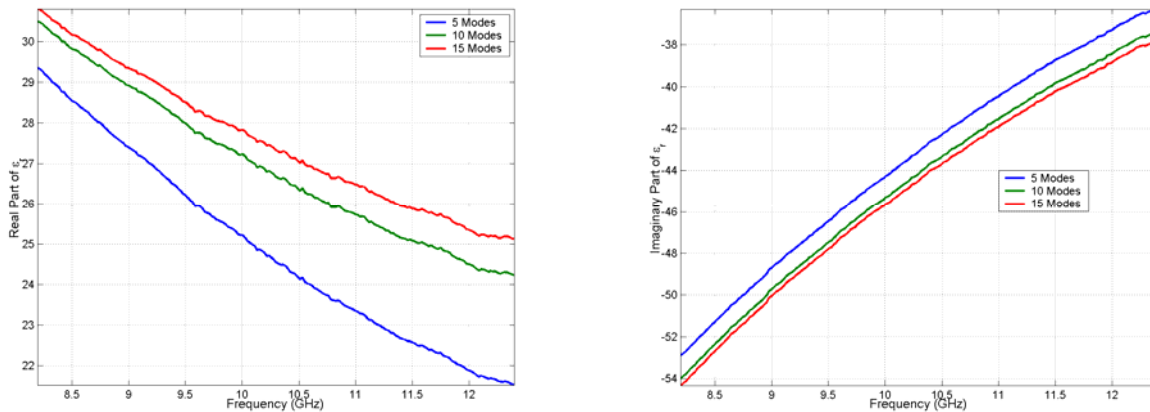
Figure 4-28. 64 Ω/sq R-card relative permittivity using 5, 10, and 15 modes of the vertical mode matching technique. On the left is the real part of the relative permittivity. On the right is the imaginary part of the relative permittivity. Values are solutions to (3.11) with a 10^{-7} tolerance.
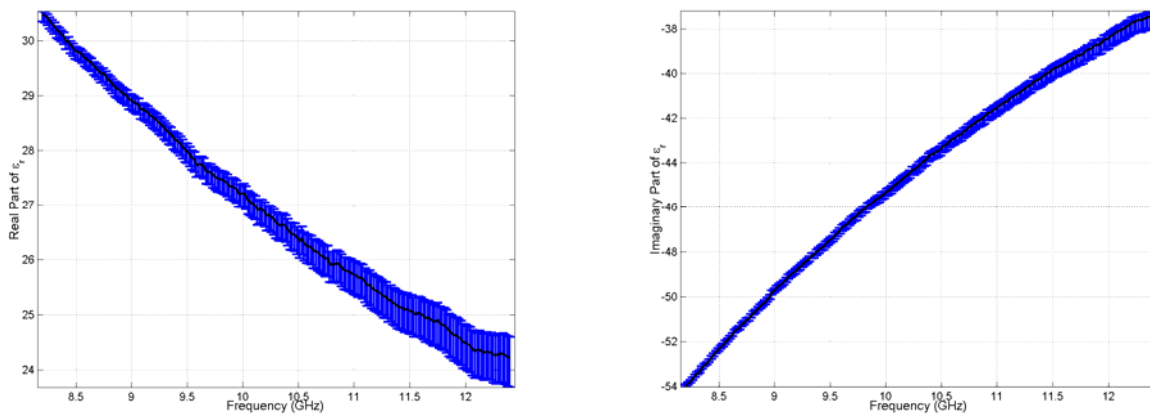
Figure 4-29. 64 Ω/sq R-card relative permittivity values obtained by the vertical mode matching technique, 10 modes, when the foam sandwich is any value within the range of Figure 4-14. On the left is the real part of the relative permittivity. On the right is the imaginary part of the relative permittivity.
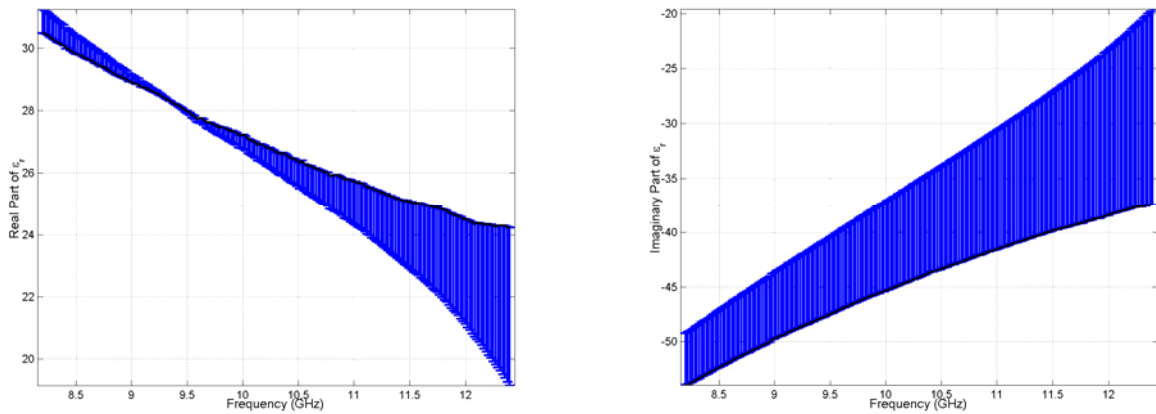
Figure 4-30. 64 Ω/sq R-card relative permittivity values obtained by the vertical mode matching technique, 10 modes, when the value of τ is changed by ± 10 %. On the left is the real part of the relative permittivity. On the right is the imaginary part of the relative permittivity.
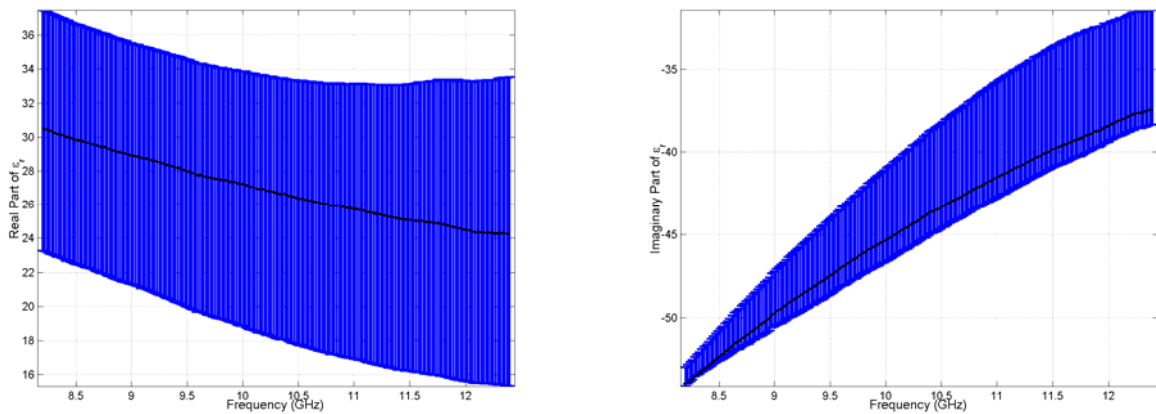
Figure 4-31. 64 Ω/sq R-card relative permittivity values obtained by the vertical mode matching technique, 10 modes, when the value of ℓ is changed by ± 10 %. On the left is the real part of the relative permittivity. On the right is the imaginary part of the relative permittivity.

4.4 Summary

When compared intra-measurement system, the *N*th order and thin sheet approximations performed as expected. The 892 Ω/sq R-card required at most only two orders to accurately converge on the solution; whereas, the 64 Ω/sq R-card, being 30 times thicker, required at least 5 orders to be accurate. When free-space data was compared to waveguide data, significant differences were discovered. It turned out that the waveguide results for the 892 Ω/sq R-card were highly dependent on the permittivity value entered for the acrylic support backing. Only a 0.5 % error in the permittivity of acrylic had a drastic impact on what the fully filled waveguide methods returned for the R-card's permittivity. The 64 Ω/sq R-card faired better in that regard; however, it did appear to be inhomogeneous. The vertical mode matching technique's results for the 892 Ω/sq R-card were fair. It produced accurate results for the R-card's loss factor (imaginary permittivity) and delivered values that were less vulnerable to the permittivity entered for the foam sandwich; however, it was unable to accurately determine the R-card's real dielectric constant. The vertical mode matching technique's results for the 64 Ω/sq R-card were better than the 892 Ω/sq R-card's. It produced accurate values for the 64 Ω/sq R-card's dielectric constant, real and imaginary. It also demonstrated the same stability to small changes in the value entered as the permittivity of the foam sandwich.

5. Conclusions and Recommendations

The problem investigated in this thesis was how to accurately determine an R-card's resistivity so that it can then be used to theoretically predict the scattering from an object utilizing an R-card. It was found that relying on a DC resistivity value provided by a four-point probe is not sufficient and material measurement techniques must be utilized to accurately account for frequency dependent reactive properties that exists in R-cards. The methods developed in chapter 3 and demonstrated in chapter 4 do exactly that. Each technique has its own strengths and weaknesses which must be taken into account when applying them.

In chapter 1 it was revealed that research into scattering prediction regarding R-cards was the impetus for this thesis, especially an RCS measurement made of the 892 Ω/sq R-card wrapped around a polystyrene foam cylinder (Figure 1-2). Using the results from free-space measurements presented in chapter 4, Figure 1-2 becomes Figure 5-1. It is evident from the figure that accounting for the R-card's reactive properties made all the difference.
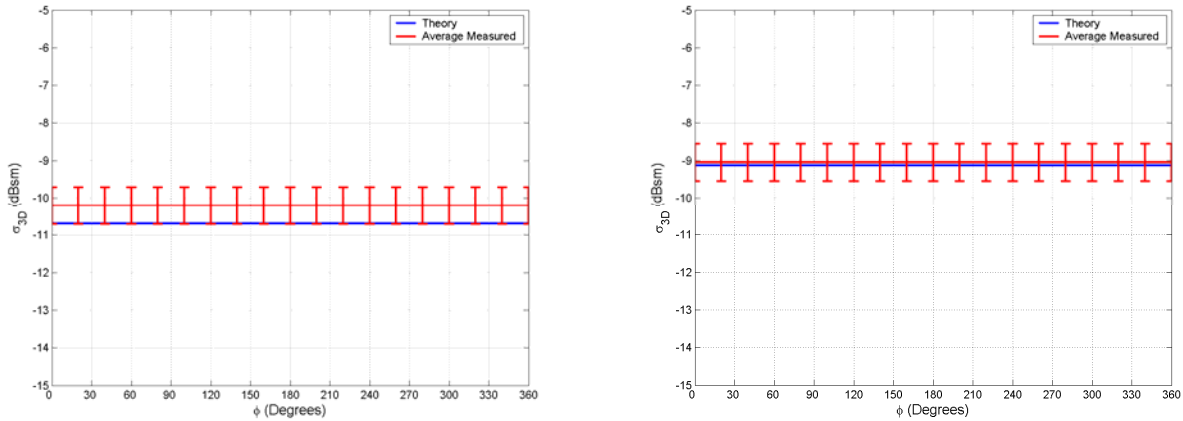
Figure 5-1. Vertical and horizontal polarization monostatic RCS plots of the 892 Ω/sq R-card. The RCS was predicted and measured at 7 GHz. In both polarizations, the theoretical RCS is within 0.5 dBsm of the measured RCS. Experience has shown a ±0.5 dBsm uncertainty in the RCS values obtained from the AFIT range.

5.1 Future Research

In regards to R-cards, one of the most interesting problems that has yet to be investigated is the flanged waveguide problem. In this problem an R-card is clamped between two waveguides that are flanged as shown in Figure 5-2. The solution of the problem involves solving two coupled magnetic field integral equations. A theoretical development of this problem would be of real benefit because of the simplicity of the actual measurement. The only requirement on the R-card sample is that it is as large as the flanges.

Other research, not necessary involving R-cards, relate to the vertical mode matching technique. It may be possible with the aid of a horizontal mode matching technique—sample lies parallel to *x*—to obtain two independent S_{21} measurements to

5-2
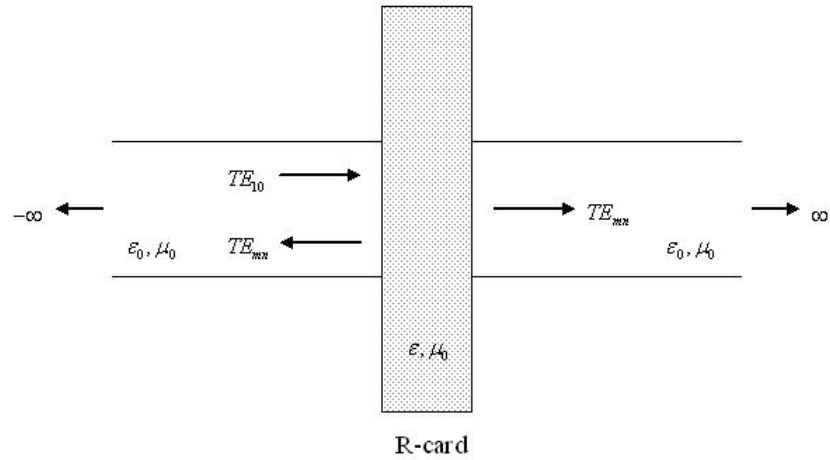
Figure 5-2. Geometry of the flanged waveguide problem.

fully characterize the permittivity and permeability of an MRAM (magnetic radar absorbing material) sample. Also, certain exotic substances require three independent measurements to determine their permittivity. It may be possible to fulfill this requirement by making a fully filled, vertical mode matching, and horizontal mode matching S_{21} measurement.

Appendix A. Integral Proofs

This appendix contains proofs for the integral relations shown in (3.84).

$$M_{nm} = \int_0^b \int_0^a \sin\left(\frac{n\pi}{a}x\right)\sin\left(\frac{m\pi}{a}x\right)dxdy = \int_0^b dy \int_0^a \sin\left(\frac{n\pi}{a}x\right)\sin\left(\frac{m\pi}{a}x\right)dx$$

$$= \frac{b}{2}\int_0^a \left[\cos\left(\frac{\pi}{a}(n-m)x\right) - \cos\left(\frac{\pi}{a}(n+m)x\right)\right]dx$$

$$= \begin{cases} \dfrac{b}{2}\displaystyle\int_0^a \left[\cos\left(\dfrac{\pi}{a}(n-m)x\right) - \cos\left(\dfrac{\pi}{a}(n+m)x\right)\right]dx & \dots n \neq m \\[2em] \dfrac{b}{2}\displaystyle\int_0^a \left[1 - \cos\left(\dfrac{2n\pi}{a}x\right)\right]dx & \dots n = m \end{cases}$$

$$= \begin{cases} \dfrac{b}{2}\dfrac{a}{\pi(n-m)}\sin\left(\dfrac{\pi}{a}(n-m)x\right)\Big|_0^a - \dfrac{b}{2}\dfrac{a}{\pi(n+m)}\sin\left(\dfrac{\pi}{a}(n+m)x\right)\Big|_0^a = 0 & \dots n \neq m \\[2em] \dfrac{b}{2}x\Big|_0^a - \dfrac{b}{2}\dfrac{a}{2n\pi}\sin\left(\dfrac{2n\pi}{a}x\right)\Big|_0^a = \dfrac{ab}{2} & \dots n = m \end{cases}$$

(A.1)

$$N_{nm} = \frac{M_{nm}}{Z_{0,m}} = \begin{cases} 0 & \dots n \neq m \\[1em] \dfrac{ab}{2Z_{0,m}} & \dots n = m \end{cases}$$

(A.2)

$$O_{nm} = \int_0^b \int_0^\tau \sin\left(\frac{n\pi}{a}x\right)\sin\left(k_{x,m}x\right)dxdy = \int_0^b dy \int_0^\tau \sin\left(\frac{n\pi}{a}x\right)\sin\left(k_{x,m}x\right)dx$$

$$= \frac{b}{2}\int_0^\tau \left[\cos\left(x\left(\frac{n\pi}{a} - k_{x,m}\right)\right) - \cos\left(x\left(\frac{n\pi}{a} + k_{x,m}\right)\right)\right]dx$$

$$= \frac{b}{2}\left(\frac{a}{n\pi - ak_{x,m}}\right)\sin\left(x\left(\frac{n\pi}{a} - k_{x,m}\right)\right)\Big|_0^\tau - \frac{b}{2}\left(\frac{a}{n\pi + ak_{x,m}}\right)\sin\left(x\left(\frac{n\pi}{a} + k_{x,m}\right)\right)\Big|_0^\tau$$

$$= \frac{b}{2}\left(\frac{a}{n\pi - ak_{x,m}}\right)\sin\tau\left(\frac{n\pi}{a} - k_{x,m}\right) - \frac{b}{2}\left(\frac{a}{n\pi + ak_{x,m}}\right)\sin\tau\left(\frac{n\pi}{a} + k_{x,m}\right)$$

(A.3)

$$P_{nm} = \int_0^b \int_\tau^{\tau+d} \sin\left(\frac{n\pi}{a}x\right)\sin\left(k_{xu,m}\left(x-\tau\right)\right)dxdy = \int_0^b dy \int_\tau^{\tau+d} \sin\left(\frac{n\pi}{a}x\right)\sin\left(k_{xu,m}\left(x-\tau\right)\right)dx \qquad \text{(A.4)}$$

$$= \frac{b}{2}\int_\tau^{\tau+d}\left[\cos\left(x\left(\frac{n\pi}{a}-k_{xu,m}\right)+k_{xu,m}\tau\right) - \cos\left(x\left(\frac{n\pi}{a}+k_{xu,m}\right)-k_{xu,m}\tau\right)\right]dx$$

$$= \frac{b}{2}\left(\frac{a}{n\pi-ak_{xu,m}}\right)\sin\left(x\left(\frac{n\pi}{a}-k_{xu,m}\right)+k_{xu,m}\tau\right)\Bigg|_\tau^{\tau+d}$$

$$-\frac{b}{2}\left(\frac{a}{n\pi+ak_{xu,m}}\right)\sin\left(x\left(\frac{n\pi}{a}+k_{xu,m}\right)-k_{xu,m}\tau\right)\Bigg|_\tau^{\tau+d}$$

$$= \frac{b}{2}\left(\frac{a}{n\pi-ak_{xu,m}}\right)\left[\sin\left(\frac{n\pi}{a}\left(\tau+d\right)-k_{xu,m}d\right) - \sin\frac{n\pi}{a}\tau\right]$$

$$-\frac{b}{2}\left(\frac{a}{n\pi+ak_{xu,m}}\right)\left[\sin\left(\frac{n\pi}{a}\left(\tau+d\right)+k_{xu,m}d\right) - \sin\frac{n\pi}{a}\tau\right]$$

$$Q_{nm} = \int_0^b \int_\tau^{\tau+d} \sin\left(\frac{n\pi}{a}x\right)\cos\left(k_{xu,m}\left(x-\tau\right)\right)dxdy = \int_0^b dy \int_\tau^{\tau+d} \sin\left(\frac{n\pi}{a}x\right)\cos\left(k_{xu,m}\left(x-\tau\right)\right)dx \qquad \text{(A.5)}$$

$$= \frac{b}{2}\int_\tau^{\tau+d}\left[\sin\left(x\left(\frac{n\pi}{a}+k_{xu,m}\right)-k_{xu,m}\tau\right) + \sin\left(x\left(\frac{n\pi}{a}-k_{xu,m}\right)+k_{xu,m}\tau\right)\right]dx$$

$$= \frac{b}{2}\left(\frac{a}{n\pi+ak_{xu,m}}\right)\left[-\cos\left(x\left(\frac{n\pi}{a}+k_{xu,m}\right)-k_{xu,m}\tau\right)\right]_\tau^{\tau+d}$$

$$+\frac{b}{2}\left(\frac{a}{n\pi-ak_{xu,m}}\right)\left[-\cos\left(x\left(\frac{n\pi}{a}-k_{xu,m}\right)+k_{xu,m}\tau\right)\right]_\tau^{\tau+d}$$

$$= \frac{b}{2}\left(\frac{a}{n\pi+ak_{xu,m}}\right)\left[\cos\frac{n\pi}{a}\tau - \cos\left(\frac{n\pi}{a}\left(\tau+d\right)+k_{xu,m}d\right)\right]$$

$$+\frac{b}{2}\left(\frac{a}{n\pi-ak_{xu,m}}\right)\left[\cos\frac{n\pi}{a}\tau - \cos\left(\frac{n\pi}{a}\left(\tau+d\right)-k_{xu,m}d\right)\right]$$

$$R_{nm} = \int\limits_{0}^{b} \int\limits_{\tau+d}^{a} \sin\left(\frac{n\pi}{a}x\right) \sin\left(k_{x,m}\left(a-x\right)\right) dx dy = \int\limits_{0}^{b} dy \int\limits_{\tau+d}^{a} \sin\left(\frac{n\pi}{a}x\right) \sin\left(k_{x,m}\left(a-x\right)\right) dx \qquad (A.6)$$

$$= \frac{b}{2} \int\limits_{\tau+d}^{a} \left[\cos\left(x\left(\frac{n\pi}{a}+k_{x,m}\right)-k_{x,m}a\right) - \cos\left(x\left(\frac{n\pi}{a}-k_{x,m}\right)+k_{x,m}a\right) \right] dx$$

$$= \frac{b}{2}\left(\frac{a}{n\pi+ak_{x,m}}\right) \sin\left(x\left(\frac{n\pi}{a}+k_{x,m}\right)-k_{x,m}a\right)\Bigg|_{\tau+d}^{a}$$

$$- \frac{b}{2}\left(\frac{a}{n\pi-ak_{x,m}}\right) \sin\left(x\left(\frac{n\pi}{a}-k_{x,m}\right)+k_{x,m}a\right)\Bigg|_{\tau+d}^{a}$$

$$= \frac{b}{2}\left(\frac{a}{n\pi-ak_{x,m}}\right) \sin\left(\frac{n\pi}{a}\left(\tau+d\right)+k_{x,m}\left(a-\tau-d\right)\right)$$

$$- \frac{b}{2}\left(\frac{a}{n\pi+ak_{x,m}}\right) \sin\left(\frac{n\pi}{a}\left(\tau+d\right)+k_{x,m}\left(\tau+d-a\right)\right)$$

Appendix B. Matlab Code

This appendix contains the `Matlab`® code used to analyze measured data.

B.1 Free-Space

B.1.1 Root Search Method.

```
function [parameters] = Newton1DSearchFS(permi, thick, maxGuess, precision)
%
% [parameters] = Newton1DSearchFS(permi, thick, maxGuess, precision)
%
% Newton1DSearchFS returns the relative permittivity and resistance of an
%   unknown material layer
%   SPECIFICALLY WRITTEN FOR FREE-SPACE MEASUREMENTS
%   1D ROOT SEARCH - RELATIVE PERMEABILITY ASSUMED TO BE FREE-SPACE
%   ASSUMES MEASURED SYSTEM DATA IS NAMED:
%       s21sample.txt
%
% ------------------------
%        |        |
%   Air  | Layer  | Air
%        |        |
% ------------------------
%        |- thick -|
%
% permi = permittivity value of the layer shown in the diagram
%    THE VALUE FOR THE UNKNOWN LAYER WILL BE THE INITIAL GUESS
% thick = thickness of the layer shown in the diagram in METERS
% maxGuess = maximum number of root search iterations
% precision = precision of root

% close all;
clc;

%%%%%%%%%%%%%%%%%%%%%%%% Measured Data Filenames %%%%%%%%%%%%%%%%%%%%%%%
load s21sample.txt;
freq = s21sample(:,1)*1e9;
%%%%%%%%%%%%%%%%%%%%%%%%%%%%%%%%%%%%%%%%%%%%%%%%%%%%%%%%%%%%%%%%%%%%%%%%%%
%%%%%%%%%%%%%%%%%%%%%%%%%%% S21_exp %%%%%%%%%%%%%%%%%%%%%%%%%%%%%%%%%%%%%%
s21samplea = s21sample(:,2);
s21sampleb = s21sample(:,3);
s21samplesys = complex(s21samplea,s21sampleb);
%%%%%%%%%%%%%%%%%%%%%%%%%%%%%%%%%%%%%%%%%%%%%%%%%%%%%%%%%%%%%%%%%%%%%%%%%%
%%%%%%%%%%%%%%%%%%%%%%%% Constants %%%%%%%%%%%%%%%%%%%%%%%%%%%%%%%%%%%%%%
u0 = 4*pi*10^-7;
e0 = 8.854e-12;
c = 1/sqrt(e0*u0);

w = 2*pi*freq;
k0 = w/c;
%%%%%%%%%%%%%%%%%%%%%%%%%%%%%%%%%%%%%%%%%%%%%%%%%%%%%%%%%%%%%%%%%%%%%%%%%%
%%%%%%%%%%%%%%%%%%%%%%%%%%%%%%%%%%%%%%%%%%%%%%%%%%%%%%%%%%%%%%%%%%%%%%%%%%
s21sys_exp = s21samplesys.*exp(-j*k0*thick);
%%%%%%%%%%%%%%%%%%%%%%%%%%%%%%%%%%%%%%%%%%%%%%%%%%%%%%%%%%%%%%%%%%%%%%%%%%
%%%%%%%%%%%%%%%%%%%%%%% 1D Newton Root Search %%%%%%%%%%%%%%%%%%%%%%%%%%%
permi(1:length(freq)) = permi;
for counFreq=1:length(freq)
    prog_str = ['Processing frequency ' num2str(counFreq) ' of ' ...
            num2str(length(freq)) ' ...'];
    disp(prog_str);
    guesses = 1;
```

```
%%%%%%%%%%%%%%%%%%%%% S21 %%%%%%%%%%%%%%%%%%%%%%%%%%%%%%%%%%%%%%%%%%
    while guesses <= maxGuess
        del_e_r = precision*permi(counFreq);
        R1 = (sqrt(u0/(e0*permi(counFreq))) - sqrt(u0/e0))/ ...
            (sqrt(u0/(e0*permi(counFreq))) + sqrt(u0/e0));
        R2 = -R1;
        T1 = 1+R1;
        T2 = 1+R2;
        A = 1/(T1*T2)*[exp(j*k0(counFreq)*sqrt(permi(counFreq))*thick) ...
                R1*exp(-j*k0(counFreq)*sqrt(permi(counFreq))*thick); ...
                R1*exp(j*k0(counFreq)*sqrt(permi(counFreq))*thick) ...
                exp(-j*k0(counFreq)*sqrt(permi(counFreq))*thick)] ...
            *[1 R2;R2 1];
        s21sys_thy = 1/A(1,1);
        R1 = (sqrt(u0/(e0*(permi(counFreq)+del_e_r))) - sqrt(u0/e0))/ ...
            (sqrt(u0/(e0*(permi(counFreq)+del_e_r))) + sqrt(u0/e0));
        R2 = -R1;
        T1 = 1+R1;
        T2 = 1+R2;
        A = 1/(T1*T2)*[exp(j*k0(counFreq)*sqrt(permi(counFreq)+del_e_r)*thick) ...
                R1*exp(-j*k0(counFreq)*sqrt(permi(counFreq)+del_e_r)*thick); ...
                R1*exp(j*k0(counFreq)*sqrt(permi(counFreq)+del_e_r)*thick) ...
                exp(-j*k0(counFreq)*sqrt(permi(counFreq)+del_e_r)*thick)] ...
            *[1 R2;R2 1];
        s21sys_thy_d = (1/A(1,1)-s21sys_thy)/del_e_r;
        if abs((s21sys_thy-s21sys_exp(counFreq))/s21sys_thy_d) <= precision
            break;
        end
        permi(counFreq) = permi(counFreq) - ...
            (s21sys_thy-s21sys_exp(counFreq))/s21sys_thy_d;
        guesses = guesses + 1;
    end
end
permi = permi.';
R = -j*sqrt(u0/e0)./(k0*thick.*(permi-1));
parameters = [permi R];
DispResults(parameters, freq);
end
%%%%%%%%%%%%%%%%%%%%%%%%%%%%%%%%%%%%%%%%%%%%%%%%%%%%%%%%%%%%%%%%%%%%
function DispResults(parameters, freq)
e_r = parameters(:,1);
R = parameters(:,2);
title_str = 'S_2_1^S^Y^S^,^T^H^Y(\epsilon_r,\omega) - S_2_1^S^Y^S^,^E^X^P(\omega) = 0';
figure;
subplot(221);
plot(freq/1e9,real(e_r),'linewidth',2);
title(title_str,'fontsize',12);
xlabel('Frequency (GHz)','fontsize',12);
ylabel('Real Part of \epsilon_r','fontsize',12,'fontweight','bold');
axis tight;
grid on;
subplot(223);
plot(freq/1e9,imag(e_r),'linewidth',2);
title(title_str,'fontsize',12);
xlabel('Frequency (GHz)','fontsize',12);
ylabel('Imaginary Part of \epsilon_r','fontsize',12,'fontweight','bold');
axis tight;
grid on;
subplot(222);
plot(freq/1e9,real(R),'linewidth',2);
title(title_str,'fontsize',12);
xlabel('Frequency (GHz)','fontsize',12);
ylabel('Real Part of R','fontsize',12,'fontweight','bold');
axis tight;
grid on;
subplot(224);
plot(freq/1e9,imag(R),'linewidth',2);
title(title_str,'fontsize',12);
xlabel('Frequency (GHz)','fontsize',12);
```

```
ylabel('Imaginary Part of R','fontsize',12,'fontweight','bold');
axis tight;
grid on;
end
```

B.1.2 Nth Order Approximation.

```
function R = OrderApproxFS(order, thick)
%
% R = OrderApproxFS(order, thick)
%
% OrderApprox returns the relative permittivity and resistivity of a sample
%   using an Nth order Maclaurin series approximation
%   SPECIFICALLY WRITTEN FOR FREE-SPACE MEASUREMENTS
%   ASSUMES MEASURED SYSTEM DATA IS NAMED:
%     s21sample.txt
%
% ----------------------
%   |        |
%  Air | Layer   | Air
%   |        |
% ----------------------
%       |- thick -|
%
% order = degree of Maclaurin polynomial retained to formulate
%   approximation
% thick = thickness of the layer shown in the diagram in METERS

% close all;
clc;

%%%%%%%%%%%%%%%%%%%%%%%% Measured Data Filenames %%%%%%%%%%%%%%%%%%%%%%%
load s21sample.txt;
freq = s21sample(:,1)*1e9;
%%%%%%%%%%%%%%%%%%%%%%%%%%%%%%%%%%%%%%%%%%%%%%%%%%%%%%%%%%%%%%%%%%%%%%%%%%
%%%%%%%%%%%%%%%%%%%%%%%% S21_exp %%%%%%%%%%%%%%%%%%%%%%%%%%%%%%%%%%%%%%%%%
s21samplea = s21sample(:,2);
s21sampleb = s21sample(:,3);
s21samplesys = complex(s21samplea,s21sampleb);
%%%%%%%%%%%%%%%%%%%%%%%%%%%%%%%%%%%%%%%%%%%%%%%%%%%%%%%%%%%%%%%%%%%%%%%%%%
%%%%%%%%%%%%%%%%%%%%%%%% Constants %%%%%%%%%%%%%%%%%%%%%%%%%%%%%%%%%%%%%%%
u0 = 4*pi*10^-7;
e0 = 8.854e-12;
N0 = sqrt(u0/e0);
c = 1/sqrt(e0*u0);
w = 2*pi*freq;
k0 = w/c;
%%%%%%%%%%%%%%%%%%%%%%%%%%%%%%%%%%%%%%%%%%%%%%%%%%%%%%%%%%%%%%%%%%%%%%%%%%
%%%%%%%%%%%%%%%%%%%%%%%%%%%%%%%%%%%%%%%%%%%%%%%%%%%%%%%%%%%%%%%%%%%%%%%%%%
s21sys_exp = s21samplesys.*exp(-j*k0*thick);
%%%%%%%%%%%%%%%%%%%%%%%%%%%%%%%%%%%%%%%%%%%%%%%%%%%%%%%%%%%%%%%%%%%%%%%%%%
%%%%%%%%%%%%%%%%%%%%%%%% Nth Order Approx %%%%%%%%%%%%%%%%%%%%%%%%%%%%%%%%
p(:,1) = -2./s21sys_exp+2+j*w*thick/c;
if mod(order,2) ~= 0
    m = floor(order/2) + 1;
    for i = 1:m
        if i == m
            p(:,i+1) = j*(-1)^(m-1)/factorial(2*m-1)*(w*thick/c).^(2*m-1);
        else
            p(:,i+1) = j*(-1)^(i-1)/factorial(2*i-1)*(w*thick/c).^(2*i-1) ...
                + 2*(-1)^(i)/factorial(2*i)*(w*thick/c).^(2*i) ...
                + j*(-1)^(i)/factorial(2*i+1)*(w*thick/c).^(2*i+1);
        end
    end
    p = fliplr(p);
    for i=1:length(p(:,1))
        tmpe_r(i,:) = roots(p(i,:)).';
```

```
        end
    for i=1:length(tmpe_r(:,1))
        for n=1:length(tmpe_r(i,:))
            if imag(tmpe_r(i,n)) <= 0
                e_r(i,1) = tmpe_r(i,n);
            end
        end
    end
else
    m = order/2;
    for i = 1:m
        if i == m
            p(:,i+1) = j*(-1)^(m-1)/factorial(2*m-1)*(w*thick/c).^(2*m-1) ...
                + 2*(-1)^(m)/factorial(2*m)*(w*thick/c).^(2*m);
        else
            p(:,i+1) = j*(-1)^(i-1)/factorial(2*i-1)*(w*thick/c).^(2*i-1) ...
                + 2*(-1)^(i)/factorial(2*i)*(w*thick/c).^(2*i) ...
                + j*(-1)^(i)/factorial(2*i+1)*(w*thick/c).^(2*i+1);
        end
    end
    p = fliplr(p);
    for i=1:length(p(:,1))
        tmpe_r(i,:) = roots(p(i,:)).';
    end
    for i=1:length(tmpe_r(:,1))
        for n=1:length(tmpe_r(i,:))
            if imag(tmpe_r(i,n)) <= 0
                e_r(i,1) = tmpe_r(i,n);
            end
        end
    end
end
Re = -j*N0./(k0*thick.*(e_r-1));
title_str = ['Order ' num2str(order) ' Maclaurin Approximation - Free-Space'];
R = [e_r, Re];
figure;
subplot(221);
plot(freq/1e9,real(e_r),'linewidth',2);
title(title_str,'fontsize',12);
xlabel('Frequency (GHz)','fontsize',12);
ylabel('Real Part of \epsilon_r','fontsize',12,'fontweight','bold');
axis tight;
grid on;
subplot(223);
plot(freq/1e9,imag(e_r),'linewidth',2);
title(title_str,'fontsize',12);
xlabel('Frequency (GHz)','fontsize',12);
ylabel('Imaginary Part of \epsilon_r','fontsize',12,'fontweight','bold');
axis tight;
grid on;
subplot(222);
plot(freq/1e9,real(Re),'linewidth',2);
title(title_str,'fontsize',12);
xlabel('Frequency (GHz)','fontsize',12);
ylabel('Real Part of R_e','fontsize',12,'fontweight','bold');
axis tight;
grid on;
subplot(224);
plot(freq/1e9,imag(Re),'linewidth',2);
title(title_str,'fontsize',12);
xlabel('Frequency (GHz)','fontsize',12);
ylabel('Imaginary Part of R_e','fontsize',12,'fontweight','bold');
axis tight;
grid on;
end
```

B.1.3 Thin Sheet Approximation.

```
function R = ResistiveFS(thick)
%
% R = ResistiveFS(thick)
%
% ResistiveFS returns the relative permittivity and resistivity of a sample
%   using resistive boundary conditions
%   SPECIFICALLY WRITTEN FOR FREE-SPACE MEASUREMENTS
%   ASSUMES MEASURED SYSTEM DATA IS NAMED:
%     s21sample.txt
%
% -----------------------
%     |         |
%  Air | Layer   | Air
%     |         |
% -----------------------
%       |- thick -|
%
% thick = thickness of the layer shown in the diagram in METERS

% close all;
clc;

%%%%%%%%%%%%%%%%%%%%%%% Measured Data Filenames %%%%%%%%%%%%%%%%%%%%%%
load s21sample.txt;
freq = s21sample(:,1)*1e9;
%%%%%%%%%%%%%%%%%%%%%%%%%%%%%%%%%%%%%%%%%%%%%%%%%%%%%%%%%%%%%%%%%%%%%%
%%%%%%%%%%%%%%%%%%%%%%%%%%%%%% S21_exp %%%%%%%%%%%%%%%%%%%%%%%%%%%%%%%%
s21samplea = s21sample(:,2);
s21sampleb = s21sample(:,3);
s21samplesys = complex(s21samplea,s21sampleb);
%%%%%%%%%%%%%%%%%%%%%%%%%%%%%%%%%%%%%%%%%%%%%%%%%%%%%%%%%%%%%%%%%%%%%%
%%%%%%%%%%%%%%%%%%%%%%%%%%% Constants %%%%%%%%%%%%%%%%%%%%%%%%%%%%%%%%%
u0 = 4*pi*10^-7;
e0 = 8.854e-12;
N0 = sqrt(u0/e0);
c = 1/sqrt(e0*u0);
w = 2*pi*freq;
k0 = w/c;
%%%%%%%%%%%%%%%%%%%%%%%%%%%%%%%%%%%%%%%%%%%%%%%%%%%%%%%%%%%%%%%%%%%%%%
%%%%%%%%%%%%%%%%%%%%%%%%%%%%%%%%%%%%%%%%%%%%%%%%%%%%%%%%%%%%%%%%%%%%%%
s21sys_exp = s21samplesys;
%%%%%%%%%%%%%%%%%%%%%%%%%%%%%%%%%%%%%%%%%%%%%%%%%%%%%%%%%%%%%%%%%%%%%%
%%%%%%%%%%%%%%%%%%%%%%%%% Thin Sheet Approx %%%%%%%%%%%%%%%%%%%%%%%%%%%
Re = s21sys_exp*N0./(2 - 2*s21sys_exp);
e_r = (-j*N0 + Re.*k0*thick)./(Re.*k0*thick);
R = [e_r, Re];
figure;
subplot(221);
plot(freq/1e9,real(e_r),'linewidth',2);
title_str = 'Resistive Boundary Condition - Free-Space';
title(title_str,'fontsize',12);
xlabel('Frequency (GHz)','fontsize',12);
ylabel('Real Part of \epsilon_r','fontsize',12,'fontweight','bold');
axis tight;
grid on;
subplot(223);
plot(freq/1e9,imag(e_r),'linewidth',2);
title(title_str,'fontsize',12);
xlabel('Frequency (GHz)','fontsize',12);
ylabel('Imaginary Part of \epsilon_r','fontsize',12,'fontweight','bold');
axis tight;
grid on;
subplot(222);
plot(freq/1e9,real(Re),'linewidth',2);
title(title_str,'fontsize',12);
xlabel('Frequency (GHz)','fontsize',12);
```

```
ylabel('Real Part of R_e','fontsize',12,'fontweight','bold');
axis tight;
grid on;
subplot(224);
plot(freq/1e9,imag(Re),'linewidth',2);
title(title_str,'fontsize',12);
xlabel('Frequency (GHz)','fontsize',12);
ylabel('Imaginary Part of R_e','fontsize',12,'fontweight','bold');
axis tight;
grid on;
end
```

B.2 Waveguide

B.2.1 Root Search Method.

```
function [parameters] = Newton1DSearchWG(numLayers, unkLayer, ...
    permi_vec, perme_vec, thick_vec, a, maxGuess, precision)
%
% [parameters] = Newton1DSearchWG(numLayers, unkLayer, ...
%   permi_vec, perme_vec, thick_vec, a, maxGuess, precision)
%
% Newton1D2DSearchWG returns the relative permittivity and permeability of an
%   unknown material layer in a stack of known layers.
%   SPECIFICALLY WRITTEN FOR WAVEGUIDE MEASUREMENTS
%   ASSUMES MEASURED SYSTEM DATA IS NAMED:
%     s21sample.txt
%
% ----------------------------------------------------------------------
%      |         |         |     |         |     |         |
%      |         |         |     |         |     |         |
%      |         |         |     |         |     |         |
%   Air | Layer 1 | Layer 2 | ... | Layer n | ... | Layer N | Air
%      |         |         |     |         |     |         |
%      |         |         |     |         |     |         |
%      |         |         |     |         |     |         |
%      |         |         |     |         |     |         |
% ----------------------------------------------------------------------
%      |-thick 1-|-thick 2-|     |-thick n-|     |-thick N-|
%
% numLayers = number of layers including unknown layer
% unkLayer = layer number of the unknown material
% permi_vec = a vector of the permittivity values of the layers in the
%   order shown in the diagram
%   THE VALUE FOR THE UNKNOWN LAYER WILL BE THE INITIAL GUESS
% perme_vec = a vector of the permeability values of the layers in the
%   order shown in the diagram
%   THE VALUE ENTERED FOR THE UNKNOWN LAYER WILL BE
%     ASSUMED TO BE TRUE
% thick_vec = a vector of the thicknesses of the layers in the order shown
%   in the diagram in METERS
% a = longest dimension of the rectangular waveguide in METERS
% maxGuess = maximum number of root search iterations
% precision = precision of root

% close all;
clc;
warning off all;

%%%%%%%%%%%%%%%%%%%%%%%% Measured Data Filenames %%%%%%%%%%%%%%%%%%%%%
load s21sample.txt;

freq = s21sample(:,3);
%%%%%%%%%%%%%%%%%%%%%%%%%%%%%%%%%%%%%%%%%%%%%%%%%%%%%%%%%%%%%%%%%%%%%%%%
%%%%%%%%%%%%%%%%%%%%%%%% S21_exp %%%%%%%%%%%%%%%%%%%%%%%%%%%%%%%%%%%%%%%
```

B-6

```matlab
    s21samplea = s21sample(:,1);
    s21sampleb = s21sample(:,2);
    s21samplesys = complex(s21samplea,s21sampleb);
    %%%%%%%%%%%%%%%%%%%%%%%%%%%%%%%%%%%%%%%%%%%%%%%%%%%%%%%%%%%%%%%%%%%%%%
    %%%%%%%%%%%%%%%%%%%%%%%%%% System Length %%%%%%%%%%%%%%%%%%%%%%%%%%%%%%
    d_system = sum(thick_vec);
    %%%%%%%%%%%%%%%%%%%%%%%%%%%%%%%%%%%%%%%%%%%%%%%%%%%%%%%%%%%%%%%%%%%%%%
    %%%%%%%%%%%%%%%%%%%%%%%%%% Constants %%%%%%%%%%%%%%%%%%%%%%%%%%%%%%%%%%%
    u0 = 4*pi*10^-7;
    e0 = 8.854e-12;
    c = 1/sqrt(e0*u0);

    w = 2*pi*freq;
    ko = w/c;
    kc = pi/a;
    kz = sqrt(ko.^2-kc^2);
    %%%%%%%%%%%%%%%%%%%%%%%%%%%%%%%%%%%%%%%%%%%%%%%%%%%%%%%%%%%%%%%%%%%%%%
    %%%%%%%%%%%%%%%%%%%%%%%%%%%%%%%%%%% %%%%%%%%%%%%%%%%%%%%%%%%%%%%%%%%%%%
    s21sys_exp = s21samplesys.*exp(-j*kz*d_system);
    %%%%%%%%%%%%%%%%%%%%%%%%%%%%%%%%%%%%%%%%%%%%%%%%%%%%%%%%%%%%%%%%%%%%%%
    %%%%%%%%%%%%%%%%%%%%%%%%% 1D Newton Root Search %%%%%%%%%%%%%%%%%%%%%%%
    permi_vec = repmat(permi_vec,length(freq),1);
    perme_vec = repmat(perme_vec,length(freq),1);
    for counFreq=1:length(freq)
        prog_str = ['Processing frequency ' num2str(counFreq) ' of ' ...
                num2str(length(freq)) ' ...'];
        disp(prog_str);
        guesses = 1;
    %%%%%%%%%%%%%%%%%%%%%%%%% S21 %%%%%%%%%%%%%%%%%%%%%%%%%%%%%%%%%%%%%%%%
        while guesses < maxGuess
            del_e_r = precision*permi_vec(counFreq, unkLayer);
            A = A_Matrix_Total(numLayers, unkLayer, kc, ko, permi_vec, ...
                perme_vec, thick_vec, w, counFreq, 1, 0, 0);
            s21sys_thy = 1/A(1,1);
            A = A_Matrix_Total(numLayers, unkLayer, kc, ko, permi_vec, ...
                perme_vec, thick_vec, w, counFreq, 2, del_e_r, 0);
            s21sys_thy_d = (1/A(1,1)-s21sys_thy)/del_e_r;
            if abs((s21sys_thy-s21sys_exp(counFreq))/s21sys_thy_d) <= precision
                break;
            end
            permi_vec(counFreq,unkLayer) = permi_vec(counFreq,unkLayer) - ...
                (s21sys_thy-s21sys_exp(counFreq))/s21sys_thy_d;
            guesses = guesses + 1;
        end
    end
    %%%%%%%%%%%%%%%%%%%%%%%%%%%%%%%%%%%%%%%%%%%%%%%%%%%%%%%%%%%%%%%%%%%%%%
    Re = -j*sqrt(u0/e0)./(ko*thick_vec(unkLayer).*(permi_vec(:,unkLayer)-1));
    parameters = [permi_vec(:,unkLayer) Re];
    DispResults(parameters, freq);
    end

    function [A] = A_Matrix_Total(numLayers, unkLayer, kc, ko, permi_vec, ...
        perme_vec, thick_vec, w, counFreq, option, del_e_r, del_u_r)
    A = eye(2,2);
    switch option
        case 1
            for counLay = 1:numLayers+1
                if counLay == 1
                    A = A*A_Matrix(kc, ko(counFreq), [1 permi_vec(counFreq,counLay)], ...
                        [1 perme_vec(counFreq,counLay)], thick_vec(counLay), ...
                        w(counFreq));
                elseif counLay == numLayers+1
                    A = A*A_Matrix(kc, ko(counFreq), [permi_vec(counFreq,counLay-1) 1], ...
                        [perme_vec(counFreq,counLay-1) 1], 0, ...
                        w(counFreq));
                else
                    A = A*A_Matrix(kc, ko(counFreq), ...
                        [permi_vec(counFreq,counLay-1) permi_vec(counFreq,counLay)], ...
                        [perme_vec(counFreq,counLay-1) perme_vec(counFreq,counLay)], ...
```

B-7

```
                        thick_vec(counLay), w(counFreq));
                end
            end
        case 2
            for counLay = 1:numLayers+1
                if counLay == 1 && counLay == unkLayer
                    A = A*A_Matrix(kc, ko(counFreq), ...
                        [1 permi_vec(counFreq,counLay)+del_e_r], ...
                        [1 perme_vec(counFreq,counLay)+del_u_r], thick_vec(counLay), ...
                        w(counFreq));
                elseif counLay == 1 && counLay ~= unkLayer
                    A = A*A_Matrix(kc, ko(counFreq), ...
                        [1 permi_vec(counFreq,counLay)], ...
                        [1 perme_vec(counFreq,counLay)], thick_vec(counLay), ...
                        w(counFreq));
                elseif counLay == numLayers+1 && counLay - 1 == unkLayer
                    A = A*A_Matrix(kc, ko(counFreq), ...
                        [permi_vec(counFreq,counLay-1)+del_e_r 1], ...
                        [perme_vec(counFreq,counLay-1)+del_u_r 1], 0, ...
                        w(counFreq));
                elseif counLay == numLayers+1 && counLay - 1 ~= unkLayer
                    A = A*A_Matrix(kc, ko(counFreq), ...
                        [permi_vec(counFreq,counLay-1) 1], ...
                        [perme_vec(counFreq,counLay-1) 1], 0, ...
                        w(counFreq));
                elseif counLay - 1 == unkLayer
                    A = A*A_Matrix(kc, ko(counFreq), ...
                        [permi_vec(counFreq,counLay-1)+del_e_r ...
                            permi_vec(counFreq,counLay)], ...
                        [perme_vec(counFreq,counLay-1)+del_u_r ...
                            perme_vec(counFreq,counLay)], ...
                        thick_vec(counLay), w(counFreq));
                elseif counLay == unkLayer
                    A = A*A_Matrix(kc, ko(counFreq), ...
                        [permi_vec(counFreq,counLay-1) ...
                            permi_vec(counFreq,counLay)+del_e_r], ...
                        [perme_vec(counFreq,counLay-1) ...
                            perme_vec(counFreq,counLay)+del_u_r], ...
                        thick_vec(counLay), w(counFreq));
                else
                    disp('Forgot a case');
                    return;
                end
            end
        otherwise
            disp('Improper Choice')
            return;
end
end

function [B] = A_Matrix(kc, ko, e_r, u_r, len, w)
%%%%%%%%%%%%%%%%%%%%%% Constants %%%%%%%%%%%%%%%%%%%%%%%%%%%%%%%%%%%
u0 = 4*pi*10^-7;
e0 = 8.854e-12;
%%%%%%%%%%%%%%%%%%%%%%%%%%%%%%%%%%%%%%%%%%%%%%%%%%%%%%%%%%%%%%%%%%%%%%
gamma1 = sqrt(kc^2 - ko^2*e_r(1)*u_r(1));
gamma2 = sqrt(kc^2 - ko^2*e_r(2)*u_r(2));
Za = w*u0*u_r(1)/(gamma1/j);
Zb = w*u0*u_r(2)/(gamma2/j);
R = (Zb-Za)/(Zb+Za);
T = 1 + R;
B = 1/T*[exp(gamma2*len) R*exp(-gamma2*len);R*exp(gamma2*len) exp(-gamma2*len)];
end

function DispResults(parameters, freq)
e_r = parameters(:,1);
Re = parameters(:,2);
title_str = 'S_2_1^S^Y^S^,^T^H^Y(\epsilon_r,\omega) - S_2_1^S^Y^S^,^E^X^P(\omega) = 0';
figure;
```

```
subplot(221);
plot(freq/1e9,real(e_r),'linewidth',2);
title(title_str,'fontsize',12);
xlabel('Frequency (GHz)','fontsize',12);
ylabel('Real Part of \epsilon_r','fontsize',12,'fontweight','bold');
axis tight;
grid on;
subplot(223);
plot(freq/1e9,imag(e_r),'linewidth',2);
title(title_str,'fontsize',12);
xlabel('Frequency (GHz)','fontsize',12);
ylabel('Imaginary Part of \epsilon_r','fontsize',12,'fontweight','bold');
axis tight;
grid on;
subplot(222);
plot(freq/1e9,real(Re),'linewidth',2);
title(title_str,'fontsize',12);
xlabel('Frequency (GHz)','fontsize',12);
ylabel('Real Part of R_e','fontsize',12,'fontweight','bold');
axis tight;
grid on;
subplot(224);
plot(freq/1e9,imag(Re),'linewidth',2);
title(title_str,'fontsize',12);
xlabel('Frequency (GHz)','fontsize',12);
ylabel('Imaginary Part of R_e','fontsize',12,'fontweight','bold');
axis tight;
grid on;
end
```

B.2.2 Nth Order Approximation.

```
function R = OrderApproxWG(order, thick_vec, backing_rel_permi, a)
%
% R = OrderApproxWG(order, thick_vec, backing_rel_permi, a)
%
% OrderApproxWG returns the relative permittivity and resistivity of a sample
%    using an Nth order Maclaurin series approximation
%    SPECIFICALLY WRITTEN FOR WAVEGUIDE MEASUREMENTS
%    ASSUMES MEASURED SYSTEM DATA IS NAMED:
%      s21sample.txt
%
% -------------------------------------
%       |          |          |
%       |          |          |
%       | Unknown  | Known    |
%   Air | Layer    | Layer    | Air
%       |          |          |
%       |          |          |
% -------------------------------------
%       |-thick 1-|-thick 2-|
%
% order = degree of Maclaurin polynomial retained to formulate
%    approximation
% thick_vec = a vector of the thicknesses of the layers in the order shown
%    in the diagram in METERS
% backing_rel_permi = relative permittivity of the support backing, or
%    known layer in the diagram
% a = longest dimension of the rectangular waveguide in METERS

% close all;
clc;

%%%%%%%%%%%%%%%%%%%%%%%% Measured Data Filenames %%%%%%%%%%%%%%%%%%%%%%%
load s21sample.txt;
freq = s21sample(:,3);
%%%%%%%%%%%%%%%%%%%%%%%%%%%%%%%%%%%%%%%%%%%%%%%%%%%%%%%%%%%%%%%%%%%%%%%%%
```

```
%%%%%%%%%%%%%%%%%%%% S21_exp %%%%%%%%%%%%%%%%%%%%%%%%%%%%%%%%%
s21samplea = s21sample(:,1);
s21sampleb = s21sample(:,2);
s21samplesys = complex(s21samplea,s21sampleb);
%%%%%%%%%%%%%%%%%%%%%%%%%%%%%%%%%%%%%%%%%%%%%%%%%%%%%%%%%%%%%%%
%%%%%%%%%%%%%%%%%%%%%% Constants %%%%%%%%%%%%%%%%%%%%%%%%%%%%%%%
u0 = 4*pi*10^-7;
e0 = 8.854e-12;
N0 = sqrt(u0/e0);
c = 1/sqrt(e0*u0);
w = 2*pi*freq;
ko = w/c;
kc = pi/a;
kz = sqrt(ko.^2-kc^2);
Z0 = 2*a*freq*N0./sqrt(4*a^2*freq.^2 - c^2);
t = thick_vec(1);
l = thick_vec(2);
%%%%%%%%%%%%%%%%%%%%%%%%%%%%%%%%%%%%%%%%%%%%%%%%%%%%%%%%%%%%%%%%%%%%%%%
%%%%%%%%%%%%%%%%%%%%%%%%%%%%%%%%%%%%%%%%%%%%%%%%%%%%%%%%%%%%%%%%%%%%%%%
s21sys_exp = s21samplesys.*exp(-j*kz*(t+l));
%%%%%%%%%%%%%%%%%%%%%%%%%%%%%%%%%%%%%%%%%%%%%%%%%%%%%%%%%%%%%%%%%%%%%%%
%%%%%%%%%%%%%%%%%%%%%%% Support Backing %%%%%%%%%%%%%%%%%%%%%%%%%%%%%%%
e = e0*backing_rel_permi;
u = u0;
N = sqrt(u/e);
Z2 = N./sqrt(1-((1/(2*a*sqrt(e*u)))./freq).^2);
kz2 = w*sqrt(e*u).*sqrt(1-((1/(2*a*sqrt(e*u)))./freq).^2);
%%%%%%%%%%%%%%%%%%%%%%%%%%%%%%%%%%%%%%%%%%%%%%%%%%%%%%%%%%%%%%%%%%%%%%%
%%%%%%%%%%%%%%%%%%%%%%%% Nth Order Approx %%%%%%%%%%%%%%%%%%%%%%%%%%%%%
psi1 = exp(j*kz2*l).*(Z2 + Z0);
psi2 = exp(-j*kz2*l).*(Z0 - Z2);
omega1 = w*N0.*Z2;
omega2 = j*w.^2*N0^2/c;
omega3 = j*c*Z0.*Z2;
omega4 = w*N0.*Z0;
omega5 = 4*Z0.*Z2.*w*N0./s21sys_exp;
tmp_p(:,1) = omega1.*(psi1 + psi2) + t*omega2.*(psi1 - psi2) ...
    + omega4.*(psi1 - psi2) - omega5;
if mod(order,2) ~= 0
    m = floor(order/2) + 1;
    for i = 1:m
        if i == m
            tmp_p(:,i+1) = (-1)^(m-1)*t^(2*m-1)/factorial(2*m-1)*omega3.*(psi1 + psi2);
        else
            tmp_p(:,i+1) = (-1)^(i)*t^(2*i)/factorial(2*i)*omega1.*(psi1 + psi2) ...
                + (-1)^(i)*t^(2*i+1)/factorial(2*i+1)*omega2.*(psi1 - psi2) ...
                + (-1)^(i-1)*t^(2*i-1)/factorial(2*i-1)*omega3.*(psi1 + psi2) ...
                + (-1)^(i)*t^(2*i)/factorial(2*i)*omega4.*(psi1 - psi2);
        end
    end
    tmp_p = fliplr(tmp_p);
    m = 1;
    for i = 1:2*length(tmp_p(1,:))-1
        if mod(i,2) == 0
            p(:,i) = zeros(length(tmp_p(:,1)),1);
        else
            p(:,i) = tmp_p(:,m);
            m = m + 1;
        end
    end
    for i=1:length(p(:,1))
        kz1(i,:) = roots(p(i,:)).';
    end
    for i = 1:length(kz1(1,:))
        tmpe_r(:,i) = (kz1(:,i).^2*a^2*c^2/pi^2 + c^2)./(4*a^2*freq.^2);
    end
    for i=1:length(tmpe_r(:,1))
        for n=1:length(tmpe_r(i,:))
            if imag(tmpe_r(i,n)) <= 0
```

B-10

```matlab
                    e_r(i,1) = tmpe_r(i,n);
                end
            end
        end
else
    m = order/2;
    for i = 1:m
        if i == m
            tmp_p(:,i+1) = (-1)^(m)*t^(2*m)/factorial(2*m)*omega1.*(psi1 + psi2) ...
                + (-1)^(m-1)*t^(2*m-1)/factorial(2*m-1)*omega3.*(psi1 + psi2) ...
                + (-1)^(m)*t^(2*m)/factorial(2*m)*omega4.*(psi1 - psi2);
        else
            tmp_p(:,i+1) = (-1)^(i)*t^(2*i)/factorial(2*i)*omega1.*(psi1 + psi2) ...
                + (-1)^(i)*t^(2*i+1)/factorial(2*i+1)*omega2.*(psi1 - psi2) ...
                + (-1)^(i-1)*t^(2*i-1)/factorial(2*i-1)*omega3.*(psi1 + psi2) ...
                + (-1)^(i)*t^(2*i)/factorial(2*i)*omega4.*(psi1 - psi2);
        end
    end
    tmp_p = fliplr(tmp_p);
    m = 1;
    for i = 1:2*length(tmp_p(1,:))-1
        if mod(i,2) == 0
            p(:,i) = zeros(length(tmp_p(:,1)),1);
        else
            p(:,i) = tmp_p(:,m);
            m = m + 1;
        end
    end
    for i=1:length(p(:,1))
        kz1(i,:) = roots(p(i,:)).';
    end
    for i = 1:length(kz1(1,:))
        tmpe_r(:,i) = (kz1(:,i).^2*a^2*c^2/pi^2 + c^2)./(4*a^2*freq.^2);
    end
    for i=1:length(tmpe_r(:,1))
        for n=1:length(tmpe_r(i,:))
            if imag(tmpe_r(i,n)) <= 0
                e_r(i,1) = tmpe_r(i,n);
            end
        end
    end
end
Re = -j*N0./(ko*t.*(e_r-1));
R = [e_r Re];
title_str = ['Order ' num2str(order) ' Maclaurin Approximation - Waveguide'];
figure;
subplot(221);
plot(freq/1e9,real(e_r),'linewidth',2);
title(title_str,'fontsize',12);
xlabel('Frequency (GHz)','fontsize',12);
ylabel('Real Part of \epsilon_r','fontsize',12,'fontweight','bold');
axis tight;
grid on;
subplot(223);
plot(freq/1e9,imag(e_r),'linewidth',2);
title(title_str,'fontsize',12);
xlabel('Frequency (GHz)','fontsize',12);
ylabel('Imaginary Part of \epsilon_r','fontsize',12,'fontweight','bold');
axis tight;
grid on;
subplot(222);
plot(freq/1e9,real(Re),'linewidth',2);
title(title_str,'fontsize',12);
xlabel('Frequency (GHz)','fontsize',12);
ylabel('Real Part of R_e','fontsize',12,'fontweight','bold');
axis tight;
grid on;
subplot(224);
plot(freq/1e9,imag(Re),'linewidth',2);
```

B-11

```
title(title_str,'fontsize',12);
xlabel('Frequency (GHz)','fontsize',12);
ylabel('Imaginary Part of R_e','fontsize',12,'fontweight','bold');
axis tight;
grid on;
end
```

B.2.3 Thin Sheet Approximation.

```
function R = ResistiveWG(thick_vec, backing_rel_permi, a)
%
% R = ResistiveWG(thick_vec, backing_rel_permi, a)
%
% ResistiveFS returns the relative permittivity and resistivity of a sample
%   using resistive boundary conditions
%   SPECIFICALLY WRITTEN FOR WAVEGUIDE MEASUREMENTS
%   ASSUMES MEASURED SYSTEM DATA IS NAMED:
%     s21sample.txt
%
% ------------------------------------
%      |          |          |
%      |          |          |
%      | Unknown  | Known    |
%   Air | Layer    | Layer    | Air
%      |          |          |
%      |          |          |
% ------------------------------------
%      |-thick 1-|-thick 2-|
%
% thick_vec = a vector of the thicknesses of the layers in the order shown
%   in the diagram in METERS
% backing_rel_permi = relative permittivity of the support backing, or
%   known layer in the diagram
% a = longest dimension of the rectangular waveguide in METERS

% close all;
clc;

%%%%%%%%%%%%%%%%%%%%%%%%% Measured Data Filenames %%%%%%%%%%%%%%%%%%%%%%%
load s21sample.txt;
freq = s21sample(:,3);
%%%%%%%%%%%%%%%%%%%%%%%%%%%%%%%%%%%%%%%%%%%%%%%%%%%%%%%%%%%%%%%%%%%%%%%%%%
%%%%%%%%%%%%%%%%%%%%%%%%%% S21_exp %%%%%%%%%%%%%%%%%%%%%%%%%%%%%%%%%%%%%%%%
s21samplea = s21sample(:,1);
s21sampleb = s21sample(:,2);
s21samplesys = complex(s21samplea,s21sampleb);
%%%%%%%%%%%%%%%%%%%%%%%%%%%%%%%%%%%%%%%%%%%%%%%%%%%%%%%%%%%%%%%%%%%%%%%%%%
%%%%%%%%%%%%%%%%%%%%%%%%%% Constants %%%%%%%%%%%%%%%%%%%%%%%%%%%%%%%%%%%%%%
u0 = 4*pi*10^-7;
e0 = 8.854e-12;
N0 = sqrt(u0/e0);
c = 1/sqrt(e0*u0);
w = 2*pi*freq;
ko = w/c;
kc = pi/a;
kz = sqrt(ko.^2-kc^2);
Z0 = 2*a*freq*N0./sqrt(4*a^2*freq.^2 - c^2);
t = thick_vec(1);
l = thick_vec(2);
%%%%%%%%%%%%%%%%%%%%%%%%%%%%%%%%%%%%%%%%%%%%%%%%%%%%%%%%%%%%%%%%%%%%%%%%%%
%%%%%%%%%%%%%%%%%%%%%%%%%% Forward %%%%%%%%%%%%%%%%%%%%%%%%%%%%%%%%%%%%%%%%
s21sys_exp = s21samplesys.*exp(-j*kz*l);
%%%%%%%%%%%%%%%%%%%%%%%%%%%%%%%%%%%%%%%%%%%%%%%%%%%%%%%%%%%%%%%%%%%%%%%%%%
%%%%%%%%%%%%%%%%%%%%%%%%%% Support Backing %%%%%%%%%%%%%%%%%%%%%%%%%%%%%%%%
e = e0*backing_rel_permi;
u = u0;
N = sqrt(u/e);
```

```
Z1 = N./sqrt(1-((1/(2*a*sqrt(e*u)))./freq).^2);
kz1 = w*sqrt(e*u).*sqrt(1-((1/(2*a*sqrt(e*u)))./freq).^2);
%%%%%%%%%%%%%%%%%%%%%%%%%%%%%%%%%%%%%%%%%%%%%%%%%%%%%%%%%%%%%%%%%%%%
%%%%%%%%%%%%%%%%%%%%%%% Thin Sheet Approx %%%%%%%%%%%%%%%%%%%%%%%%%%
psi1 = j*(Z1.^2).*sin(kz1*l) + 2*Z0.*Z1.*cos(kz1*l) + j*(Z0.^2).*sin(kz1*l);
psi2 = (Z0.^2).*Z1.*cos(kz1*l) + j*Z0.*(Z1.^2).*sin(kz1*l);
Re = s21sys_exp.*psi2./(2*Z0.*Z1 - s21sys_exp.*psi1);
e_r = (-j*N0 + Re.*ko*t)./(Re.*ko*t);
R = [e_r Re];
figure;
subplot(221);
plot(freq/1e9,real(e_r),'linewidth',2);
title_str = 'Resistive Boundary Condition - Waveguide';
title(title_str,'fontsize',12);
xlabel('Frequency (GHz)','fontsize',12);
ylabel('Real Part of \epsilon_r','fontsize',12,'fontweight','bold');
axis tight;
grid on;
subplot(223);
plot(freq/1e9,imag(e_r),'linewidth',2);
title(title_str,'fontsize',12);
xlabel('Frequency (GHz)','fontsize',12);
ylabel('Imaginary Part of \epsilon_r','fontsize',12,'fontweight','bold');
axis tight;
grid on;
subplot(222);
plot(freq/1e9,real(Re),'linewidth',2);
title(title_str,'fontsize',12);
xlabel('Frequency (GHz)','fontsize',12);
ylabel('Real Part of R_e','fontsize',12,'fontweight','bold');
axis tight;
grid on;
subplot(224);
plot(freq/1e9,imag(Re),'linewidth',2);
title(title_str,'fontsize',12);
xlabel('Frequency (GHz)','fontsize',12);
ylabel('Imaginary Part of R_e','fontsize',12,'fontweight','bold');
axis tight;
grid on;
end
```

B.2.4 Vertical Mode Matching Technique.

```
function parameters = ModeMatching1DSearchKx(permi_vec, perme_vec, ...
    thick_vec, len, a, numModes, maxIterations, precision)
%
% parameters = ModeMatching1DSearchKx(permi_vec, perme_vec, thick_vec, ...
%   len, a, numModes, maxIterations, precision)
%
% ModeMatching1DSearchKx returns the relative permittivity of a sample
%   stacked horizontally in a wavegude using S21
%   S21_thy(w,e) - S21_exp = 0
%   ASSUMES MEASURED SYSTEM DATA IS NAMED:
%     s21sample.txt
%
%
% -----------------------------------------------
%             |            3            |
%             |                         |
%             |-------------------------|
%             |            2            |          ---> z
%             |-------------------------|
%             |                         |
%             |            1            |
% -----------------------------------------------
%             |------ length -----|
%
```

```matlab
% 1 & 3 are the same known material
% 2 is the unknown material
%
%
% permi_vec = a vector of the permittivity values of the layers in the
%   order shown in the diagram
%   THE VALUE FOR LAYER 2 WILL BE THE INITIAL GUESS
% perme_vec = a vector of the permeability values of the layers in the
%   order shown in the diagram
%   THE VALUE ENTERED FOR LAYER 2 WILL BE ASSUMED TO BE TRUE
% thick_vec = a vector of the thicknesses of the layers in the order shown
%   in the diagram in METERS
% len = length of the sample in METERS
% a = longest dimension of the rectangular waveguide in METERS
% numModes = number of modes to calculated
% maxIterations = maximum number of root search iterations
% precision = precision of root


% close all;
% clc;
warning off all;

%%%%% Measured Data Filename
load s21sample.txt;

freq = s21sample(:,3);
%%%%%
%%%%% S21_exp
s21samplea = s21sample(:,1);
s21sampleb = s21sample(:,2);
s21samplesys = complex(s21samplea,s21sampleb);
%%%%%
%%%%% Constants
u0 = 4*pi*10^-7;
e0 = 8.854e-12;
c = 1/sqrt(e0*u0);

w = 2*pi*freq;
kx0 = pi/a*[1:numModes];
kx0 = repmat(kx0,length(w),1);
k0 = w*sqrt(e0*u0);
k0 = repmat(k0,1,numModes);
gamma0 = (kx0.^2 - k0.^2).^(1/2);
%%%%%
%%%%% S21_exp
s21sys_exp = s21samplesys.*exp(-gamma0(:,1)*len);
%%%%%

tau = thick_vec(1);
d = thick_vec(2);
initial_guess = permi_vec(1,2);
permi_vec = repmat(permi_vec,length(w),1);
for i = 1:length(w)
    prog_str = ['Processing frequency ' num2str(i) ' of ' ...
        num2str(length(freq)) ' ...'];
    disp(prog_str);
    guesses = 1;
    if i > 1
        for k = i-1:-1:1
            if ~isnan(permi_vec(k,2))
                permi_vec(i,2) = permi_vec(k,2);
                break;
            elseif k == 1
                permi_vec(i,2) = initial_guess;
            else
            end
        end
    end
```

```matlab
    while guesses < maxIterations
        inter_param = InterParameters(numModes, a, permi_vec(i,:), 0, ...
            perme_vec, w(i), tau, d, maxIterations, ...
            precision, gamma0(i,:));
        A_Mat = BuildMatrix(numModes, a, inter_param, len, tau, d);
        b_Vec = BuildVector(numModes, a, inter_param(5,:));
        sol = A_Mat\b_Vec;
        s21sys_thy = sol(3*numModes+1);
        del_permi = precision*permi_vec(i,2);
        inter_param = InterParameters(numModes, a, permi_vec(i,:), ...
            del_permi, perme_vec, w(i), tau, d, maxIterations, ...
            precision, gamma0(i,:));
        A_Mat = BuildMatrix(numModes, a, inter_param, len, tau, d);
        b_Vec = BuildVector(numModes, a, inter_param(5,:));
        sol = A_Mat\b_Vec;
        s21sys_thy_deriv = (sol(3*numModes+1)-s21sys_thy)/del_permi;
        if abs((s21sys_thy-s21sys_exp(i))/s21sys_thy_deriv) <= precision
            break;
        end
        permi_vec(i,2) = permi_vec(i,2) - ...
            (s21sys_thy-s21sys_exp(i))/s21sys_thy_deriv;
        if isnan(permi_vec(i,2))
            break;
        end
        guesses = guesses + 1;
    end
end
Re = -j*sqrt(u0/e0)./(k0(:,1)*thick_vec(2).*(permi_vec(:,2)-1));
parameters = [permi_vec(:,2) Re];
DispResults(parameters, freq, numModes);
end

function inter_param = InterParameters(numModes, a, permi_vec, ...
    del_permi, perme_vec, w, tau, d, maxIterations, precision, gamma0)
u0 = 4*pi*10^-7;
e0 = 8.854e-12;
permi_vec(2) = permi_vec(2) + del_permi;
permi_vec = permi_vec*e0;
perme_vec = perme_vec*u0;
gamma = FindGamma(numModes, a, permi_vec, perme_vec, w, ...
    tau, d, maxIterations, precision);
kx = (w^2*permi_vec(1)*perme_vec(1) + gamma.^2).^(1/2);
kxu = (w^2*permi_vec(2)*perme_vec(2) + gamma.^2).^(1/2);
Y = (-kx*perme_vec(2)./(perme_vec(1)*kxu).*cos(kx*tau).*sin(kxu*d) ...
    - sin(kx*tau).*cos(kxu*d))./sin(kx*(a-tau-d));
Z0 = j*w*u0./gamma0;
Z = j*w*perme_vec(1)./gamma;
Zu = j*w*perme_vec(2)./gamma;
psi1 = kx*perme_vec(2)./(perme_vec(1)*kxu).*cos(kx*tau);
psi2 = -sin(kx*tau);

inter_param = [gamma;
               kx;
               kxu;
               Y;
               Z0;
               Z;
               Zu;
               psi1;
               psi2];
end

function A = BuildMatrix(numModes, a, inter_param, len, tau, d)
gamma = inter_param(1,:);
kx = inter_param(2,:);
kxu = inter_param(3,:);
Y = inter_param(4,:);
Z0 = inter_param(5,:);
Z = inter_param(6,:);
```

```
Zu = inter_param(7,:);
psi1 = inter_param(8,:);
psi2 = inter_param(9,:);

psi1 = repmat(psi1,numModes,1);
psi2 = repmat(psi2,numModes,1);
Y = repmat(Y,numModes,1);
Z0 = repmat(Z0,numModes,1);
Z = repmat(Z,numModes,1);
Zu = repmat(Zu,numModes,1);
gamma = repmat(gamma,numModes,1);

M = M_SubMatrix(numModes, a);
N = N_SubMatrix(numModes, a, kx, tau);
P = P_SubMatrix(numModes, a, kxu, tau, d);
R = R_SubMatrix(numModes, a, kxu, tau, d);
Q = Q_SubMatrix(numModes, a, kx, tau, d);

S1 = -N - psi1.*P + psi2.*R + Y.*Q;
S2 = N./Z + psi1./Zu.*P - psi2./Zu.*R - Y./Z.*Q;
S3 = -S2;

A = [-M                          -S1                      ...
     -S1                          zeros(numModes,numModes);
     -M./Z0                      -S2                      ...
     -S3                          zeros(numModes,numModes);
      zeros(numModes,numModes)    S1.*exp(-gamma*len) ...
      S1.*exp(gamma*len)          M;
      zeros(numModes,numModes)    S2.*exp(-gamma*len) ...
      S3.*exp(gamma*len)         -M./Z0];
end

function b = BuildVector(numModes, a, Z0)
Z0 = Z0.';
m = M_SubVector(numModes, a);
b = [ m;
     -m./Z0;
      zeros(numModes,1);
      zeros(numModes,1)];
end

function M_Mat = M_SubMatrix(numModes, a)
M_Mat = zeros(numModes, numModes);
for m = 1:numModes
    M_Mat(m,m) = 1/2*a;
end
end

function N_Mat = N_SubMatrix(numModes, a, kx, tau)
for n = 1:numModes
    for m = 1:numModes
        N_Mat(n,m) = 1/2*(a/(n*pi-a*kx(m)))*sin(tau*(n*pi/a-kx(m))) ...
            - 1/2*(a/(n*pi+a*kx(m)))*sin(tau*(n*pi/a+kx(m)));
    end
end
end

function P_Mat = P_SubMatrix(numModes, a, kxu, tau, d)
for n = 1:numModes
    for m = 1:numModes
        P_Mat(n,m) = 1/2*(a/(n*pi-a*kxu(m))) ...
            *(sin(n*pi/a*(tau+d) - kxu(m)*d) - sin(n*pi/a*tau)) ...
            - 1/2*(a/(n*pi+a*kxu(m))) ...
            *(sin(n*pi/a*(tau+d) + kxu(m)*d) - sin(n*pi/a*tau));
    end
end
end

function R_Mat = R_SubMatrix(numModes, a, kxu, tau, d)
```

B-16

```
for n = 1:numModes
    for m = 1:numModes
        R_Mat(n,m) = 1/2*(a/(n*pi-a*kxu(m))) ...
            *(-cos(n*pi/a*(tau+d) - kxu(m)*d) + cos(n*pi/a*tau)) ...
            + 1/2*(a/(n*pi+a*kxu(m))) ...
            *(-cos(n*pi/a*(tau+d) + kxu(m)*d) + cos(n*pi/a*tau));
    end
end
end

function Q_Mat = Q_SubMatrix(numModes, a, kx, tau, d)
for n = 1:numModes
    for m = 1:numModes
        Q_Mat(n,m) = 1/2*(a/(n*pi-a*kx(m))) ...
            *sin(n*pi/a*(tau+d)+kx(m)*(a-tau-d)) ...
            - 1/2*(a/(n*pi+a*kx(m)))*sin(n*pi/a*(tau+d)+kx(m)*(tau+d-a));
    end
end
end

function M_Vec = M_SubVector(numModes, a)
M_Vec = zeros(numModes,1);
M_Vec(1) = 1/2*a;
end

function gammaM = FindGamma(numModes, a, permi_vec, perme_vec, ...
    w, tau, d, maxIterations, precision)
e = permi_vec(1);
u = perme_vec(1);
eu = permi_vec(2);
uu = perme_vec(2);

delta_d = 0.01;
%%%%% Initial Gamma Guess - Empty
gamma = (([1:numModes]*pi/a).^2 - w^2*e*u).^(1/2);
%%%%%
for m = 1:numModes
    d_step = delta_d*d;
    tau_step = tau + d - d_step;
    while d_step <= d
        guesses = 1;
        while guesses < maxIterations
            eigen_eq = GammaEigenFunction(gamma(m), 0, tau_step, ...
                d_step, a, e, u, eu, uu, w);
            del_gamma = precision*gamma(m);
            eigen_eq_deriv = (GammaEigenFunction(gamma(m), del_gamma, ...
                tau_step, d_step, a, e, u, eu, uu, w) - eigen_eq)/del_gamma;
            if abs(eigen_eq/eigen_eq_deriv) <= precision
                break;
            end
            gamma(m) = gamma(m) - eigen_eq/eigen_eq_deriv;
            guesses = guesses + 1;
        end
        d_step = d_step + delta_d*d;
        tau_step = tau + d - d_step;
    end
end
gammaM = gamma;
end

function eigFuncValue = GammaEigenFunction(gamma, del_gamma, tau, d, ...
    a, e, u, eu, uu, w)
gamma = gamma + del_gamma;
kx = (w^2*e*u + gamma^2)^(1/2);
kxu = (w^2*eu*uu + gamma^2)^(1/2);
eigFuncValue = (exp(j*kxu*d)+exp(-j*kxu*d))* ...
    (exp(j*kx*(a-d))-exp(-j*kx*(a-d))) ...
    + uu*kx/(2*u*kxu)*(exp(j*kxu*d)-exp(-j*kxu*d))* ...
    (exp(j*kx*(a-d))+exp(j*kx*(a-2*tau-d))+ ...
```

```
            exp(-j*kx*(a-2*tau-d))+exp(-j*kx*(a-d))) ...
        + u*kxu/(2*uu*kx)*(exp(j*kxu*d)-exp(-j*kxu*d))* ...
        (exp(j*kx*(a-d))-exp(j*kx*(a-2*tau-d))- ...
            exp(-j*kx*(a-2*tau-d))+exp(-j*kx*(a-d)));
end

function DispResults(parameters, freq, numModes)
e_r = parameters(:,1);
Re = parameters(:,2);
title_str = [num2str(numModes) ' Modes'];
figure;
subplot(221);
plot(freq/1e9,real(e_r),'linewidth',2);
title(title_str,'fontsize',12);
xlabel('Frequency (GHz)','fontsize',12);
ylabel('Real Part of \epsilon_r','fontsize',12,'fontweight','bold');
axis tight;
grid on;
subplot(223);
plot(freq/1e9,imag(e_r),'linewidth',2);
title(title_str,'fontsize',12);
xlabel('Frequency (GHz)','fontsize',12);
ylabel('Imaginary Part of \epsilon_r','fontsize',12,'fontweight','bold');
axis tight;
grid on;
subplot(222);
plot(freq/1e9,real(Re),'linewidth',2);
title(title_str,'fontsize',12);
xlabel('Frequency (GHz)','fontsize',12);
ylabel('Real Part of R_e','fontsize',12,'fontweight','bold');
axis tight;
grid on;
subplot(224);
plot(freq/1e9,imag(Re),'linewidth',2);
title(title_str,'fontsize',12);
xlabel('Frequency (GHz)','fontsize',12);
ylabel('Imaginary Part of R_e','fontsize',12,'fontweight','bold');
axis tight;
grid on;
end
```

References

[1]   J. Lee, M. J. Havrilla, J. E. Luminati, M. W. Hyde, and E. J. Rothwell, "Scattering from a cylindrical resistive sheet using a modified PO current," in press., 2005.

[2]   D. K. Schroder, *Semiconductor Material and Device Characterization*. New York: John Wiley & Sons, 1990.

[3]   R. E. Collin, *Field Theory of Guided Waves*, 2nd ed. New York: IEEE Press, 1991.

[4]   R. F. Harrington, *Time-Harmonic Electromagnetic Fields*. New York: IEEE Press, 2001.

[5]   C. A. Balanis, *Advanced Engineering Electromagnetics*. New York: John Wiley & Sons, 1989.

[6]   T. B. A. Senior and J. L. Volakis, *Approximate Boundary Conditions in Electromagnetics*. London: IEEE Press, 1995.

[7]   K. Sarabandi and F. T. Ulaby, "Technique for measuring the dielectric constant of thin materials," *IEEE Trans. Instrum. Meas.*, vol. 37, no. 4, pp. 631-636, Dec. 1988.

[8]   E. F. Knott, J. F. Shaeffer, and M. T. Tuley, *Radar Cross Section*, 2nd ed. Raleigh, NC: SciTech Publishing, 2004.

[9]   A. E. Bogle, "Electromagnetic material characterization using a partially filled rectangular waveguide," M.S. thesis, Michigan State University, East Lansing, Michigan, 2004.

[10]   Personal Communication with Rodney George, AFRL/SNS, Wright-Patterson Air Force Base, Ohio, Dec. 16, 2005.

[11]   K. J. Cassell, "Investigation of time-domain and frequency-domain free-space material measurements," M.S. thesis, Air Force Institute of Technology, Wright-Patterson Air Force Base, Ohio, 2006.

[12]   S. P. Dorey, "Stepped waveguide electromagnetic material characterization technique," M.S. thesis, Air Force Institute of Technology, Wright-Patterson Air Force Base, Ohio, 2004.

[13]   M. J. Havrilla, "Analytical and experimental techniques for the electromagnetic characterization of materials," Ph.D. dissertation, Michigan State University, East Lansing, Michigan, 2001.

[14]   L. F. Chen, C. K. Ong, C. P. Neo, V. V. Varadan, and V. K. Varadan, *Microwave Electronics Measurement and Materials Characterization*. New York: John Wiley & Sons, 2004.

[15]   T. B. A. Senior, "Combined resistive and conductive sheets," *IEEE Trans. Antennas Propagat.*, vol. AP-33, no. 5, pp. 577-579, May 1985.

[16]   R. F. Harrington and J. R. Mautz, "An impedance sheet approximation for thin dielectric shells," *IEEE Trans. Antennas Propagat.*, vol. AP-23, pp. 531-534, July 1975.

[17]   J. W. Schultz, "Numerical analysis of transmission line techniques for RF material measurements," *24th Annual Meeting & Symposium of the Antenna Measurement Techniques Association (AMTA)*, Cleveland, Ohio, Nov. 3-8, 2002.

[18]   W. B. Wier, "Automatic measurement of complex dielectric constant and permeability at microwave frequencies," *Proc. IEEE*, vol. 62, pp. 33-36, Jan. 1974.

REPORT DOCUMENTATION PAGE

1. REPORT DATE (DD-MM-YYYY) 23-03-2006	**2. REPORT TYPE** **Master's Thesis**	**3. DATES COVERED** (From – To) Sep 2005 – Mar 2006

4. TITLE AND SUBTITLE Determining the Resistivity of Resistive Sheets Using Transmission Measurements	**5a. CONTRACT NUMBER**
	5b. GRANT NUMBER
	5c. PROGRAM ELEMENT NUMBER

6. AUTHOR(S) Hyde, Milo, W., IV, Captain, USAF	**5d. PROJECT NUMBER**
	5e. TASK NUMBER
	5f. WORK UNIT NUMBER

7. PERFORMING ORGANIZATION NAMES(S) AND ADDRESS(S) Air Force Institute of Technology Graduate School of Engineering and Management (AFIT/EN) 2950 Hobson Way WPAFB OH 45433-7765	**8. PERFORMING ORGANIZATION REPORT NUMBER** AFIT/GE/ENG/06-24

9. SPONSORING/MONITORING AGENCY NAME(S) AND ADDRESS(ES) N/A	**10. SPONSOR/MONITOR'S ACRONYM(S)**
	11. SPONSOR/MONITOR'S REPORT NUMBER(S)

12. DISTRIBUTION/AVAILABILITY STATEMENT
        APPROVED FOR PUBLIC RELEASE; DISTRIBUTION UNLIMITED.

13. SUPPLEMENTARY NOTES

14. ABSTRACT

  In September 2005, radar cross section (RCS) measurements were made of resistive sheets, or R-cards, wrapped around a polystyrene foam cylinder to compare with a newly developed theoretical RCS prediction technique. The resistivities of the R-cards were initially measured with a direct current (DC) four-point probe. When the RCS measurements were compared to the theoretical predictions, it became clear that DC resistivity alone is not sufficient to accurately predict the scattering from an R-card. This thesis presents alternating current (AC) methods for determining the resistivity of an R-card. Both free-space and waveguide techniques are presented.

  Experimental verification of the techniques is performed using two R-cards with DC resistivities 892 Ω/sq and 64 Ω/sq. The techniques are compared intra- and inter-measurement apparatus. An error analysis is also performed to demonstrate the sensitivity of the techniques to errors in the measurements of the thickness or the permittivity of the support backing.

15. SUBJECT TERMS
    Resistive Sheet, R-card, Wave Transmission, Free-Space, Focused Arch, Waveguide, Resistivity, Permittivity

16. SECURITY CLASSIFICATION OF:			**17. LIMITATION OF ABSTRACT**	**18. NUMBER OF PAGES**	**19a. NAME OF RESPONSIBLE PERSON** Dr. Michael J. Havrilla (ENG)
REPORT U	**ABSTRACT** U	**c. THIS PAGE** U	**UU**	126	**19b. TELEPHONE NUMBER** (Include area code) (937) 255-3636, ext 7252 michael.havrilla@afit.edu